SYNTHESIS OF SILVER DOPED MULTI-WALLED CARBON NANOTUBES FOR THE TREATMENT OF FISHPOND WASTEWATER

BY

ALIYU, Saadatu
MEng/SEET/2017/6713

DEPARTMENT OF CHEMICAL ENGINEERING
FEDERAL UNIVERSITY OF TECHNOLOGY, MINNA

OCTOBER, 2021

SYNTHESIS OF SILVER DOPED MULTI-WALLED CARBON NANOTUBES FOR THE TREATMENT OF FISHPOND WASTEWATER.

BY

ALIYU, Saadatu
MEng/SEET/2017/6713

A THESIS SUBMITTED TO THE POSTGRADUATE SCHOOL FEDERAL UNIVERSITY OF TECHNOLOGY, MINNA, NIGERIA IN PARTIAL FULFILMENT OF THE REQUIREMENTS FOR THE AWARD OF THE DEGREE OF MASTER OF ENGINEERING IN CHEMICAL ENGINEERING

OCTOBER, 2021

ABSTRACT

Agglomeration of the carbonaceous material during and after the synthesis carbon nanotubes affects and limits its efficiency hence there is need to modify the surface of raw CNTs and enhance its adsorption capacity and dispersion rate. This study is aimed at the development of silver Nanoparticles doped on multi- walled carbon nanotube for the treatment of fish pond wastewater. This study investigated the treatment of fishpond wastewater using nanocomposites via batch adsorption by purified carbon nanotube and silver doped carbon nanotubes (CNTs) as nano-adsorbents. Synthesis of silver nanoparticles (AgNPs) was done using *Carica papaya* leaf extract. The synthesized AgNPs was confirmed by UV spectra, Fourier Transform Infrared Spectroscopy (FTIR), X-ray diffraction (XRD) and High-resolution transmission electron microscopy (HRTEM). The peaks in XRD pattern are associated with that of face centered cubic (FCC) form of metallic silver. The results of HRTEM confirmed that the size of AgNPs are between 11-30 nm. Fe–Ni/kaolin catalyst was used for the production of carbon nanotubes (CNTs) by catalytic chemical vapour deposition method followed by acid purification treatment and doping with silver nanoparticles to give purified carbon nanotubes (P-CNTs) and silver doped carbon nanotubes (Ag-CNTs) respectively. The as-synthesized CNTs, P-CNTs and Ag-CNTs were characterized by HRTEM, High-resolution scanning electron microscopy (HRSEM), FTIR and Brunauer Emmett Teller (BET). The adsorption behavior of P-CNTs and Ag-CNTs to remove specifically Fe, Mn and Zn from fishpond wastewater were examined by the batch adsorption process as a function of different contact time, adsorbent dosage and temperature. The HRSEM/HRTEM/BET analysis confirmed that both nano adsorbents were tube-like in nature, highly porous and crystalline, with Ag-CNTs possessing high surface area (1068 m^2/g) than P-CNTs (268.40 m^2/g). The order of maximum Mn, Zn and Fe removal by the nano-adsorbents at equilibrium time of 100 min are as follows: Ag-CNTs (91.92%, 88.53% and 89.23%)>P-CNTs (91.85%, 81.60% and 52.14%). Equilibrium sorption data were better described by Freundlich isotherm than Langmuir isotherm. The adsorption kinetics for Mn, Zn and Fe removal from fishpond wastewater fitted well to the pseudo-second-order model. Thermodynamics analysis of the adsorption process revealed negative values of enthalpy ($\Delta H°$) for Mn, Fe and Zn respectively on Ag-CNTs which indicates that the adsorption is exothermic in nature and for P-CNTs negative values of $\Delta H°$ for Mn and Fe except Zn has positive $\Delta H°$ and endothermic in nature. The Gibbs free energy ($\Delta G°$) was negative which showed the feasibility and spontaneity of adsorption process, except Zn adsorbed by P-CNTs which possesses positive $\Delta G°$. The change entropy ($\Delta S°$) was positive which signifies a better adsorption of the heavy metals and increase randomness except for Zn adsorbed by P-CNTs with negative $\Delta S°$ which signifies decrease in randomness of the process. In this study the adsorption isotherm and kinetic model was best fitted to Freundlich isotherm and pseudo-second-order model, which shows that it is a multilayer phenomenon. The adsorption process was spontaneous, random and exothermic in nature.

TABLE OF CONTENTS

CHAPTER TWO

LIST OF TABLES

LIST OF FIGURES

LIST OF PLATES

CHAPTER ONE

1.0 INTRODUCTION

1.1 Background to the Study

Wastewater is any water that has been contaminated by human activities; combination of domestic, industrial, commercial or agricultural use, surface runoff or storm water and any sewer inflow or sewer infiltration (Luo *et al.*, 2014; Tilley, 2014).

Wastewaters are characterized with high concentrations of nutrients and solid materials which are usually discharged into water streams and rivers without any form of treatment. This practice introduces non-native species into the water causing pollution, changes in river hydrology and other environmental issues. In addition, increasing environmental awareness, coupled with more stringent regulation standards, has triggered various industries to challenge themselves in seeking appropriate ways of treating the wastewater generated (Teh *et al.*, 2016). The use of highly nutritious feeds and other chemical products, has generated wastes that are difficult to curtail and toxic to aquatic lives. Nitrogenous wastes are the major component of aquaculture waste. They are highly toxic to macro-fauna in the open water body. An increase in ammonia concentrations could elevate blood ammonia making it highly toxic to fish same as suspended solids which causes interstitial clogging and substrate embeddedness in fish (Omitoyin *et al.*, 2017).

These problems and the remarkable growth in fish farming, necessitated measures for the control of fish farm effluent and wastewater control, the pollutants from fish farms include fish metabolic products as well as faeces which are by-products of the composition of food and fish feeding methods (Anijiofor *et al.*, 2018). Some of the parameters of interest from

fish wastewater that can affect aquatic environment include, physical parameters such as pH, Total Suspended Solids (TSS), Total Dissolved Solids (TDS), Turbidity and Colour, Organic pollutants which are indicated by Chemical Oxygen Demand (COD) and Biochemical Oxygen Demand (BOD) and nutrients such as, Ammonia (NH_3), Total Nitrogen (TN) and Total Phosphorous (TP). Water sources, water scarcity and nature of additives used in fish farming are factors that determined the level of pollution that has been made to the fish and fishpond. It is therefore, important to treat water discharge from fish pond for reuse and to protect the environment around fish farms.

The existing technologies of wastewater treatments, such as sedimentation, flocculation, dis-infection, filtration, ozonation, and UV (ultraviolet) light have several drawbacks such as high-energy requirement, incomplete pollutant removal and generation of toxic sludge. In this context, there is a requirement for more efficient and powerful technologies for treatment of municipal and industrial wastewaters (Ferroudj *et al.*, 2013). Among the various emerging technologies, the advancement in nanotechnology has proved an incredible potential for the remediation of wastewater. In wastewater treatment application, a variety of efficient, eco-friendly and cost-effective nanomaterials have been developed having unique functionalities for effective decontamination of industrial effluents, surface water, ground water and drinking water (Khan *et al.*, 2016).

Nanotechnology has been cited, in different literatures, as one of the most advanced processes for wastewater treatment especially in the use of nano materials such as Nano-adsorbent which are chemically active and have high adsorption capacity for remediation of wastewater (Kyzas and Matis 2015). Examples of nano-adsorbent are carbon nanotubes, carbon nanofibres, metallic nanoparticles, graphenes, zeolites amongst others.

Carbon nanotubes (CNTs) are carbon material in the form of tubes and made of rolled up graphene layers. A single-walled CNTs consists of one layer of tube, while multi-walled CNTs are formed from more than a layer of tube. The tubes diameter is in nanometer range and a few micrometers in length. There are several methods to synthesize CNTs such as arc discharge, laser ablation, electrolysis, flame synthesis and catalytic chemical vapour deposition (CCVD). CCVD method is the most widely used due to its ability to control the growth directions and scale up the production in large quantity (Alfarisa *et al.*, 2016).

During the last decades, extensive research has led to the development of versatile methods for modifying carbon nanotubes (CNTs) and to obtain derivatives with more attractive features. Metallic nanoparticles such as silver nanoparticles (AgNPs) have received attention due to their antimicrobial and adsorptive potentials (Farid *et al.*, 2018). Green synthesis of nanoparticle is being imployed in the synthesis of silver nanoparticles because of its eco-friendly nature. Numerous studies report on the use of plant extracts to synthesis AgNPs with significant antimicrobial activities: leaf extracts of *Xanthium strumerium* (Rough cocklebur), *Murrayakoenigii* (curry), *Ocimum sanctum* (Tulsi), seed extracts of *Acacia farnesiana* (Acacia), *Macrotyloma uniflorum* (Horsegram), and even fruit extracts of *Musa paradisiacal* (banana peels) (Jerushka *et al*., 2018). In these studies, the plant extract is from *Carica papaya* (Pawpaw) leaf which serve as reducing and/or capping agents in the reaction with silver nitrate ($AgNO_3$), a commonly used precursor in silver nanoparticle synthesis.

1.2 Statement of the Research Problem

Direct application of colloidal silver nanoparticles might cause some problems such as their tendency to aggregate in aqueous media that gradually reduces their efficiency during long-

term use. Multi-walled carbon nanotubes (MWCNTs) have been extensively employed as a novel adsorbent for the removal of various organic and inorganic pollutants from wastewater due to its large specific surface area, high aspect ratio and above all exceptional hollow and layered structures (Hamzat *et al.*, 2019) Despite these remarkable properties of Carbon nanotubes (CNTs) (Thostenson *et al*., 2001), agglomeration of the carbonaceous material during and after the synthesis affects and limits its efficiency hence there is need to modify the surface of raw CNTs and enhance its adsorption capacity and dispersion rate (Lu *et al.*, 2008).

1.3 Aim and Objectives of the study

This study is aimed at the development of silver Nanoparticles doped on multi- walled carbon nanotube for the treatment of fish pond effluent. The aim was achieved by the following objectives.

1. Synthesis and characterize multi-walled carbon nanotube via chemical vapour deposition method with Fe-Ni/kaolin as the catalyst.
2. Green synthesis of silver nanoparticles with extract from *Carica Papaya* leaves as reducing and stabilizing agent.
3. Develop nanoadsorbent by doping silver nanoparticles on the matrix of multiwalled carbon nanotube through wet impregnation method.
4. Analysis of fish pond wastewater to determine physico- chemical parameters such as pH, turbidity, conductivity, TDS, colour, DO, COD, BOD and TP, TA and inorganic pollutants such as Fe, Mn, and Zn and total bacterial count before and after treatment.

5. Investigate the effect of contact time, mass of adsorbent and temperature on the efficient removal of heavy metals from fish pond wastewater using batch adsorption process.

1.4 Justification of the study

Adsorption techniques when combine with nanotechnology is considered a rational route to improve the treatment technologies due to their unique properties. Green synthesis methods of silver nanoparticle is simple, cost effective, high yield and wipe out the use of toxic chemicals. Catalytic chemical vapour deposition is a simple, economical and versatile method of producing high quality CNTs, high yield of bulk product and less quantity of unpurified nanotubes. Doping of Ag-NPs onto the matrix carbon nanotubes (CNTs) will not only enhance their antibacterial efficacy, biocompatibility and durability, hence reduces their bio-toxicity and their absorption into the body as well as excretion into the environment (Zhang *et al.*, 2014).The as-synthesized Ag-CNTs could hinder the growth of bacteria by direct contact, in which the cell membrane was ruptured and surface charge interactions between Ag-CNTs and the bacteria were initiated, it showed strong antibacterial efficacy against *Escherichia coli* compared to the AgNPs and CNTs This may be attributed to the synergic effect of CNTs and AgNPs in the nanocomposite (Dawadi *et al.*, 2021).There is still lack of information on the use Ag/CNTs for water treatment in aquaculture.

1.5 Scope of the study

In this study, Fe-Ni/Kaolin catalyst was synthesized and characterized for CNTs production via chemical catalytic vapour deposition method and doping of CNT with silver nanoparticles to produce nano- adsorbents for treatment of fish pond wastewater.

CHAPTER TWO

2.0 LITERATURE REVIEW

2.1 Water

Water is one of the most plentiful and essential compounds, occurring as a liquid on Earth's surface under normal conditions, which makes it invaluable for human uses and as plant and animal habitat (Westall and Brack 2018).Water is the environment of fish and other aquatic organism, it's the physical support in which living organisms carried out there life function, they can neither survive nor reproduce outside it. Water molecules contains 1 molecule of oxygen and 2 hydrogen atom connected by covalent hydrogen bond, 70- 71% of the earth surface is water out of which 97.5% is salt water while the remaining 2.8% is fresh water (Gleick, 2019). Water plays an important role in the world economy approximately 70% of the freshwater used by humans goes to agriculture (Chen *et al.,* 2018),fishing in salt and fresh water bodies is a major source of food in many parts of the world. Water provides safe neighborhoods for young fish, hiding spot by fish is crucial when it comes to mating, fish follow the food and helps fish protect their growing families.

2.2 Wastewater

Wastewater (or waste water) is any water that has been contaminated by human use. Wastewater is "used water from any combination of domestic, industrial, commercial or agricultural activities, surface runoff or storm water, and any sewer inflow or sewer infiltration". Therefore, wastewater is a byproduct of domestic, industrial, commercial or agricultural activities. The characteristics of wastewater vary depending on the source. Types of wastewater include: domestic wastewater from households, municipal wastewater from communities (also called sewage) and industrial wastewater. Wastewater can contain physical, chemical and biological pollutants (Tilley, 2014).

2.3 Fish

Fish are gill-bearing aquatic craniate animals that lack limbs with digits. They form a sister group to the tunicates, together forming the olfactores. Included in this definition are the living hagfish, lampreys, and cartilaginous and bony fish as well as various extinct related groups. The earliest organisms that can be classified as fish were soft-bodied chordates that first appeared during the Cambrian period. Although they lacked a true spine, they possessed notochords which allowed them to be more agile than their invertebrate counterparts (en.wikipedia.org). Fish are very diverse animals and can be categorized in many ways. This article is an overview of some of ways in which fish are categorized. Although most fish species have probably been discovered and described, about 250 new ones are still discovered every year. According to Fish Base, 34300 species of fish had been described as of September 2020. That is more than the combined total of all other vertebrate species: mammals, amphibians, reptiles and birds (Kohnen *et al.*, 2005).

2.4 Fish Pond

A fish pond, is a controlled pond, artificial lake, or reservoir that is stocked with fish and is used in aquaculture for fish farming, or is used for recreational fishing or for ornamental purp oses (en.wikipedia.org). Fish ponds are also being promoted in developing countries. They provide a source of food and income from the sale of fish for small farmers and can also supply irrigation needs and water for livestock (FAO, 2018).A large part of the world's fish culture production relies on the use of freshwater ponds which hold and exchange water, receive fertilizer or feed, and allow for holding, rearing and harvesting of fish. The proper preparation and construction of such ponds and their associated structures are essential for successful fish farming. Good ponds should be inexpensive relatively to construct, easy to maintain and efficient in allowing good water and fish management (Savary, 2020).

2.5 Fish Feeds

Fish need to be provided with enough nutritious food in order to attain maturity within a short period of time under culture conditions. There are two main types of fish feeds natural food and artificial feeds natural food can be stimulated to developing a pond through pond fertilization, fertilized pond will have tiny plants (phytoplankton) and animals (zooplankton) that can only be seen under a microscope (Ronga *et al.*, 2019). Artificial feeds are those feeds prepared and given to fish, the nutrients in these feeds are well balanced to meet the nutritional needs of the cultured fish species. The nutrients that should be included in fish feeds include; protein for body building, fat for normal functioning of the body and for energy, carbohydrates for energy, mineral salts for bone structure and body functions, vitamins for good health. Locally available ingredients such as fish meal, soya, maize and wheat are some ingredients that provide the nutrients listed above (Kemigabo *et al.*, 2017).

Prepared or artificial feeds should supply all the ingredients (protein, carbohydrates, fats, vitamins, and minerals) necessary for the optimal growth and health of the fish. Majority of fish farmers uses ingredients, typically made up of the following components and percentage ranges: protein, 18-50 percent; lipids, 10-25 percent; carbohydrate, 15-20 percent; ash, <8.5 percent; phosphorus, <1.5 percent; water, <10 percent; and trace amounts of vitamins and minerals. The nutritional content of the feed depends on what species of fish is being cultured and at what life stage (Craig *et al.*, 2017).

Any feed that is not eaten by the fish drops into the pond water, the excess feed dropping into the water may be a result of two things. Either as the result of over feeding by farmer or the feed is of poor quality and the fish only eat a small proportion. Either way, the uneaten feed drops into the pond and starts rotting (decomposing). Anything that rots in the pond takes up the fresh air (oxygen) that the fish needs for breathing, and produces bad gases example ammonia that are poisonous to fish, under such conditions the fish gets stressed and stops eating. In extreme cases the fish dies (Abdel-Tawwab *et al.*, 2020).

2.5.1 Sources of Aquaculture Waste

2.5.1.1 *Feed*

Feed is an extremely important factor of production in aquaculture and its level of importance depends on the type of culture technique. In an extensive system, feed supply to fish is mainly dependent on the environment. This type of culture system is primarily outdoors and does not meet the current demand for aquaculture products. In semi-intensive culture, fish are stocked at a moderate to relatively high density and rely on food both from

natural production and supplemental feed from the culturists (Dauda *et al.*, 2018). In intensive systems, natural food production is not relied upon, using very high quality artificial feed targeted towards fast growth instead. Feed has been reported to be the major source of waste in aquaculture systems. The effect of waste production due to fish feed varies with the amount of supplemental feed. Waste production from feed depends on so many factors, including its nutrient composition, method of production (extruded/pelleted), ratio of feed size to fish size, quantity of feed per unit time, feeding method, and storage time.

2.5.1.2 *Chemicals*

Chemicals are used in aquaculture in the form of medications, disinfectants, and anti foulants. The medications are used for chemotherapeutic purposes, which include the antibiotics being used for prophylaxis and curative purposes (Dauda *et al*., 2019), salts, mainly, are used to reduce stress in fish, lime is being used to treat pond bottoms for acidity during pond preparation, and other chemicals considered not harmful to fish are also used. Although these chemicals are important to fish culture, they may also constitute a nuisance to the environment (Boyd and McNevin 2015). As the water is released from the ponds, it flows into the environment. The effect of these chemical wastes depends on the concentration of chemicals used, the farm size, and the size of the receiving environment. The effect could be health issues, like anemia, nausea, vomiting, skin irritations, and stomach cramps. Too many zinc could injure the pancreas and upset the protein metabolism of human leading to arteriosclerosis (Zhang *et al.*, 2019).

2.5.1.3 *Pathogens*

This group of waste is rarely considered in aquaculture systems, especially when it is below the level that affects the cultured fish. The World health organisation (WHO) has settled on a

geometric mean of 104 fecal coliforms (FC) per 100 mL of fish pond water and less than one helminthes egg per liter (arithmetic mean) (Willmon, 2018). Influent to the pond may have a geometric mean of 105 FCU per 100 mL to take into account the effects of pathogen removal which occur in the fish pond once the wastewater enters the pond (WHO, 2006). However, discharging pathogens with the wastewater may negatively affect the aquatic organisms in the natural water bodies. Natural water bodies have their own pathogenic load and receiving additional loads from fish culture systems may cause stress or the outright death of aquatic organisms. The discharge of pond effluent is rampant in semi-intensive pond aquaculture, which is more common in Africa (Kar *et al.*, 2017), where organic fertilizers used in aquaculture resulted in a high level of pathogens. Four organic fertilizers (blood cow waste, cow manure, pig manure, and poultry manure) contribute to a high level of fecal streptococci (Dauda *et al.*, 2018).

2.6. Components of Waste from Aquaculture Systems

Components of waste produced from aquaculture systems have been characterized by many authors (Dauda *et al.*, 2019). This write up will be narrowed to those major aquaculture wastes from feed. Generally, wastes from aquaculture can be classified into solid wastes and dissolved wastes.

2.6.1 Solid wastes

Solid wastes are primarily derived from the uneaten feed and fecal droppings of cultured fish (Galasso *et al.*, 2017). They occasionally include those fish that do not survive the culture process. Solid wastes can be further classified as suspended and settled solids. The suspended solids are fine particles and remained suspended in the water, except when a method of coagulation or sedimentation is employed, and are the most difficult type of solids to remove

from culture systems (Zhang *et al.*, 2018) The settled solids are larger particles that settle within a short period of time and can be easily removed from the culture column. Solid wastes are regarded to be very dangerous because they can clog the fish gills and lead to death, especially in the case of large settled particles (Dauda *et al.*, 2019). If left for a long time and allowed to decompose, these wastes lead to increases in both the total suspended and total dissolved solids. They may also increase the nitrogenous compounds and stress the cultured fish (Dauda *et al.*, 2019). If solid wastes in aquaculture remain within the culture system, their aerobic bacterial activity will increase the chemical oxygen demand and biochemical oxygen demand and depletes oxygen within the culture medium.

2.6.2 Dissolved wastes

Dissolved wastes are products of food metabolism in fish or decomposed, uneaten feed. In dissolved wastes, the two major components of concern are nitrogen (N) and phosphorus (P) products. These two elements constitute important components of protein, which is the main component of fish feed (Montoneri, 2017). Fish, irrespective of species, require a high dietary crude protein ranging from 25 to 50%. The high protein fish feeds contain high amounts of nitrogen and phosphorus, yet less than 50% of these potential water pollutants (nitrogen and phosphorus) are retained in the body of the fish. Hence, a large percentage is transferred into the culture water, where it becomes a nuisance, and, when finally released, has a lot of environmental impacts. These nutrients, when released into water at high concentrations, can harm fish and other inhabitants of aquatic ecosystem. They can also lead to increase in both dissolved and total suspended solids, as well as water turbidity it is possible that these dissolved nutrients have little or no significant effect on the cultured fish, depending on the concentrations. However, releasing of culture water of poor quality may

have a significant impact on the aquatic organisms in the receiving water bodies. It is possible that these dissolved nutrients have little or no significant effect on the cultured fish, depending on the concentrations (Dauda *et al.*, 2019). However, releasing of culture water of poor quality may have a significant impact on the aquatic organisms in the receiving water bodies when the concentration is high, it results to eutrophication of the receiving water bodies.

2.7. Water Quality Parameters

Water quality refers to the chemical, physical, biological, and radiological characteristics of water (Papagiannis *et al.*, 2018 ; Krenkel, 2012). It is a measure of the condition of water relative to the requirements of one or more biotic species and/or to any human need or purpose. It is most frequently used by reference to a set of standards against which compliance can be assessed. The most common standards used to assess water quality relate to health of ecosystems, safety of human contact and drinking water.

2.7.1 Chemical Oxygen Demand

Chemical Oxygen Demand (COD) is an indicative measure of the amount of oxygen that can be consumed by reactions in a measured solution. It is commonly expressed in mass of oxygen consumed over volume of solution, which in SI units is milligrams per liter (mg/L). A COD test can be used to easily quantify the amount of organics in water. The most common application of COD is in quantifying the amount of oxidizable pollutants found in surface water (lakes and rivers) or waste water (Gogoi *et al.,* 2018). COD is useful in terms of water quality by providing a metric to determine the effect an effluent will have on the receiving body, much like biochemical oxygen demand (BOD). Many governments impose strict regulations regarding the maximum chemical oxygen demand allowed in wastewater before it can be returned to the environment. For example, in Switzerland, a maximum oxygen demand between 200 and 1000mg/L must be reached before wastewater or industrial water can be returned to the environment (Alisawi, 2020;Sawyer *et al.*, 2003).

2.7.2 Biochemical oxygen demand

Biochemical Oxygen Demand BOD, is the amount of dissolved oxygen needed (demanded) by aerobic biological organisms to break down organic material present in a given water sample at certain temperature over a specific time period. The BOD value is most commonly expressed in milligrams of oxygen consumed per liter of sample during 5days of incubation at 20°C and is often used as a surrogate of the degree of organic pollution of water (Prazeres *et al.*, 2019; Sawyer *et al.*, 2003). BOD can be used as a gauge of the effectiveness of wastewater treatment plants. It is listed as a conventional pollutant in the U.S. Clean Water Act. BOD is similar in function to COD in that both measure the amount of organic compounds in water. However, COD is less specific, since it measures everything that can be chemically oxidized, rather than just levels of biodegradable organic matter (Di Fraia *et al.*, 2018). BOD could have significant impacts on fishes, food security and livelihoods, severely affecting poor rural communities that rely on freshwater fisheries. Severe organic pollution already affects around one seventh of all river stretches in Africa, Asia and Latin America and has been steadily increasing for years (UNEP, 2016).

2.7.3 Turbidity

Turbidity is a measure of the cloudiness/clarity of water. Cloudiness is caused by suspended solids mainly soil particles (sand, silt, clay), microscopic plants and animals that are suspended in the water column. Moderately low levels of turbidity may indicate a healthy, well-functioning ecosystem, with moderate amounts of microscopic plants and animals present to fuel the food chain. However, higher levels of turbidity pose several problems for stream systems (Bajpai *et al.*, 2019). Higher turbidity levels are often associated with higher levels of viruses, parasites and some bacteria because they can sometimes attach themselves

to the dirt in the water. Therefore, we must be cautious of turbid water as it usually has more pathogens, so drinking it increases chances of becoming sick. Turbidity blocks out the light needed by submerged aquatic vegetation. It also can raise surface water temperatures above normal because suspended particles near the surface facilitate the absorption of heat from sunlight (Shirke *et al* ., 2016). The increase in turbidity will severely effect aquatic metabolism thus will affect the fertility and fish size in the water ecosystem (Wang *et al.*, 2019).

2.7.4 Hydrogen ion concentration (pH)

Hydrogen ion concentration (pH) is a measure of acidity of a solution, commonly expressed as the negative logarithm of the hydrogen concentration.

$$pH = -\log_{10}[H^+]$$

Determining the value of physical and chemical properties of water such as pH is very important as it reflects the water quality of the area. (Rakotondrabe *et al.,* 2018; Ferreira *et al.,* 2011). The pH scale is represented as ranging from 0-14. pH 0-6 show that the solution is acid, pH 7 the solution is neutral and for pH 8-14 the solution is in base condition. Acid condition increase when pH values decrease and alkaline condition increase when the pH values increase. The natural water bodies pH influence chemical and biological reaction adjust the metal ions solubility and could influence biological aquatic life. For instance, the fish species viability could not survive in waters with pH below of 5.5 (Zamora-Ledezma *et al.,* 2021). The reduced rate of photosynthetic activity, the assimilation of carbon dioxide and bicarbonates which are ultimately responsible for increase in pH, the low oxygen values coincided with high temperature during the summer month (Yadav *et al.,* 2016).

2.7.5 Dissolved oxygen (DO)

Dissolved oxygen (DO) describe the concentration of molecular oxygen in the water and it dependents on the temperature of the water and the biological demand of the system. DO is supplied to water through several method; direct diffusion of oxygen from the atmosphere, wind and wave action; and photosynthesis. It is used in aerobic decomposition of organic matter, respiration of aquatic organism and chemical oxidation of mineral (Mader *et al.*, 2017). As DO is used by many organisms in the water, it tends to change rapidly. The quantity of oxygen that the water can hold depends on the temperature, salinity and pressure of the water. Gas solubility increases with decreasing salinity. Fresh water holds more oxygen than saltwater (vanVliet *et al.*, 2021). Gas solubility decreases as pressure decreases. The amount of oxygen absorbed in water decreases as altitude increases because of the decrease in relative pressure. Levels of dissolved oxygen vary depending on factors including water temperature, time of day, season, depth, altitude, and rate of flow. Water at higher temperatures and altitudes will have less dissolved oxygen. Dissolved oxygen reaches its peak during the day. At night, it decreases as photosynthesis has stopped (Vijay *et al.*, 2016)

2.7.6 Temperature

Temperature refers to degree of hotness or coldness and it can be measured in degree Celsius. Water temperature needs to be monitored regularly as outside tolerable temperature range, disease and stress will become more prevalent. Among the consequences of temperature changes are; photosynthetic activity, diffusion rate or gases, amount of oxygen that can be dissolved (Almahdi, 2017). The aesthetic objective for temperature of less than or equal to 15 degrees Celsius is adopted from the 'Guidelines for Canadian Drinking Water', which has been accepted by the Ministry of Health Services for application in British Columbia.

Objectives are derived from criteria by considering the local water quality, water uses, water movement, waste discharges, and socio-economic factors. Temperature is important because of its influence on water chemistry. The rate of chemical reactions generally increases at higher temperature (Xu *et al.*, 2018). Water, particularly groundwater, with higher temperatures can dissolve more minerals from the rocks. Therefore, it will have a higher electrical conductivity. Temperature exerts a major influence on biological activity and growth. Temperature governs the kinds of organisms that can live in rivers and lakes (Cheo, 2016)

2.7.7 Electrical conductivity

Electrical conductivity is the ability of any medium, water in this case, to carry an electric current. The presence of dissolved solids such as calcium, chloride, and magnesium in water samples carries the electric current through water. Conductivity does not have direct impact on human health. It is determined for several purposes such as determination of mineralization rate (existence of minerals such as potassium, calcium, and sodium) and estimating the amount of chemical reagents used to treat this water(Siddiqui and Pandey 2019). High conductivity may lead to lowering the aesthetic value of the water by giving mineral taste to the water. For the industrial and agricultural activity, conductivity of water is critical to monitor. Water with high conductivity may cause corrosion of metal surface of equipment such as boiler. It is also applicable to home appliances such as water heater system and faucets. Food-plant and habitat-forming plant species are also eliminated by excessive conductivity (Nassehinia *et al.*, 2020).

2.7.8 Heavy metals analysis

The presence of heavy metals in drinking water higher than a certain concentration can cause detrimental impacts on human health. Therefore the determination of heavy metals in drinking water is an important parameter, and most of the studies on fish pond wastewater quality involved investigation of heavy metals. Some heavy metals such as Cu, Zn, Mg, Fe, Cd, Pb, Mn, Cr, As, Hg, Sn and Cd occurs naturally in rocks and soils and enters water when there is contact with soft groundwater or surface water. Moreover, it may be introduced by paints, pigments, plastic stabilizers, mining and smelting operations, and other industrial operations (Solgi *et al.*, 2020).Some of the effect of poisoning by heavy metal to the fish are; the body surface of the fish covered with mucus, the respiratory epithelium of the gills damaged and the fish die with symptoms of suffocation. Some affect maturation, hatchability and development of larvae in rainbow trout (Demeke and Tassew 2016).

Heavy metals have tendency to bio-accumulate which entails an increase in the amount/concentration of a mineral or substance in a living organism over time due to the bodies inability to remove such a substance (Jamshaid *et al.*, 2017).Heavy metals are known to have rather harmful effects on the human body such as inhibited or reduced growth, cancerous cell growth, damage of body organs, damage of the nervous system, and in cases of extreme level of exposure may result in loss of life (death).Moreover, the cardiovascular diseases, kidney-related problems, neurocognitive diseases, and cancer (Ayangbenro and Babalola 2017).

2.8 Silver Nanoparticles

Nanoparticles of silver are of size between 1 nm and 100 nm, which is frequently described as being 'silver' some are composed of a large percentage of silver oxide due to their large ratio of surface-to-bulk silver atoms. Silver (Ag) is a transition metal element having atomic

number 47 and atomic mass 107.87 g/mol. The medicinal uses of silver have been documented since 1000 B.C. Silver nanoparticles possess an effective anti-bacterial activity and they are widely recognized as being effective because of their enormous high surface area. For a long time silver has been known to have a disinfecting effect and has found applications in many traditional medicines and culinary items (Dixit and Tripathi 2019); (Shirley *et al.*, 2010). Silver nano particles are spherical or flake-like high surface area metal particles having high antibacterial activity. Numerous shapes of nanoparticles can be constructed depending on the application at hand. Commonly used are spherical silver nanoparticles but diamond, octagonal and thin sheets are also popular (Zhang *et al.*, 2016). Silver nanoparticles (AgNPs) are increasingly used in various fields, including medical, food, health care, consumer, and industrial purposes, due to their unique physical and chemical properties. Which include optical, electrical, and thermal, high electrical conductivity and biological properties (Gurunathan *et al.*, 2015). Due to their peculiar properties, they have been used for several applications, including as antibacterial agents, in industrial, household, and healthcare-related products, in consumer products, medical device coatings, optical sensors, and cosmetics, in the pharmaceutical industry, the food industry, in diagnostics, drug delivery and anticancer agents (Chernousova and Epple 2013).

2.8.1 Methods of Synthesis of silver nanoparticle

2.8.1.1 *Wet chemistry*

The most common methods for nanoparticle synthesis fall under the category of wet chemistry, or the nucleation of particles within a solution. This nucleation occurs when a silver ion complex, usually $AgNO_3$ or $AgClO_4$, is reduced to colloidal silver in the presence of a reducing agent (Rasheed *et al.*, 2018). When the concentration increases enough,

dissolved metallic silver ions bind together to form a stable surface. The surface is energetically unfavorable when the cluster is small, because the energy gained by decreasing the concentration of dissolved particles is not as high as the energy lost from creating a new surface (Polte, 2015). When the cluster reaches a certain size, known as the critical radius, it becomes energetically favorable, and thus stable enough to continue to grow. This nucleus then remains in the system and grows as more silver atoms diffuse through the solution and attach to the surface (Cobos *et al.*, 2020; Perala and Kumar 2013). When the dissolved concentration of atomic silver decreases enough, it is no longer possible for enough atoms to bind together to form a stable nucleus. At this nucleation threshold, new nanoparticles stop being formed, and the remaining dissolved silver is absorbed by diffusion into the growing nanoparticles in the solution.

As the particles grow, other molecules in the solution diffuse and attach to the surface. This process stabilizes the surface energy of the particle and blocks new silver ions from reaching the surface. The attachment of these capping/stabilizing agents slows and eventually stops the growth of the particle. The most common capping ligands are tri sodium citrate and polyvinyl pyrolidone (PVP), but many others are also used in varying conditions to synthesize particles with particular sizes, shapes, and surface properties (Lounsbury *et al.*, 2016).

2.8.1.2 *Monosaccharide reduction*

There are many ways silver nanoparticles can be synthesized; one method is through monosaccharide. This includes glucose, fructose, maltose maltodextrin but not sucrose. It is also a simple method to reduce silver ions back to silver nanoparticles as it usually involves a one-step process (Fetouh *et al.*, 2020; Iravani *et al.*, 2014). Another method of silver

nanoparticle synthesis includes the use of reducing sugars with alkali starch and silver nitrate. The reducing sugars have free aldehyde and ketone groups, which enable them to be oxidized into gluconate (Olsson *et al.*, 2020).The monosaccharide must have a free ketone group because in order to act as a reducing agent it first undergoes tautomerization. In addition, if the aldehydes are bound, it will be stuck in cyclic form and cannot act as a reducing agent. For example, glucose has an aldehyde functional group that is able to reduce silver cations to silver atoms and is then oxidized to gluconic acid (U.S. National Institute of Standards and technology). The reaction for the sugars to be oxidized occurs in aqueous solutions.

2.8.1.3 *Citrate Reduction*

An early, and very common, method for synthesizing silver nanoparticles is citrate reduction. This method was first recorded by M. C. Lea, who successfully produced a citrate-stabilized silver colloid in 1889 (Talaveraz *et al.*, 2019; Gottschalk and Nowack 2011) Citrate reduction involves the reduction of a silver source particle, usually $AgNO_3$ or $AgClO_4$, to colloidal silver using trisodium citrate, $Na_3C_6H_5O_7$. The synthesis is usually performed at an elevated temperature (~100 °C) to maximize the monodispersity (uniformity in both size and shape) of the particle. In this method, the citrate ion traditionally acts as both the reducing agent and the capping ligand, making it a useful process for AgNPs production due to its relative ease and short reaction time. However the silver particles formed may exhibit broad size distributions and form several different particle geometries simultaneously (Oprica *et al*., 2020). The addition of stronger reducing agents to the reaction is often used to synthesize particles of a more uniform size and shape.

2.8.1.4 *Polyol process*

The polyol process is a particularly useful method because it yields a high degree of control over both the size and geometry of the resulting nanoparticles. In general, the polyol synthesis begins with the heating of a polyol compound such as ethylene glycol, 1,5-pentanediol, or 1,2-propylene glycol (Shao *et al.*, 2015). Ag^{+} species and a capping agent are added (although the polyol itself is also often the capping agent). The Ag^{+} species is then reduced by the polyol to colloidal nanoparticles. The polyol process is highly sensitive to reaction conditions such as temperature, chemical environment, and concentration of substrates. Therefore, by changing these variables, various sizes and geometries can be selected for such as quasi-spheres, pyramids, spheres, and wires (Khodashenas and Ghorbani 2019; Rycenga *et al.*, 2011).

2.8.1.5 *Biological synthesis*

The biological synthesis of nanoparticles has provided a means for improved techniques compared to the traditional methods that call for the use of harmful reducing agents like sodium borohydride. Many of these methods could improve their environmental footprint by replacing these relatively strong reducing agents. (Bang *et al.*, 2019; Shankar *et al.*, 2003).In most of the cases, the silver nanoparticles formed are highly unstable and necessitate the addition of a separate capping agent which renders it unstability. In contrast, the green synthesis of silver nanoparticles gained a lot of attention owing to the instinctive features such as usage of natural resources, rapidness, eco-friendliness and benignancy. These appealing features are essential in medical applications. The other advantages of green synthesis include well-defined and controlled size of the nanoparticles. They are devoid of contaminants and the process is easy to scale-up (Selvaraj *et al.*, 2019). One of the green methods of synthesis of nanoparticles is the utilization of various plants and their parts. The

various biomolecules present in the plant extract such as enzymes, proteins, flavonoids, terpenoids and cofactors act as both reducing and capping agents (Bagherzade *et al.*, 2017). The plant-mediated synthesis of nanoparticles is relatively fast as there is no need of maintaining specific media and culture conditions, unlike microbial synthesis.

2.8.1.6 *Nanoparticles synthesis approach*

There are two general approaches to the synthesis of nanomaterials and the fabrication of nanostructures: Bottom up and top down approach (Obaid *et al.*, 2017). Bottom-up approach include the miniaturization of materials components (up to atomic level) with further self assembly process leading to the formation of nanostructures. During self-assembly the physical forces operating at nanoscale are used to combine basic units into larger stable structures. Typical examples are quantum dot formation during epitaxial growth and formation of nanoparticles from colloidal dispersion. Top-down approach use larger (macroscopic) initial structures, which can be externally-controlled in the processing of nanostructures. Typical examples are etching through the mask, ball milling, and application of severe plastic deformation (Soni *et al.*, 2018). Nanoparticle synthesis can be done by different methods like physical, chemical and green methods (Kalantari *et al.*, 2019;Wei *et al.*, 2015).

The physical methods include: laser ablation, lithography and high-energy irradiation. The physical method involves the use of costly equipment, high temperature and pressure, large space area for setting up of machines (Rajkumar *et al.*, 2020). In the chemical approach, chemical reduction, electrochemistry, and photochemical reduction are the most common methods for synthesis of nanoparticles. The chemical method involves the use of toxic chemicals which can be hazardous to the environment (Soni *et al.*, 2018). Moreover the

toxicity of the chemicals used in physical and chemical methods make it unsafe for use in medical field. As compared to conventional methods, biological methods are considered safe and ecologically sound for the nanomaterial fabrication. Therefore an environment and eco-friendly approach for synthesis of nanoparticles using microorganisms and different plants commonly referred to as Green Approach is the most researched area for synthesis of nanoparticles holds immense potential.

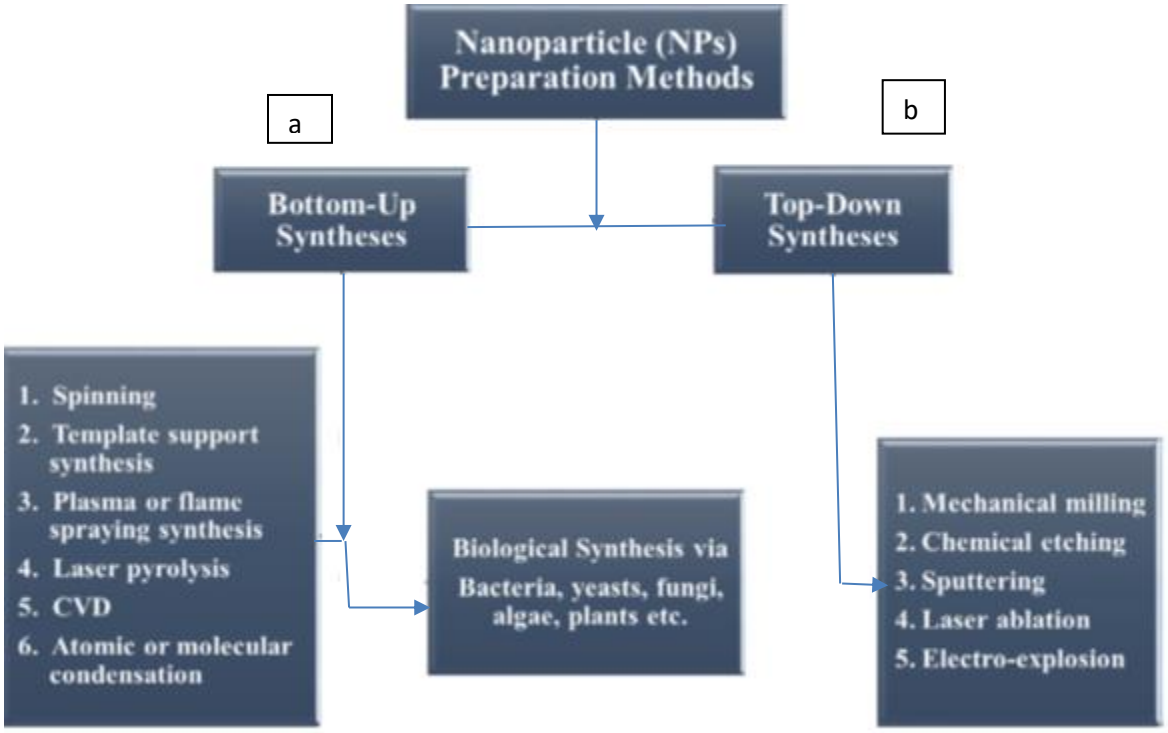

Figure 2.1: Typical synthetic methods for NPs for the (a) bottom-up and (b) top-down approaches. (Barua *et al.*, 2017)

The green biosynthesis of nanoparticles can be achieved by selecting an environmentally acceptable solvent with eco-friendly reducing and stabilizing agents. These biological systems can transform inorganic metal ions into metal nanoparticles via the reductive capacities of the proteins and metabolites present in these organisms (Makarov *et al.*, 2014).

2.9 Carbon Nanotube

Carbon is an astonishing element, not only due to the reason that it is the element necessary for all life processes, but also because of the fact that it can occur in various allotropic forms (Mabena *et al.*, 2011). Conventionally, carbon materials consist of graphite blocks, the category under which activated carbons, carbon blacks, and diamonds are present. The recently developed materials of carbon include nanotextured and nanosized carbons. Nanotextured carbons cover a large variety of carbon structures, from carbon fibers, pyrolytic carbons, or glass-like carbons, to diamond-like carbon materials. The nanosized carbons (or nanocarbons) comprise fullerenes, grapheme and CNTs (Kharlamova and Eder 2020). Radushkevish and Lukyanovich first detected and described CNTs in 1952, later the SWCNTs were observed by Oberin in 1976(Rahman *et al.*, 2019). The discovery of CNTs in recent history is ascribed to Iijima, who for the first time, described multi-walled carbon nanotubes (MWCNTs) in carbon soot obtained during C_{60} carbon molecule fabrication in an arc evaporation test. CNT is a beehive-shaped tube, having unique 1D nanostructures with carbon atoms belonging to sp^2 hybridization. They have a thickness of approximately 1/50,000th of human hair (Burakova *et al.*, 2018); (Dresselhaus *et al.*, 1995). CNTs exist in three unique geometries, which are armchair, zig-zag, and chiral (Figure 2.2). The mechanical, electrical, optical, and other properties of CNTs are determined by the chirality. It has been reported that the electrical properties of CNTs are influenced by the chiral vector and corresponding pairs of integers. Depending on rolling up of the grapheme sheets, CNTs can be either narrow-band semiconductors or metals. Thus, some nanotubes behave more like silicon, while others show higher conductivities than that of copper (Rahman *et al.*, 2019). CNTs have a high surface area, high tensile strength and low density, CNTs also have good

mechanical, electrical, vibrational and thermal properties. MWCNTs have a very high structural rigidity and speculated their possible use in composite materials with improved mechanical properties (Ramoraswi 2014)

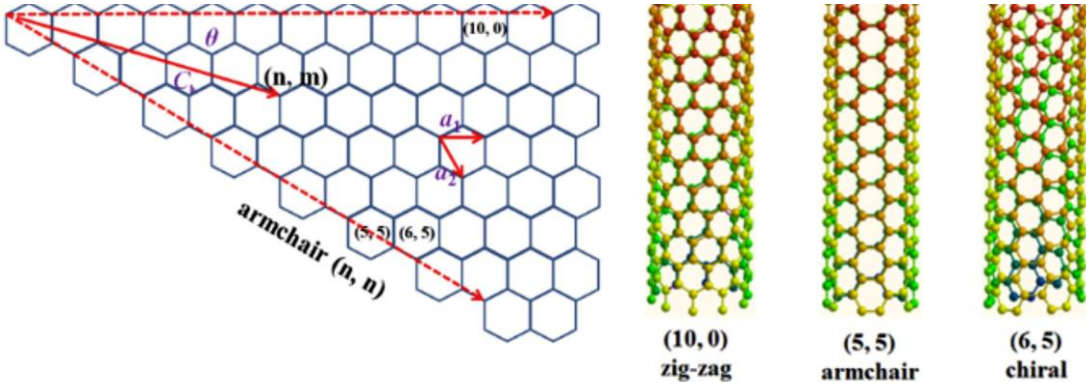

Figure 2.2: Geometries of CNTs. reproduced with permission from (Kim *et al.* 2016)

Taking into account the number of layers of CNTs, they may be single-walled carbon nanotube

(SWCNTs) or multi-walled carbon nanotubes (MCWNTs) (Figure 2.2). Most SWCNTs have a diameter extending from 0.4 to >3 nm, whereas the length can extend to a few millions times the diameter. Conceptualizing the wrapping of a layer of graphene into the shape of a tube gives the structure of SWCNTs, while multiple rolled layers (concentric tubes) of graphene constitute MWNTs. In MWCNTs, the interlayer space is approximately equal to the space between the graphene sheets in graphite, which is 3.4 Å. The diameter ranges from 1.4 to at least 100 nm for MWCNTs (Tang *et al*., 2001).

Figure 2.3: (**a**) Structure of SWCNT (**b**) MWCNT. Reproduced with permission from (Al Moustafa *et al.*, 2016)

2.9.1 Synthesis of carbon nanotubes

Carbon nanotubes are broadly synthesized via three major methods: arc discharge, laser ablation, and chemical vapour deposition. Although scientist are investigating further on cost effective methods to synthesis these structures, however chemical vapour deposition is deemed the best technique for sizeable scale synthesis of carbon nanotubes. (Obasogie *et al.*, 2018)

2.9.1.1 *Arc discharge method*

The arc discharge method is a well-known method for the formation of CNTs. Figure 2.3 illustrates the 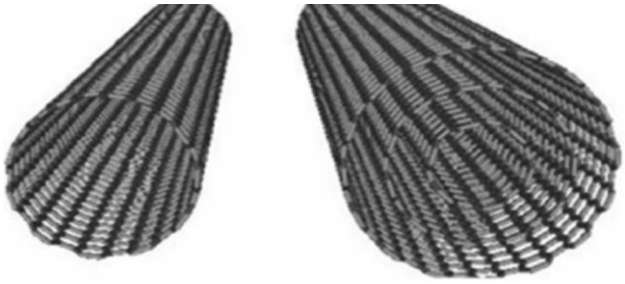 schematic diagram of Arc discharge method. In this method, a buffer gas such as helium is introduced in a chamber containing a cathode, a graphite anode, and vaporized carbon molecules. The chamber also contains a small amount of metal catalysts such as nickel, cobalt or iron. Under applied pressure, the chamber is heated to 4000 K, and a direct current (DC) is passed through the sample. In the

progression of this technique, nearly half of the vaporized carbon solidifies on the tip of cathode in the form of a "hard cylindrical deposit". Condensation of the remaining carbon occurs, forming "cathode soot" on the cathode, and "chamber soot", which is present all over the walls of the chamber (Figure 2.4). The chamber and the cathode soot yield either SWCNTs or MWCNTs. The selection of the inert gas and the added metallic catalyst decides whether the resultant CNTs are SWCNTs or MWCNTs (Eatemadi *et al.*, 2014) For the production of SWCNTs, catalyst precursors are necessary for growth in the arc discharge, while the anode is immersed with a metal catalyst, such as Fe, Co, Ni, Y, or Mo (Hirlekar *et al.*, 2009) Studies have revealed that SWCNTs with a diameter of 1.4 nm can be synthesized by Ni-Y graphite mixtures, giving yields of <90 %(Dresselhaus *et al.*, 1998). The advantage of this method is the high yield of nanotubes. However, the little control over the orientation of the nanotubes is the key disadvantage that ultimately affect their activity. Furthermore, due to the involvement of a catalyst in the production of SWCNTs, the products need to be purified (Eatemadi *et al.*, 2014).

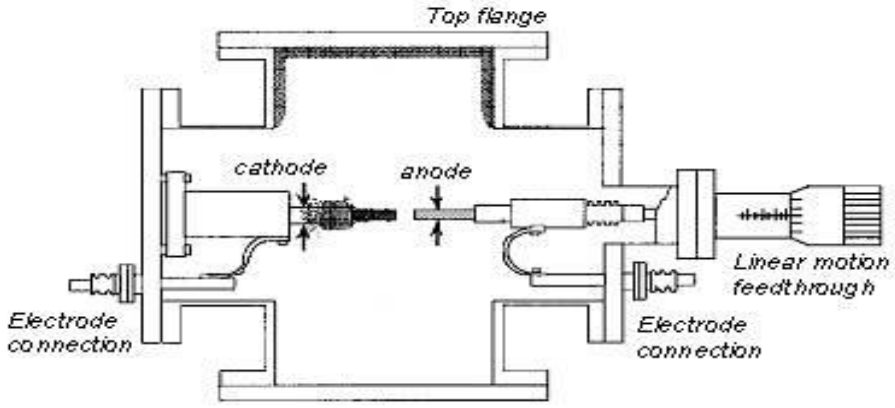

Figure 2.4: Schematic diagram showing the Arc discharge apparatus (Rahman *et al.*, 2019)

2.9.1.2 ***Laser ablation method***

The laser ablation technique and the arc discharge method are similar in principles and mechanisms; however, they are different by the input energy sources. In the laser ablation method, the required energy is provided by a laser. Figure 2.5 shows the schematic structure of an experimental setup. A tube made up of a quartz-containing graphite block is heated in a furnace at 1200 ^{0}C, using a high-power laser in the presence of metal particles as catalysts (Eatemadi *et al.*, 2014). A stream of argon is the vaporized carbon, which condenses downstream onto the cooler walls of the quartz. SWCNTs and metallic particles are present in this condensation. It has been reported in literature that, the laser power can influence the diameter of the CNTs. The diameter of the tube becomes thinner as the laser pulse power is increased (Hirlekar *et al.*, 2009).The SWCNTs produced by this method are of high purity and quality. The position where the carbon atom starts to condense should be set up as a curved sheet of graphene with a metal catalyst atom nearby for the proper fabrication of the condensed nanotubes. When carbon atoms begin to assign for the formation of rings, the proper electronegative properties of the metallic atom prevent the open edge from closing (Eatemadi *et al.*, 2014). The main advantages of this technique include relatively low metallic impurities, and a relatively high yield, due to the vaporization tendency of the metallic atoms from the end of the tube, once it is closed. The key drawback of this technique is that the synthesized nanotubes may not be regularly straight, and have some degree of branching. Furthermore, this procedure involves. Fabrication of the condensed nanotubes graphite rods of high purity, and requires high powers of lasers, and the amount of CNTs produced are not as great as in the arc-discharge technique.

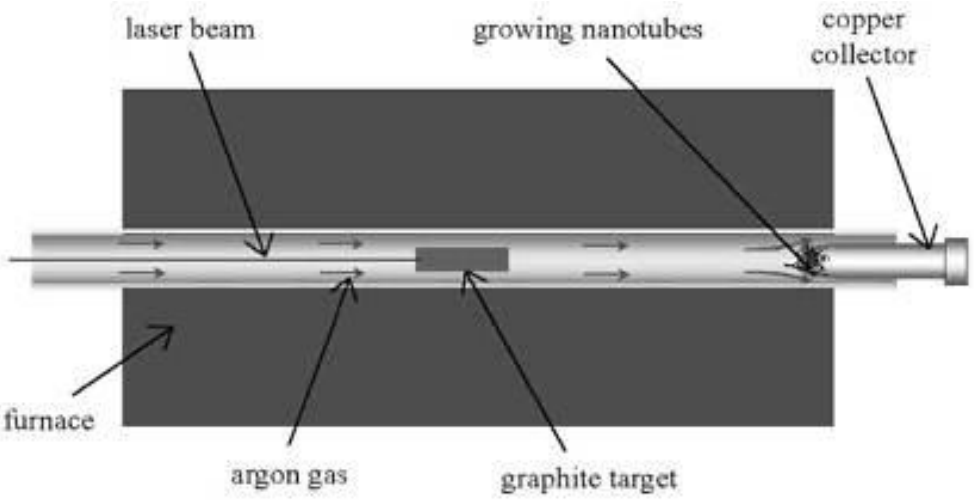

Figure 2.5: laser ablation method for producing CNTs (Rahman *et al.*, 2019)

2.9.1.3 *Catalytic chemical vapor deposition (CCVD) method*

The catalytic chemical vapor deposition (CCVD) system is a proficient method which can be utilized to scale up the generation of CNTs and is the most generally utilized technique for fiber, filament and nanotubes synthesis (Rahman *et al.*, 2019). The experiment is mostly performed at atmospheric pressure in a flow furnace. The modality of the furnace is of two types. Horizontal configuration, and vertical configuration. The application of the horizontal furnace is dominant. The catalyst here is implanted in a quartz or ceramic boat, which is planted into a quartz tube. The reaction mixture consists of an inert hydrocarbon, and a source of hydrocarbon. This mixture is passed through a catalyst bed at temperatures in a range of 500 ^{0}C to 1100 ^{0}C. Afterwards, the temperature of the system is cooled to room temperature. The vertical configuration of the furnace is typically implemented in the sustained mass production of carbon nanotubes/fibers. The carbon source and catalyst, are both introduced at the topmost part of the furnace. The resultant filaments build up

throughout the flight, and then accumulated at the lower portion of the chamber. Ultrafine metal catalyst particles are inaugurated either directly to the reactor, or are manufactured in situ, utilizing precursors like metallocenes (Rahman *et al.*, 2019). Commonly used metal catalysts are Ni, Co, Fe, or their combinations, as Ni-Y, Fe-Ni, Co-Ni, (Eatemadi *et al.*, 2014; Zhang *et al.*, 2016) synthesized MWCNTs with diameter of 40–60 nm by the catalytic decomposition of methane at a temperature of about 680 ^{0}C for 120 min, using catalyst nickel oxide–silica binary aerogels (Rahman *et al.*, 2019).

The advantages of CVD method it has easy process of production, it produces long tube length and the diameter of the CNTs produced can be well controlled, also the production can be scaled up easily, (Aliyu *et al.*, 2017). It is a simple and economic technique for synthesizing CNTs at low and ambient temperature, it also has a better control on the growth parameters and CNTs produced of relatively high purity, high size control and few defects. (Poulsen *et al.*, 2015)

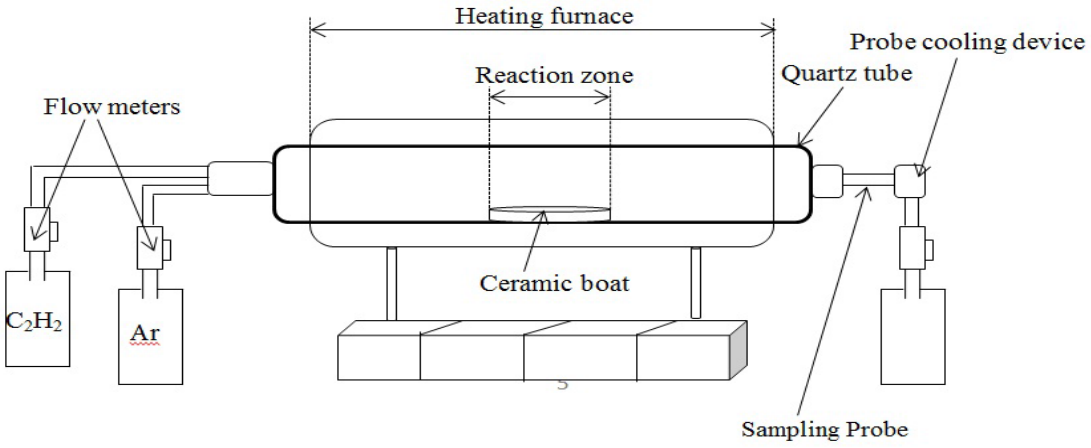

Figure 2.6: Schematic diagram of the Chemical Catalytic Vapour Depositor(Kumar and Ando 2010)

2.9.1.4. *Flame synthesis method*

Flames offer the potential for the fabrication of CNTs in large amounts at considerably lower cost, as compared to the existing methods. It is capable of producing nanotubes of carbon on required surfaces, and specifically in a controllable way. There are three essential constituents that are necessary for the production of CNTs. These are: metallic catalyst particles, a heat source, and a source of carbon. The catalytic precursors, in the flame synthesis method are usually introduced into the flame system, where they undergo nucleation and finally condense into solid spherical metallic nanoparticles. Flame parameters can also be applied to obtain suitable flame conditions, which would enable the fabrication of ideal sizes of catalyst particles for the growth and inception of CNTs. The catalyst properties and alteration of the flame parameters can remarkably influence the heat and carbon source, the activation and deactivation of catalyst particles, and the formation of catalysts, as well as the morphology of the final synthesized products (Cao *et al.*, 2020) As a consequence, several flame patterns, including premixed, partially premixed, and inverse diffusion flames, have been used for the production of CNTs and Nano fibers (Liu *et al.*, 2015).

2.9.1.5. *Saline solution method*

Using a saline solution method for the production of CNTs, a stainless steel mesh or carbon paper is used as a substrate, which is submerged in a saline solution of a metal catalyst, preferably Co: Ni, in a 1:1 ratio, and a carbon containing a gas source such as ethylene is passed through the substrate. An electrical current is applied for heating the substrate. As a result, a reaction takes place between the gas and the catalyst to yield CNTs supported on the conductive substrate (Chinnappan *et al.*, 2016).

2.9.1.6 *Spray pyrolysis method*

Spray pyrolysis is a favorable technique for the production of CNTs on different surfaces. This method is a modified form of the CVD method. Using spray pyrolysis (or injection CVD) technique, high purity MWCNTs can be obtained by using different aromatic and aliphatic hydrocarbons and ferrocene as a catalyst precursor (Kumar *et al.*, 2020). In this technique, the system is well sealed to prevent leakages. The system uses a thermolyne single zone split tube furnace with a quartz tube. A vacuum tight assembly is built for the solution. Samples are placed on a quartz or stainless steel boat, which is about nine inches from the center of the tube furnace. Pure argon is introduced in the quartz tube reactor. The furnace is heated in the presence of argon flow (50 sccm). When the injector head reaches 170 ^{0}C, the argon flow rate is increased to 100 sccm, and the mixture of ferrocene dissolved in xylene is rapidly injected until the solution reaches the injector head. This results in the production of black CNTs powder, (Annu *et al.*, 2017).

2.10 Growth Mechanism of CCVD

Growth mechanisms of carbon nanotubes are still debated. Based on the reaction conditions and post deposition product analyses, several groups have proposed several possibilities which are often contradicting. Therefore no single CNT growth mechanism is well established till date. Nevertheless, widely-accepted most general mechanism can be outlined as follows. Hydrocarbon vapor when comes in contact with the “hot” metal nanoparticles, first decomposes into carbon and hydrogen species; hydrogen flies away and carbon gets dissolved into the metal. After reaching the carbon-solubility limit in the metal at that temperature, as-dissolved carbon precipitates out and crystallizes in the form of a cylindrical network having no dangling bonds and hence energetically stable. Hydrocarbon

decomposition (being an exothermic process) releases some heat to the metal's exposed zone, while carbon crystallization (being an endothermic process) absorbs some heat from the metal's precipitation zone.(Kumar and Ando 2010).

2.10.1 Tip-growth

In the other case, the catalyst–substrate interaction is strong (metal has an obtuse contact angle with the substrate), initial hydrocarbon decomposition and carbon diffusion take place similar to that in the tip-growth case, but the CNT precipitation fails to push the metal particle up; so the precipitation is compelled to emerge out from the metal's apex (farthest from the substrate, having minimum interaction with the substrate). First, carbon crystallizes out as a hemispherical dome (the most favorable closed-carbon network on a spherical nanoparticle) which then extends up in the form of seamless graphitic cylinder. Subsequent hydrocarbon deposition takes place on the lower peripheral surface of the metal, and as dissolved carbon diffuses upward. Thus CNT grows up with the catalyst particle rooted on its base; hence, this is known as "base-growth model (Baker *et al.*, 1975). Formation of single- or multi-wall CNT (SWCNT or MWCNT, respectively) is governed by the size of the catalyst particle. (Sinnott *et al.*, 1999) Broadly speaking, when the particle size is a few nm SWCNT is formed and particles of few tens nm wide favor MWCNT formation.

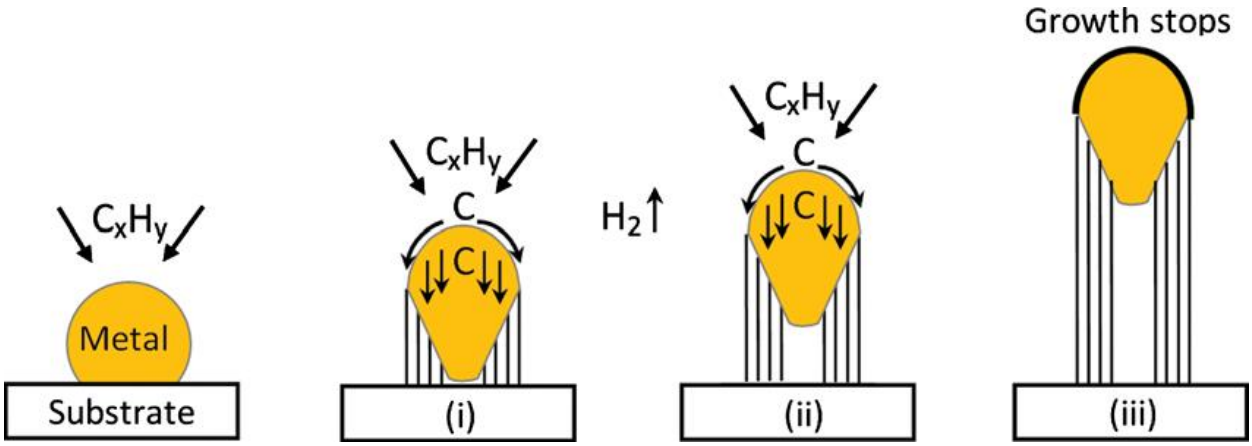

Figure 2.7 Tip Growth Mechanism of CNT (Baker *et al.*, 1975)

2.10.2 Base-growth

Now there are two general cases. (Figure 2.8) When the catalyst substrate- interaction is weak (metal has an acute contact angle with the substrate), hydrocarbon decomposes on the top surface of the metal, carbon diffuses down through the metal, and CNT precipitates out across the metal bottom, pushing the whole metal particle off the substrate (as depicted in step (i)). As long as the metal's top is open for fresh hydrocarbon decomposition (concentration gradient exists in the metal allowing carbon diffusion), CNT continues to grow longer and longer (ii). Once the metal is fully covered with excess carbon, its catalytic activity ceases and the CNT growth is stopped (iii). This is known as "tip-growth model.(Baker *et al.*, 1972).

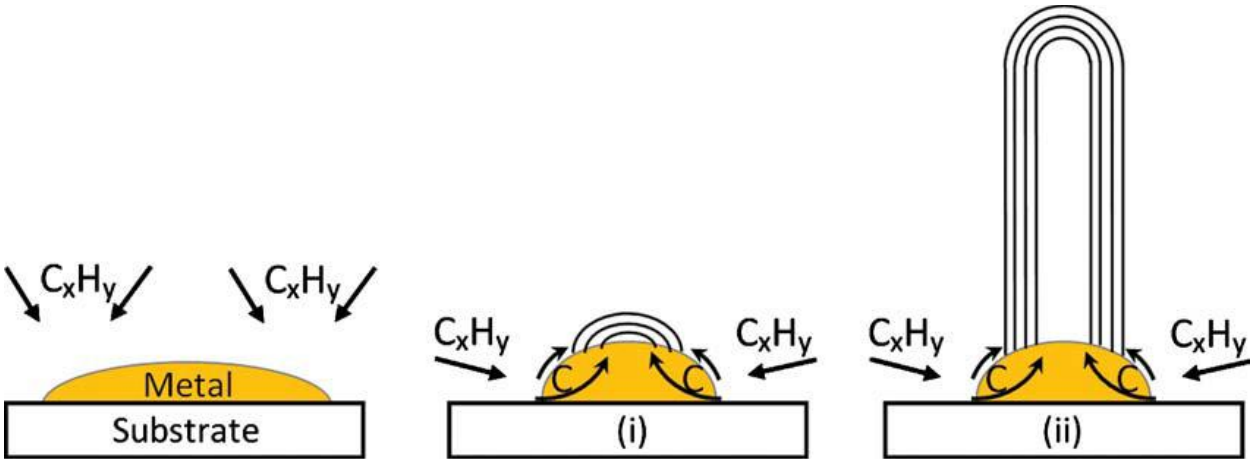

Figure 2.8: Base Growth Mechanism of CNT (Baker *et al.*, 1975)

2.11 Purification of CNTs

As-synthesized CNTs prepared by the above methods inevitably contain carbonaceous impurities and metal catalyst particles, and the amount of the impurities commonly increases with the decrease of CNT diameter. The fundamental problems that still exist are how to (1) obtain uniform dispersions of the carbon nanotubes in dispersing media or polymer solutions. (2) remove impurities, such as amorphous carbons and metallic catalysts and the impurities in unpurified carbon nanotubes severely reduce the mechanical or electrical properties the as-produced CNTs soot contains a lot of impurities. Up to now, all currently known production methods generate CNTs with impurities (Saifuddin *et al.*, 2013). Purification difficulties are considerable because CNTs are insoluble and, hence, liquid chromatography is limited thus, extensive research has been dedicated to the purification of carbon nanotubes in order to remove foreign nanoparticles that modify the physic chemical properties of carbon nanotubes.

2.11.1 Chemical purification

The most commonly used chemical purification involves the oxidation of as-synthesized CNTs in both wet and dry conditions. The wet condition generally refers to the oxidation using a solution of concentrated acids or strong oxidants; meanwhile the dry condition mainly refers to the oxidation by air, oxygen, or other gases at a controlled temperature. The key idea of this approach is a selective oxidative etching process, based on the fact that amorphous carbon and carbon particles can be eliminated more easily than CNTs due to their higher oxidation reaction rate than CNTs. The high oxidative activity demonstrated by the amorphous carbon is due to the presence of hanging bonds with high energy, which can be easily oxidized; meanwhile the higher reactivity of the carbon nanoparticles can be attributed to their big curvature and pentagonal carbon ring (Liu *et al.*, 2014)

2.11.1.1 *Gas phase oxidation*

In general, chemical oxidation includes gas phase oxidation (using air, O_2, Cl_2, H_2O, etc.), liquid phase oxidation (acid treatment and refluxing, etc.), and electrochemical oxidation. Tubes are heated at a controlled rate either in wet air or vacuum or other oxidizing agents for an extended time at about 330 ^{0}C.This is a good way to remove carbonaceous impurities. The disadvantages of this method are that it often opens the end of CNTs, cuts CNTs, damages surface structure and introduces oxygenated functional groups (–OH, –C=O, and–COOH) on CNTs. Metal particles cannot be directly removed, and further acid treatment is needed.(Yasunori *et al.*, 2002).

2.11.1.2 *Liquid Phase Oxidation*

Usually, the acid treatment will remove the metal catalyst and some fullerenes. Reflux in HNO_3, HCl, or other acid for period of time ranging from 4 to 48 hours. HNO_3 is the only acid that does not cause degradation to tubes (unless left in HNO_3 for extended time frames, usually >16 hours). the metal catalyst is solvated while the CNTs remain in suspended form.(Cao *et al.*, 2003).

2.11.1.3 *Electrochemical oxidation*

CNTs with fewer defects show higher electrochemical oxidation resistance than CNTs with more defects. Suitable for purifying CNT arrays without destroying their alignment. the CNTs electrode is immersed in 0.2 M HNO_3 solution or 0.2 M HCl (purging with N_2 for 20 min prior to use) and the potential was cycled between +1.00 and +2.00 V at a scan rate of 50 mV s−1.reases the specific area of nanotubes by cutting off the nanotube tips and by converting the surface property of nanotubes from the hydrophobic state to the hydrophilic state (Fang *et al.*, 2004).

2.11.2 Physical purification

To reduce the damage caused by direct oxidation or changing their natural surface properties Physical method makes it possible to achieve this methods such as sonication, filtration and have been used to purify CNTs.

2.11.2.1 *Filtration*

This technique is often used in conjunction with oxidation, the acid decomposition products are highly soluble in basic solution and CNTs are not and are separated using a basic solution of pH 11 and altered using 3–5 μm filter, often under vacuum. This removes nanospheres,

metal nanoparticles, polyatomic carbons, and fullerenes, without any noted negative effects (Saifuddin *et al.*, 2013)

2.11.2.2 *Sonication*

CNTs are suspended in distilled water, toluene, or acid solution and sonicated for 5–30 minutes.This separates tubes from attached particles, creating dispersion of nanotubes and other particles for better centrifugation the separation of the particles is highly dependable on the surfactant, solvent, and reagent used. The solvent influences the stability of the dispersed tubes in the system.(Yu *et al.*, 2007).

2.11.2.3 *Magnetic*

CNTs is suspended in soap or toluene and nanoparticle powder (ZrO_2, $NHCl_4$, $CaCo_3$, diamond) is added. This particles will attach to the CNTs and make them magnetic. The slurry is sonicated for 2 hour and subsequently the magnetic particles are trapped using permanent magnetic poles. This is then followed by chemical treatment. This removes catalyst materials and small inorganic particles. Few to no known negative effects.(Zambrano *et al.*, 2016).

2.11.2.4 *Microwave purification*

CNTs are sonicated, then diluted in HNO_3 (or other acid). Microwaved at 100–200 W, and microwave is ramped up to ∼200 ^{0}C over 30 min. Microwave is then held at temperature 200 ^{0}C for 30–90 minutes. This removes amorphous carbon, metals, and other nanoparticles, with no known negative effects.(Ma *et al.*, 2008).

2.12 Functionalization of Carbon Nanotubes

The carbon atoms in nanotubes are great at forming covalent bonds with many other types of atoms for several reasons: Carbon atoms have a natural capacity to form covalent bonds with many other elements because of a property called electronegativity. Electronegativity is a measure of how strongly an atom holds onto electrons orbiting about it. The electronegativity of carbon (2.5) is about in the middle of the range of electronegativity of various substances from potassium (0.8) to fluorine. Because carbon has electronegativity in the middle of the range, it can form stable covalent bonds with a large number of elements.

- All the carbon atoms in nanotubes are on the surface of the nanotube and therefore accessible to other atoms.
- The carbon atoms in nanotubes are bonded to only three other atoms, so they have the capability to bond to a fourth atom.

These factors make it relatively easy to covalently bond a variety of atoms or molecules to nanotubes, which changes the chemical properties of the nanotube. (This method is called Functionalization). Taking this bonding thing further, if the molecules attached to the carbon nanotubes also attach to carbon fibers, the functionalized carbon nanotubes can bond to the fibers in a composite, producing a stronger material (Varshney, 2014).

2.13 Properties of Carbon Nanotubes

Characteristics of carbon nanotubes comprise of density, lattice structure, electrical and mechanical likewise thermal conductivity depending upon its structural form. Amongst the important factors affecting their structure, are type and diameter of nanotubes. CNTs act like graphite due to wider diameters. A reduction in the diameter of the nanotubes will dictate the inherent properties relying more on its particular form. CNTs have high aspect ratio (length/diameter) and high surface area. CNTs possess high aspect ratio greater than

$1x10^3$:$1x10^0$. Furthermore, the density of CNTs with a value of 1.34 g/cm^3 is less than of Al of about 2.7g/cm^3. In addition, CNTs are virtually chemically inactive, thus no reaction with other materials is feasible (Aliyu *et al.*, 2017).CNTs have outstanding electronic, optical, thermal, chemical, and mechanical characteristics. The best known thermal conductor prior to CNT was diamond. But the thermal conductivity of CNTs is at least twice that of diamond. The extraordinary mechanical strength of the CNTs is due the sp^2 carbon-carbon bonding. The nanotubes exhibiting a high mechanical strength with a Young's modulus value of 1000 GPa, (approximately five times higher than that of steel), are considered the best for a variety of applications. CNTs can have a breaking strain or tensile strength of approximately 63 GPa, which is about 50 times greater, compared to that of the steel. CNTs have extraordinary electrical properties, due to their peculiar electronic structure and the 1D character of graphite. Their electrical resistance is extremely low, because resistance occurs when an electron in the crystal structure collides with some defect in the material through which it is passing, but electrons are not easily scattered in CNTs (Rahman *et al.*, 2019).

2.14 Some of the existing Wastewater Treatment Techniques

2.14.1 Coagulation flocculation sedimentation

Coagulation flocculation sedimentation is one of the most used methods, especially in the conventional treatment process. Active on suspended matter, colloidal type of very small size, their electrical charge give repulsion and prevent their aggregation. Adding in water electrolytic products such as aluminium sulphate, ferric sulphate, ferric chloride, giving hydrolysable metallic ions or organic hydrolysable polymers (polyelectrolyte) can eliminate the surface electrical charges of the colloids. This effect is named coagulation normally the colloids bring negative charges so the coagulants are usually inorganic or organic cationic

coagulants in water(Konnola and Joseph 2016). The metallic hydroxides and the organic polymers, besides giving the coagulation, can help the particle aggregation into flocks, thereby increasing the sedimentation. The combined action of coagulation, flocculation and settling is named clariflocculation. Settling needs stillness and flow velocity, so these three processes need different reactions tanks. This processes use mechanical separation among heterogeneous matters, while the dissolved matter is not well removed (clariflocculation can eliminate a part of it by absorption into the flocks). The dissolved matter can be better removed by biological or by other physical chemical processes (Ruben *et al.*, 2000). However, additional chemical load on the effluent (which normally increases salt concentration) increases the sludge production and leads to the uncompleted dye removal.

2. 14.1 Chlorination

Chlorine is used to destroy disease-causing organisms in water, an essential step in delivering safe drinking water and protecting public health. Chlorine is by far the most commonly used disinfectant in all regions of the world, and has helped to virtually eliminate waterborne diseases such as cholera, typhoid and dysentery. Chlorination is effective against many pathogenic bacteria, but at normal dosage rates it does not destroy all viruses, cysts, or worms (Daniels and Mesner 2010), chlorine kills microbes but also reacts with organic matter already in water to form toxic chemicals, the organochlorines. The organochlorine commonly found at the highest concentration is chloroform, which is carcinogenic (Gribble, 2003).

2.14.2 Ultraviolet light/lamps

Ultraviolet radiation has commonly been used to eradicate microorganisms in water. Mercury low pressure lamps generating 254 nm UV light are an effective means of disinfecting water.

The adsorption of UV light by the DNA and proteins in the microbial cell inactivates the microorganism. Most ultraviolet purification systems are combined with various forms of filtration. UV light is only capable of destroying microorganisms such as bacteria, viruses, fungi, algae, yeast, and acolytes like *Cryptosporidium* and *Giardia*. UV light generally has no impact on chlorine, volatile organic chemicals (VOCs), heavy metals, and other chemical contaminants (Arnold and Rainbow 1996).

A major disadvantage of UV filtration is that it does not leave dis-infection residuals that are needed to persist in maintaining clean water. UV-disinfected water may become re-contaminated if exposed to further bacterial contamination

2.14.3 Reverse osmosis

Reverse osmosis (RO) is a filtration method that removes many types of large molecules and ions from solutions by applying pressure to the solution when it is on one side of a selective membrane. The result is that the solute is retained on the pressurized side of the membrane and the pure solvent is allowed to pass to the other side. The membrane does not allow large molecules or ions through the pores, but allows smaller components of the solution to pass freely (Rananga 2013). Reverse osmosis, however, involves a diffusive mechanism so that separation efficiency is dependent on solute concentration, pressure, and water flux-rate. Reverse osmosis is most commonly known for its use in purification of sea water, by removing salt and other substances (Westerhoff *et al.,* 2009).

One of the disadvantages of reverse osmosis from a health perspective is that it de-mineralizes water. Trace minerals are important to human health since research has shown that drinking de-mineralized water on a regular basis caused digestive problems and

nutritional deficiencies. While reverse osmosis is effective for removing a variety of contaminants in water, it does not remove volatile organic chemicals, chlorine and chloramines, pharmaceuticals, and a host of other synthetic chemicals found in municipal water (Pomerantz *et al.*, 2006).

Water entering the reverse osmosis system should also be free of bacteria. While reverse osmosis systems do remove nearly all microorganisms, the risk of contamination through tiny leaks or deteriorating parts, prevents reverse osmosis systems from being used to actively remove bacteria (Uchymiak *et al.*, 2009)

2. 14.4 Nanotechnology in wastewater treatment

Using nanoparticles could chemically degrade pollutants instead of simply moving them somewhere else, including pollutants for which existing technologies are inefficient or cost prohibitive. suggested that nanotechnology offers more effective, efficient, durable, and affordable approaches to removing specific types of pollutants from water (Tiwari *et al.*, 2008).

Metal nanoparticles have been investigated extensively in recent years because of their size-dependent electronic and optical properties and the possibility of arranging them in micro- and nano-assemblies (Schmid and Chi 1998) Much effort has been devoted to the synthesis and characterisation of stable dispersions of nanoparticles made of silver, gold, and other noble metals (El-Sayed, 2001). The major focus will be to review the use of metal nanoparticles for the removal of contaminants such as organics, inorganic, heavy metals, and micro-organisms, in waste water. Metal nanoparticles have two key properties that make them particularly attractive as sorbents, they have much larger surface areas than bulk

particles and they can also be functionalised with various chemical groups to increase their affinity towards target compounds (Tiwari *et al.*, 2008).

Silver nanoparticles possess an effective anti-bacterial activity and they are widely recognised as being effective because of their enormous high surface area. For a long time silver has been known to have a disinfecting effect and has found applications in many traditional medicines and culinary items (Shrivastava *et al.*, 2007). Recently silver nanoparticles, as well as various silver-based compounds containing ionic silver (Ag^{+}) or metallic silver (Ag^{0}) exhibiting antimicrobial activity have been synthesized (Baker *et al.*, 2005) Antibacterial activity of the silver-containing materials can be used, for example, in medical applications in order to reduce infections Silver ions have been demonstrated to be useful and effective in bactericidal applications, but due to the unique properties of nanoparticles, nanotechnology now presents a reasonable alternative for the development of new bactericides. Metal particles in the nanometre size range exhibit physical properties that are different from both the ionic and the bulk materials. This makes them exhibit remarkable properties such as increased catalytic activity due to morphologies with highly active facets (Doraiswamy and Marks 1996)

2.15 Catalyst

A catalyst is described as a substance that increases the rate at which a chemical reaction approaches equilibrium without itself becoming permanently involved in the reaction. But the main role of catalyst in CNT growth is to decompose hydrocarbon molecules. The catalyst material is one of the most important key parameters, that determines the morphology, type (SWNT or MWNT), diameter and also growth mechanism in the production of CNTs. CNT formation is affected by method of catalyst preparation, the nature

and pore size of the support, the nature of the metal (Ahmed, 2016).Iron, Nickel, molybdenum, cobalt, copper and gold nanoparticles have played role as a catalyst either in purified metallic shape or as alloys. The advantageous roles of these metallic nanoparticles include high soluble carbon, carbon diffusion rates and elevated melting point temperature. The effect of time, temperature, mass of support and stirring speed are some the factors taken into consideration.(Roul *et al.*, 2017).

2.16. Adsorption

The adsorption process is a surface phenomenon in which the adsorbate is accumulated on the adsorbent surface. When a solution containing absorbable solute comes into contact with a solid with a highly porous surface structure, liquid–solid intermolecular forces of attraction cause some of the solute molecules from the solution to be concentrated or deposited on the solid surface (Gao *et al.*, 2012). In case of bulk materials, all the bonding requirements (ionic, covalent, or metallic) of the material constituent atoms are filled by other atoms in the material. However, the atoms on the surface of the adsorbent are not wholly surrounded by other adsorbent atoms, therefore they can attract adsorbates (Mahmoodian *et al.*, 2015).

The exact nature of the bonding depends on the details of the species involved, but the adsorption process is generally classified as physisorption (an adsorbate bound to the surface by weak van der Waals forces), chemisorption(an adsorbate tethered through covalent bonding (Tyagi) or due to electrostatic attraction (Semwal and Gupta 2017). Two substances are involved in the adsorption process, one is the solid or liquid on which the adsorption occurs, and it is called the adsorbent. The second substance that is absorbed is known as the adsorbate. The extent of adsorption depends on the nature of adsorbate and adsorbent, the surface area of adsorbent, activation of adsorbent and experimental conditions such as

temperature, pressure and volume or mass of adsorbent or adsorbate. Adsorbents with high surface reactivity, surface area and with a high number of the vacant site are in demand. Several adsorbents (natural or synthetic) such as polymers, activated carbon, agro-industrial wastes, and zeolite are used (Otunola and Ololade 2020).

2.17 Adsorption Isotherms

Adsorption isotherm is the amount of adsorbate on the adsorbent as a function of its pressure (if gas) or concentration (if liquid) at constant temperature (Bousskri *et al.*, 2015). Adsorption isotherm is defined as a graphical representation showing the relationship between the amount adsorbed by a unit weight of adsorbent and the amount of adsorbate remaining in a test medium at equilibrium, and it shows the distribution of adsorbable solute between the liquid and solid phases at various equilibrium concentrations. The three well known isotherms are (a) Freundlich, (b) Langmuir, and (c) BET adsorption isotherm (Desta, 2013).

2.17.1 Langmuir isotherm

Langmuir adsorption which was primarily designed to describe gas-solid phase adsorption is also used to quantify and contrast the adsorptive capacity of various adsorbents (Elmorsi, 2011) . Langmuir isotherm accounts for the surface coverage by balancing the relative rates of adsorption and desorption (dynamic equilibrium). Adsorption is proportional to the fraction of the surface of the adsorbent that is open while desorption is proportional to the fraction of the adsorbent surface that is covered (Ayawei *et al.*, 2017).

The Langmuir isotherm model is expressed in it non-linear form as shown in equation 2.1

$$q_e = \frac{q_m k_l c_e}{1+k_L c_e} \qquad 2.1$$

The linear form can be written as

$$\frac{1}{qe} = \frac{1}{al}.\frac{1}{Ce} + \frac{kl}{al} \qquad 2.2$$

The parameter k_L and a_L were obtained from the slope and intercept plot of $1/q_e$ against $1/c_e$.

Where $a_L = q_m k_l$

Where Ce is concentration of adsorbate at equilibrium (mg g−1). KL is Langmuir constant related to adsorption capacity (mg g−1), which can be correlated with the variation of the suitable area and porosity of the adsorbent which implies that large surface area and pore volume will result in higher adsorption capacity. The essential characteristics of the Langmuir isotherm can be expressed by a dimensionless constant called these separation factor RL (Ayawei *et al.*, 2015).

Where KL is Langmuir constant (mg g−1) and Co is initial concentration of adsorbate (mg g−1).RL values indicate the adsorption to be unfavourable when RL> 1, linear when RL = 1, favourable when 0 <RL< 1, and irreversible when RL = 0.

2.17.2 Freundlich isotherm.

Freundlich isotherm is applicable to adsorption processes that occur on heterogonous surfaces. This isotherm gives an expression which defines the surface heterogeneity and the exponential distribution of active sites and their energies (Ayawei *et al.*, 2015). The linear form of the Freundlich isotherm is as follows: The Freundlich isotherm is given in its non-linearized form as presented in equation 2.3

$$q_e = k_f c_e^{\,1/n} \qquad 2.3$$

The linear form is given as

$$logq_e = logk_f + \frac{1}{n} logc_e \quad 2.4$$

Freundlich constants, KF and 1/n, are related to adsorption capacity and intensity of adsorption, respectively. The values of n and KF can be calculated from the slope and intercept of the plot of log qe versus log Ce derived from Equation (2.3). The magnitude of the exponent 1/n gives an indication of the favorability of adsorption. The Freundlich adsorption isotherm represents the relationship between the corresponding adsorption capacity qe (mg/g) and the concentration of the metal in solution at equilibrium Ce (mg/L). The lot of log (qe) versus log (Ce) for various initial concentrations was found to be linear (Elsayed *et al.*, 2020). It also indicates the relative distribution of the energy and the heterogeneity of the adsorbate sites. (Ayawei *et al.*, 2017).

2.18 Adsorption Kinetics

Initial adsorption kinetic data (covering initial ~2 h period) were fitted to pseudo-first-order (PFO), pseudo-second-order (PSO), Elovich, and intraparticle models. PFO and PSO are the most popular kinetic models derived by assuming rate is a linear function of and proportional to square of the number of available adsorption sites respectively, as follows:

2.18.1 Pseudo-first order kinetics

Lagregren showed that the rate of adsorption of solute on the system is based on the adsorption capacity and follows a pseudo-first-order equation (Kean and Thanou 2010).

The non-linear form of pseudo-first-order equation is given by Equation 2.5

$$\frac{dq_t}{dt} = k_1(Qe - Qt) \quad 2.5$$

Where q_e and q_t are the adsorption capacities at equilibrium and at time (t). After integration and applying boundary condition t = 0 to t = t, $q_t = 0$ to $q_t = q_t$. Equation 2.5 becomes

$$\log(q_e - q_t) = \log q_e - \frac{K}{2.303} t \quad 2.6$$

k is the first order adsorption rate constant (min-1) which was calculated from slope of the plot log (q_e/q_t) against t. The adsorption capacity (q_e) can be determined using mass balance equation.

$$q_e = \frac{(c_o - c_e)v}{M} \quad 2.7$$

The adsorption capacity q_t at time t can be determine using

$$q_t = \frac{(c_o - c_t)v}{M} \quad 2.8$$

Co is the concentration of heavy metal ion before interaction with the adsorbent, *Ct* is the concentration of heavy metal ion after interaction with the adsorbent, v is the volume of initial metal ions in solution used in (L) and M is the mass of adsorbent used (in g).

2.18.2 The pseudo – second order kinetics

The pseudo – second order kinetic equation is expressed as

$$\frac{dq_t}{dt} = k_2(q_e - q_t)^2 \quad 2.9$$

Where q_e and q_t are the adsorption capacity at equilibrium and at time t (mgg^{-1}) respectively and k_2 is the rate constant of the pseudo-second order equation (gmg^{-1} min^1). For the

boundary condition t = 0 to t = t and q_t = 0 to q_t = q_t, the integrated form of the equation becomes(Zawani 2009;Mahmoud *et al.*, 2020).

$$\frac{t}{q_t} = \frac{1}{k_2 q_e^2} + \frac{t}{q_e} \quad 2.10$$

Where h (mg.g-1.mm-1) can be regarded as the initial sorption rate as qt/t = 0. Hence h = $k_2 q_e^2$.

$$\frac{t}{q_t} = \frac{1}{h} + \frac{t}{q_e} \quad 2.11$$

k_2 = rate constant of the Pseudo second-order (g.mg-1.min-1). The plot of (t/q_t) and *t* should give a linear relationship from which q_e and K_2 can be determined from the slope and intercept of the plot respectively

2.18.3 Elovich model

Elovich model is applicable for chemisorption processes (Shiosaki *et al.*, 1994). The equation is often used valid for adsorption surface that is heterogeneous. Equation 2.12

$$qt = \frac{1}{\beta}\text{In}(\alpha\beta) + \frac{1}{\beta}\text{Int} \quad 2.12$$

Where α, is the initial adsorption arte (mg/gmin) and β is related to the extent of surface coverage and the activation energy for chemisorption (g/mg), a plot of q_t against Int gives a straight line with a slope of 1/β and an intercept of 1/β In (αβ) with correlation coefficient.

2.19 Thermodynamics studies

The spontaneity of the sorption of the adsorbates-adsorbents can be assessed through thermodynamic parameters such as enthalpy change (ΔH^0), Gibb's free energy (ΔG) and

entropy change (ΔS). Any reaction where (and (ΔH^0) are negative whereas (ΔG) is positive implies a spontaneous reaction (Vardevanyan *et al.*, 2016). change in enthalpy (ΔH), were computed by the following expression.

$$\ln Kc = \frac{\Delta S}{R} - \frac{\Delta H}{RT} \quad 2.13$$

$$\Delta G = RT \ln Kc \quad 2.14$$

$$Kc = \frac{qe}{Ce} \quad 2.15$$

Where Kc is the equilibrium constant and R (8.314 J/mol K) is the gas constant and T is the absolute temperature (Jethave *et al.*, 2017).

CHAPTER THREE

3.0 MATERIALS AND METHODS

3.1 Materials

The kaolin used as a catalyst support in this study was sourced from Kankara in Kastina State of Nigeria. All the chemical and gas used are of analytical grade with percentage purity of 99.9% are presented in Table 3.1 while Table 3.2 shows the list of equipment used in this study.

Table 3.1: List of Chemicals and Gases used for the research

Chemical	Manufacturer	Purity
Kaolin	Kankara Katsina state, Nigeria	99.9
$Fe(NO_3)_3.9H_2O$	Guangdong guanghuasci-tech co., ltd, china.	99.9
$Ni(NO_3)_2.6H_2O$	Guangdong guanghuasci-tech co., ltd, china.	99.9
Acetylene gas (C_2H_2)	BOC Gases Nigeria plc.	99.9
Argon (Ar)	BOC Gases Nigeria plc.	99.9
Sodium hydroxide pellet	Burgoyne &co.,Mumbai India	99.9
HNO_3	Burgoyne &co., Mumbai India	99.9
$AgNO_3$	Burgoyne &co., Mumbai India	99.9
Distilled Water	Step-B FUT, Minna	

The water used was distilled water generated in the step-B laboratory FUT Minna.

Table 3.2: List of Equipments/Apparatus Used for the research

Equipment	**Manufacturer**	**Model**
CVD	Zhengzhou Equipment co., ltd	TZ-1200NT
TGA	Perkin Elmer, USA	TGA 4000
Surface area and pore size Analyser	Quantachrome, UK	NOVA 4200e
HRSEM	Netherland	Joel JEM 100S
HRTEM	Netherland	Philips CM20FEG
XRD	USA	Philips PW1800
XRF	USA	Philips PW2400
FTIR	Perkin Elmer, USA	-
Digital Weighing balance	Ohaus Corporation, USA	Weda, T18
Magnetic Stirrer	Gallenkamp, England	78HW-1 Constant
Furnace	Gallenkamp, England	Nabertherm
Sonicator	Shanghai Bilon co., ltd	BL30-720A
pH meter		BDH, 1-14

3.2 Methodology

Carbon nanotubes (CNTs) were produced by a catalytic chemical vapour deposition method (CCVD). The CCVD method requires a carbon source and a catalyst. In this study, CNTs were made by the decomposition of acetylene (C_2H_2) over Fe-Ni/kaolin catalyst prepared by wet impregnation method.

3.2.1 Preparation of Fe-Ni/Kaolin catalyst

The preparation of the catalyst was carried out using wet impregnation method. The metallic salts containing 4.04 g of $Fe(NO_3).9H_2O$ and 2.91 g of $Ni(NO_3).6H_2O$ were mixed in a beaker. The weighed sample of the Fe and Ni nitrates were mixed and dissolved in 50 ml distilled water to make a 0.2 M Fe-Ni (50:50 w/w) precursor solution. The kaolin support 8 g was added to the mixture and stirred at 120 rpm for 30 min on a magnetic stirrer. The metal-support mixture was then oven dried in a furnace at temperatures 120 ^{0}C for a period of 8 hrs, cooled to room temperature, ground and finally screened through a 150 µm sieve see plate1 (a and b). The catalyst powders was then calcined at 500 ^{0}C for 16 hrs in a furnace in order to decompose the nitrates and the sample was weighed and recorded to determine the yield, using the relationship in Equation 3.1 and 3.2.

$$Catalyst\ yeild\ before\ calcination = \frac{weight\ before\ ovendrying - weight\ after\ ovendrying}{weight\ befor\ ovendrying} * 100 - - - -(3.1)$$

$$Catalyst\ yeild\ after\ calcination = \frac{weight\ before\ calcination - weight\ after\ calcination}{weight\ before\ calcination} * 100 - - - -(3.2)$$

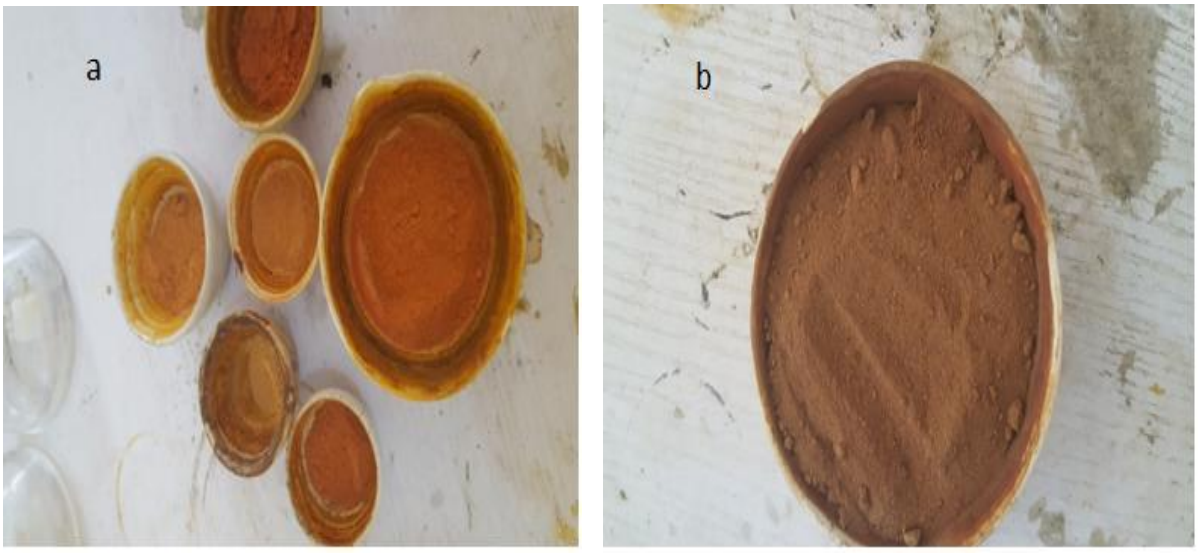

Plate I :(a) Fe-Ni/kaolin after oven drying (b) Ground and screened Fe-Ni/kaolin after oven drying.

3.2.2 Carbon nanotube syntheses

CNTs were synthesized by decomposition of carbon source (acetylene) in a tubular quartz reactor placed horizontally in furnace as shown in Plate II.

1. Pressure gauge
2. Quartz tube
3. Furnace
4. Vent pipe
5. Work bench
6. Control panel
7. Gas pipe
8. Flow meter
9. Vacuum pump
10. Program board

Plate II: Set-up of catalytic CVD for CNTs synthesis in step-B lab, FUT MINNA.

The furnace was electronically controlled such that the heating rate, reaction temperature and gas flow rates could be accurately maintained as desired. Catalyst of 1.0 g were spread to form a thin layer in a quartz boat and placed in the centre of the quartz tube. The furnace was then heated at 10 ^{0}C/min while argon (Ar) was flowing into the system at 30 ml/min to ensure an inert environment, removal of contaminant and to prevent the oxidation of the samples before and after the reaction time. Once the temperature reached the set reaction temperature (750 ^{0}C), the Argon flow rate was set to (230 ml/min) and C_2H_2 was introduced at a flow rate of 150 ml/min in order to start the initiation of CNTs growth. After the setup reaction time of 45 min, the C_2H_2 flow was stopped and the furnace was left to cool down to

room temperature under a continuous flow of Argon at 30 ml/min. The boat was then removed from the reactor and the product formed (CNTs) was weighed and recorded as shown in Plate III, to determine the CNTs yield (%) using the relationship presented in the following equation.

$$\text{CNTs yield (\%)} = \frac{weight\ product - weight\ catalyst}{weight\ catalyst} * 100\% \quad (3.3)$$

Plate III: Carbon Nanotubes synthesized

3.2.3 Purification of the as-synthesized CNTs

Acid treatment method described by Wang *et al.* (2012) was followed for the purification of the raw CNTs. About 300 mL of HNO_3 and H_2SO_4 mixture (v/v 1:3) was mixed with 5 g of the synthesized CNTs in an ultrasonic bath sonicated at 40 ^{0}C for 90 min. This was done to remove residual Fe, Ni, amorphous carbon and support material (kaolin) that remained in as-synthesized CNTs and also to introduce oxygen onto the surface of the CNTs. The CNTs was cooled to room temperature and continuously washed with distilled water and filtered until

the pH of 7 was obtained. The wet purified CNTs (P-CNTs) were oven dried at 120 ^{0}C for 12 h.

3.2.4 Preparation of plant extract

Carica papaya leaves were washed several time with distilled water and dried to remove the residual moisture under room temperature. Then ground into powder with mortar and pestle. Ten (10 g) of powdered leaves is mixed with 100 mL of distilled water and heated at 60 ^{0}C for 30 min until the solution changed colour to light yellow it was then cooled to room temperature and filtered through Whatman filter no.1 and maintained at 4 °C for further studied.

3.2.5 Quantitative phytochemical screening

3.2.5.1 Total flavonoids determination

Aluminum chloride colorimetric method was used for flavonoids determination (Chang *et al.*, 2002). Each plant extracts (0.5 ml) was separately mixed with 1.5 ml of methanol, 0.1 ml of 10% aluminum chloride, 0.1 ml of 1 M sodium acetate and 2.8 ml of distilled water. The mixture was kept at room temperature for 30 min, the absorbance of the reaction mixture was then measured at 415 nm with a double beam spectrophotometer (USA). The calibration curve was prepared by preparing quercetin solution.

3.2.5.2 Determination of total phenol content

The total phenol content of the extracts was determined using the method reported by Singleton *et al*., (1999). Appropriate dilutions of the extracts (0.5ml) were oxidized with 2.5mL of 10% Folin–Ciocalteau's reagent (v/v) and neutralized by 2.0 ml of 7.5% sodium

carbonate. The reaction mixture was incubated for 40 min at 45°C and the absorbance was measured at 765 nm in the spectrophotometer. The total phenol content was subsequently calculated using gallic acid as standard.

3.2.5.3 Tannin determination.

A known weight (0.2g) was measured into a 50ml beaker containing 20 ml of 50% methanol and covered with para film and placed in a water bath at 77-80^{O}C for one hour. The mixture was Shake thoroughly to ensure a uniform mixing and filtered using a double layered whatman NO 41 filter paper into a 100ml volumetric flask with 20mls of water,2.5 ml folin-Ciocalteu reagent, and 10ml of 17% Na_2CO_3 were added and also mixed properly. The mixture was made up to mark with water mixed well and allowed to stand for 20 min. A bluish-green colour was developed at the end of range 0-10 ppm. The absorbance of tannin acid standard solution as well as sample were read after colour development on a spectrophotometer at wave length of 760 nm (A.O.A.C,1984).

3.2.6 Synthesis of silver nanoparticles (AgNPs)

In green synthesis of AgNPs, Silver nitrate aqueous solution (1mM) was prepared by weighing 169.87mg (0.16987g) of the silver nitrate crystals using a weigh balance and dissolved in 100cm^3 of distilled water (10 mM stock of $AgNO_3$). The obtained silver nitrate solution was kept in a brown reagent bottle and used for synthesis of silver nanoparticles. About 5ml of aqueous extract of pawpaw leafs (Plate IV (a)).was added to 95 ml of aqueous solution of 1mM $AgNO_3$, and heated on a magnetic stirrer at 60 °C for 30 min. The formation of brown colour indicated synthesis of silver nanoparticles (Plate IV(b)).The

solution was cooled to room temperature and transferred to an opaque brown bottle. The obtained AgNP was characterized using Particle sizer, and UV-vis spectroscopy.

Plate IV: (a) aqueous extract of pawpaw leafs (b) AgNPs from pawpaw leaf extract.

3.2.7 Preparation of silver doped multi walled carbon nanotubes (Ag-CNTs)

In order to introduce AgNP to the P-CNT surface, the method followed previous reported procedure of, (Sneha *et al.*, 2016).Different volume of 20, 40, 60, 80 and 100 ml of AgNP solution into 0.1g each of P-CNTs. The mixture was sonicated for 18 h at 60 ^{0}C, and then later centrifuged for 10 min. After centrifugation, the black solid residue was washed with distilled water until it reached the pH of 7. Ag-CNTs was obtained which was oven-dried for characterization.

3.2.8 Characterization of synthesize nanomaterials

The support material (kaolin), synthesized catalyst, as-prepared CNTs purified CNTs, AgNPs, Ag-CNTs. XRF, TGA and BET were used as the main characterization technique for

the support material (kaolin) to determine elemental composition, thermal stability and surface area of the kaolin respectively. TGA, BET, FTIR, XRD, EDX/HRSEM, and SAED/HRTEM were technique used to determine the quality of the catalyst (Fe-Ni/kaolin catalyst). While, TGA, BET, XRD, EDX/HRSEM, SAED/HRTEM and XPS were used to characterized the as-prepared and purified CNTs, AgNPs and Ag-CNTs

3.2.8.1 *X-ray fluorescence procedure*

Philips PW2400 analyser was used to determine the elemental composition of the kaolin sample. About 300mg of kaolin sample was prepared by pressing it into cellulose before analysing on a Philips PW2400 XRF spectrometer using calibration software prepared from standard reference materials to determine the elemental composition of the sample.

3.2.8.2 *Thermalgravimetric analysis*

In this study, a Perkin Elmer STA 4000 analyser was used to test the thermal stability of the samples. A known weight (15 mg) of samples was put into a ceramic pan placed in integrated furnace in the equipment. After which the samples were heated from room temperature to 900 ^{0}C at 10 ^{0} C/min under nitrogen gas flow at 20 ml/min and pressure of 2.5 bar. The traces were recorded as weight loss versus temperature for TGA.

3.2.8.3 *BET surface area and pore size analyser*

BET surface area and total pore volume analysis was performed using NOVA 4200e Quantachrome instrument analyser. Samples of 300 mg were degassed at 150 ^{0}C for 4 hrs under a flow of nitrogen gas to remove the impurities and water moisture. The nitrogen gas was used as the adsorbate. The surface areas and pore size distributions were then obtained at

-196 ^{0}C. The pore size distribution with specific surface areas of the samples, were determined via nitrogen adsorption/desorption according to the BET method.

3.2.8.4 *Fourier transforms infrared*

Fourier transform infrared (FTIR) spectrometer was used to study the structural to functional changes in the sample. This analysis was carried out using Perkin Elmer Frontier FTIR spectrometer. In a typical analysis 10mg wafer of the sample consisting of 1% of the sample and 99% KBr window was used. The mixture was pressed under pressure of about 12MPa to produce a thin film wafer. The wafer was inserted in the sample holder of the FTIR equipment, then, FTIR spectra of the sample was recorded from 400 to 4000cm^{-1} resolution operated at scan speed of 0.125 /cm/s. Prior to the sample analysis background spectrum of air at ambient condition was ran.

3.2.8.5 *X-ray diffraction*

XRD patterns were recorded from Bragg's angle of 10º to 80º using PW1800 diffractometer operated at continuous scanning, scanning speed of 5º/min, generator settings of 55 mA and 40kV,and CuKa node material. For preparation, 15mg of the samples were gently ground, placed on a sample holder and the surface was smoothed with an object slide for the analysis.

3.2.8.6 *High resolution scanning electron microscopy*

The high resolution scanning electron microscopy (HRSEM) was operated in combination with energy-dispersive x-ray spectroscopy (EDX) to determine the local elemental composition. This analysis was carried out using Joel JEM 100S HRSEM operating at 80kV.

In a typical run a very small amount of the samples; less than 1.0mg was picked with a tweezer and was treated with methanol. The solutions were sonicated for 10mins to ensure particles dispersion and 2 drops were placed on the sample stab. The stab containing the treated sample was placed in the sputter coater for surface polishing with gold or platinum film. After the sample preparation and sputtering the sample stab was placed in the analysis chamber of the HRSEM equipment, the vaccum was put on. When the vaccum was about $9.634 * 10^{-5}$ torr the scanning was commenced. The magnification and voltage were set and the focus of the microscope was manipulated until a sharp clear image was obtained and picture captured.

3.2.8.7 *High resolution transmission electron microscopy*

High resolution transmission electron microscopy, and selected area electron diffraction (SAED) were performed with a Philips CM2OFEG 200 KeV TEM. In a typical run a very small amount of the samples; less than 1.0mg was picked with a tweezer and was treated with methanol. The solutions were sonicated for 10mins to ensure particle dispersion and 2 drops were placed on the sample stab. The sample stab was placed in the analysis chamber of the HRTEM equipment, the vaccum was put on. When the vaccum was about $9.634 * 10^{-5}$torr the beam gun was shot. The magnification and voltage were set and the focus of the microscope was manipulated until a sharp clear image was obtained and the picture captured.

3.2.8.8 *Particle size analysis (DLS Techniques)*

The particle size and hydrodynamic diameter were determined using zetasizer Nano- S at scattering angle of 173 ºC operating at 25ºC with equilibrating time of 10sec per runs. 1mg of the samples were dispersed in 10ml of an organic solvent (methanol) by means of a sonication (Misonix 3000; power: 1W/ml, pulse on: 3sec, pulse off: time: 1min) and a

centrifugation (5 min at 3000 rpm). The supernatant (free of larger aggregates) then transferred into a polystyrene quartz cuvette using a syringe with 0.23 µm filter and placed in the zetasizer Nano-S cuvette holder immediately for analysis. Each DLS measurement was averaged over 20 runs (10 sec per run).

3.2.8.9 *X-ray photo electron spectroscopy (XPS) silver nanoparticle*

The XPS analyses were carried out with a PHI 5400 XPS spectrometer using a non monochromatic MgK_α X-ray source (1253.6 eV, 15 kV, 200 W) and hemispherical sector analyser. The instrument work function was calibrated to give a binding energy (BE) of 83.96 eV for the Au $4f_{7/2}$ line for metallic gold and the spectrometer dispersion was adjusted to give a BE of 932.67 eV for the Cu $2p_{3/2}$ line of metallic copper. The photoelectron take-off angle for all measurements was $45^{0.}$ Survey scan analyses were carried out with a pass energy of 178.95 eV in steps of 0.25 eV and scan rate of 2.5 eV/s High resolution analyses were carried out with a pass energy of 44.75 eV, step size 0.125 eV and scan rate of 0.625 eV/s. Charge correction was not done (Standard practice is by referencing to the adventitious carbon peak at 284.8 eV).The analyses area was 3 x 10 mm^2. The base pressure in the working chamber was < 5 x 10^{-9}Torr measured by a nude ionization gauge. The powders were mounted on a vacuum friendly C-tape and stick to the Mo specimen holder. No sputtering or charge neutralization was used.

3.9 Characterization of fish pond wastewater

The fish pond wastewater was collected from FAIB Construction International, fish pond Minna, Niger State, Nigeria. The physicochemical parameters of the wastewater were carried out and the inorganic constituents of the wastewater were determined using the American

Public Health Association (APHA) method (2017). The pH of the wastewater was determined by pH metre. In the same vein, pH and electrical conductivity were estimated using a multi-parameter analyser C 3010 while dissolved oxygen (DO) metre was used to determine the level of DO. The following chemical parameters: chemical oxygen demand (COD), biochemical oxygen demand (BOD), total dissolved solid (TDS) alkalinity, the total amount of nitrate, sulphate, phosphate, ammonium, chloride, magnesium, potassium, calcium were determined by the standard method described by the APHA.

3.9.1 Determination of turbidity

The turbidity of fishpond wastewater was measured by turbidity meter. The turbidity meter was first calibrated by cal 800 NTU, cal 200 NTU and cal 100 NTU and the sample cell was then filled with the wastewater connected to a sample holder, the turbidity meter machine was then switched on to read the turbidity. The method employed for this analysis was nephelometric.

3.9.2 Determination of pH

The method used for the determination of pH in this analysis was electrometric the protective cap of the pH meter was removed and turned on and the pH meter probe or electrode was immersed into buffer 7 solution for calibration. After calibration the pH meter probe was rinsed with distilled water to avoid contamination then immersed into the water sample. The water sample was stirred with pH meter probe gently until the display on the pH meter was stabilized. The pH value was recorded accordingly after the reading had been stabilized. The pH meter electrode or probe was rinsed with distilled water to minimize contamination after each test.

3.9.3 Determination of conductivity

The conductivity of the sample was measured by conductivity meter. This was actually carried out by calibrating the meter according to the manufacturer's specification for the equipment. The machine was switched on and the conductivity probe was immersed into the sample to measure the conductivity.

3.9.4 Determination of dissolved oxygen

The dissolve oxygen was measured by dissolve oxygen meter. The process involve setting up a multi-layer and electrodes according to manufacturer instruction. The electrode was properly rinsed with distilled water and cleaned with soft tissue paper before immersing into the sample to take the measurement,

3.9.5 Determination of alkalinity

Titration method was used for determination of alkalinity. This was performed by measuring 100mL of the sample into a conical flask followed by addition of 2-3 drops of phenolphthalein indicator. The color changed to pink as the flask was swirled on the burette Phenolphthalein indicator. The color changed to pink as the flask was swirled on the burette (initial burette reading taken). This was then titrated against 0.01M HCl to obtained a colorless end point. Similarly, 2-3 drops of bromocresol green-methyl orange was added to the same solution which changed the colour blue (final burette reading taken). The difference between the initial and the final reading gave total alkalinity present in the sample.

3.9.6 Determination of Chemical Oxygen Demand

Chemical oxygen demand was measured by an instrument called COD rector, it was carried out by pre-heating the rector to temperature of 150 ^{0}C followed by homogenizing 100 mL of sample in a blender for 30 secs after which a stored program for chemical oxygen demand was set and the measurement taken.

3.9.7 Determination of Biochemical Oxygen Demand.

The BOD determination is an empirical test in which standardized laboratory procedures are used to determine the relative oxygen requirements of wastewaters, effluents and polluted waters (APHA, 1985).

The method consists of placing a sample in a full, airtight bottle and incubating the bottle under specified conditions for a specific time. Dissolved oxygen (DO) is measured initially and after. The BOD is calculated from the difference between the initial and final DO (APHA, 1985). Normally a 5-day BOD test period is used where samples are incubated in the dark (to restrict algal growth) at 20 ^{0}C (the temperature believed to be reasonably representative of field conditions).The BOD is calculated from equation 3.4.

$$BOD = DOi - DOf/(Vs/Vb) \quad 3.4$$

Where,

BOD_5 =Biochemical oxygen demand at t days (mg/L), DO_i = Initial dissolved oxygen in sample bottle (mg/L), DO_f =final dissolved oxygen in sample bottle (mg/L),

Vb = sample bottle volume usually 300 mL, Vs = sample volume (mL).

3.10 Adsorption experiment

The adsorption efficiencies of P-CNTs and Ag-CNTs for the removal of organic and inorganic contaminants of the fish pond wastewater were evaluated at different contact time, dosage of adsorbent and temperature via batch adsorption process. To investigate effect of contact time, 0.1 g of P-CNTs and Ag-CNTs were individually dispersed into 250 mL conical flask containing 50 mL of the fish pond wastewater. The mixture was corked and stirred on magnetic stirrer at 190 rpm under room temperature and shaking was done at pre-determined time interval of 20, 40, 60, 60, 80, 100 and 120 min, respectively. The effect of

adsorbent dosage is carried out by adding different amount of nano-adsorbents: 0.1, 0.2, 0.3, 0.4 and 0.5 g to 50 mL of fish pond wastewater in 250 mL conical flask. The mixture was shaken on a magnetic stirrer for 100 min under constant room temperature and stirring speed. The effects of temperature on the selected heavy metals were performed by adding 0.1 g each of P-CNTs and Ag-CNTs nano-adsorbent to 50 mL of fish pond wastewater in 250 mL conical flask. The temperature is varied from 303 K to 343 K while the stirring speed and the volume of the adsorbate were kept constant. After equilibrium time of 100 min was reached, the sample solutions were filtered through a 0.45 mm membrane filter and the filtrate was analyzed for the removal of contaminants using AAS PG 990 model.

Data analysis

The amount of metal adsorbed by each adsorbent was calculated by using the following Equation

$$Q = \frac{(c_o - c_e)v}{W} * 100 \qquad 3.4$$

where C_0 is the initial concentration of the metal in the fishpond wastewater before adsorption in mg L, Ce is the concentration of metal ion in the filtrate after adsorption in mgL, W is the weight of the adsorbent (mg), V is the volume of adsorbate (L) and Q is the amount of metal ion adsorbed In (mg/g) on each adsorbent.

The metal removal efficiency (E) is given by the following Equation3.5

$$E = \frac{(c_o - c_e)}{c_o} * 100 \qquad 3.5$$

Where Co and Ce are the initial and concentration of the metal in the waste water and filtered water before and after adsorption in mg/l respectively, and E is the percentage metal removal (Hamzat *et al.*, 2019).

CHAPTER FOUR

4.0 RESULTS AND DISCUSSION

4.1 Phytochemical Analysis of the Extract

Table 4.1 present, the qualitative result of some phytochemicals (such as tannins, phenols and flavonoids) present in the aqueous extract of pawpaw leaves. From Table 4.1, tannins had the maximum concentration levels (19.11 ± 0.13 mg/g) followed by phenols (8.91 ± 0.21 mg/g) and flavonoid (3.73 ± 0.10 mg/g) respectively. The phytochemical constituent of pawpaw leaf extract was also reported to be (0.001 ± 0.10 mg/g) for tannins, (0.011 ± 0.01 mg/g) for phenol, (0.013 ± 0.01 mg/g) for flavonoid by (Bamisaye *et al.*, 2019).Which implies that the phytochemical screening and quantitative estimation of the aqueous extracts of pawpaw leaves obtained in this study were very rich in phenols, flavonoids, and tannins and several studies reported that these phytoconstituents play an important role in the biochemical reduction of silver ions to silver nanoparticles as well as stabilizing and capping the synthesized nanoparticles (Mohanta *et al.*, 2017).

Table 4.1: The Phytochemical constituents of Pawpaw leaf extract

Plant extract	**Phytochemical**	**Concentration(mg/g)**
Pawpaw leaf	Tannins	19.11 ± 0.13
	Flavonoid	3.73 ± 0.10
	Total Phenol	8.91 ± 0.21

4.1.1 Uv-vis spectroscopy analysis of silver nanoparticles

Biosynthesis of AgNPs was accompanied with a distinct colour change. At the beginning, the colour of $AgNO_3$ solution was colourless. After 30 min of continuous stirring at 70 ^{0}C the

plant extract, the colour of the mixture turned brownish. This colour change was considered an indication of successful synthesis of AgNPs (Chandhuru *et al.,* 2019).The formation of silver nanoparticles in aqueous solution was confirmed by measuring the absorption spectra with a light wavelength in the range of 200-800 nm from Figure 4.1,

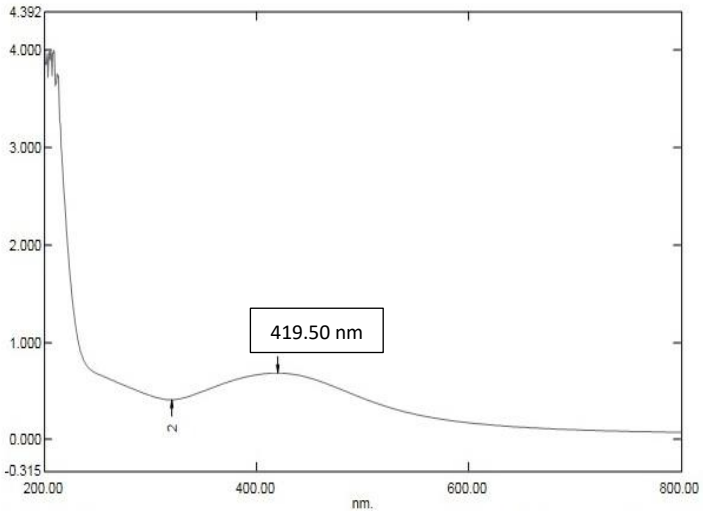

Figure 4.1: UV-VIS Spectrum of Silver Nanoparticles

A prominent peak was observed at 419.50 nm. The colour change in the aqueous solution could be due to the surface excitation of the plasmon resonance phenomenon of silver metal (Shameli *et al.,* 2014). This occurs due to mutual oscillation of the conduction electrons on the surface of the metal nanoparticles when they align in resonance with the irradiated light of the wave (Amendola *et al.,* 2017).The combined oscillation of free electrons within the metal nanoparticles and the surface resonance permit the scattering and absorption of light at a particular frequency, and thus, provide the characteristic colour of each nanoparticles (Aroca *et al.*, 2006).

4.1.2 X-ray diffraction of silver nanoparticles

The XRD pattern of synthesized AgNPs using *Carica Papaya* leaf extract is shown in Figure 4.2. The XRD was carried out to determine the crystalline nature of AgNPs and the resulted diffraction peaks of different intensities were found at 2Θ angles of 38.35°, 44.87°, 64.83°,77.76° and 81.74 representing (111), (200), (220), (311) and (200) face centered cubic structure of silver which were compared with the standard powder diffraction card of Joint Committee on Powder Diffraction Standards (JCPDS).The obtained result is very close to the XRD analysis of Chandhru *et al.* (2019) who reported 2Θ values of 38.21°, 44.40°, 64.37°, 77.79° and 81.58^0 for silver nanoparticles. Interactions between these phytochemicals and silver ions cause the bioreduction of silver nitrate and synthesis of AgNPs.

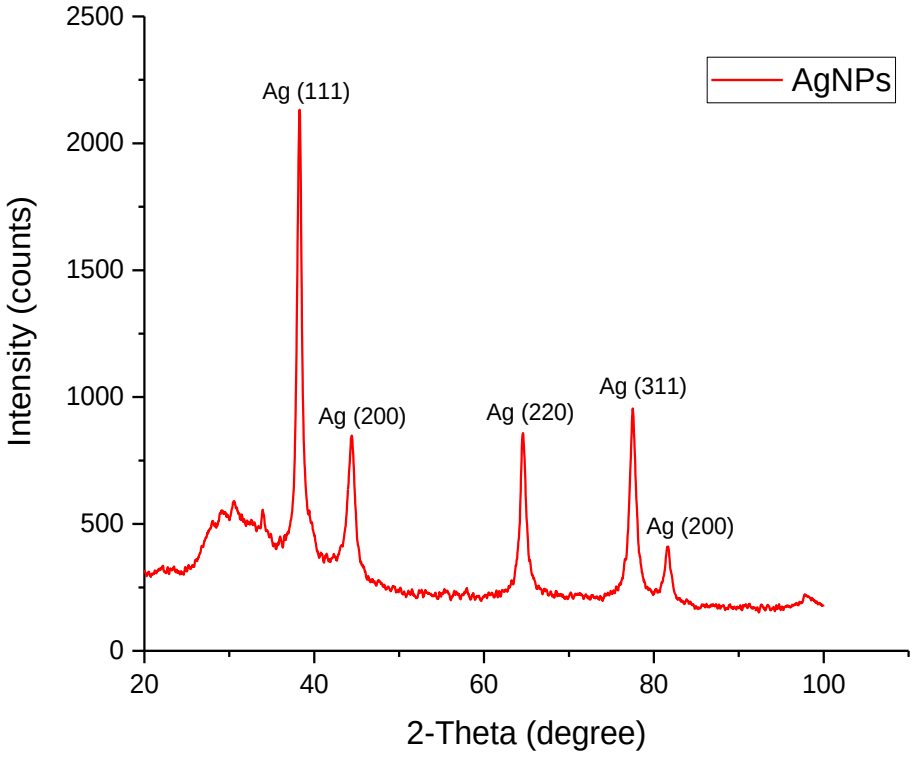

Figure 4.2: XRD pattern of AgNPs

From Figure 4.2 the observed Bragg peaks might have resulted from some bioorganic compounds/proteins present in the *Carica Papaya* leaf extract (Sagadevan *et al.,* 2019); Kotakadi *et al.*, 2014). The average crystallite sizes of Ag nanoparticles were estimated using Debye Scherrer's Equation (Ajitha *et al.,* 2015) in Equation 4.1 and estimated to be 11.35 nm.

$$\tau = (K\lambda)/\beta\cos\theta \qquad 4.1$$

where, τ is the particle size; K is a dimensionless shape factor, its value is 0.94 nm, λ is the X-ray wavelength (0.154nm), β is full width half maximum (FWHM) of the peaks and θ is the Bragg's angle.

4.1.3 TEM-SAED silver nanoparticles

The TEM analysis was carried out to investigate the size and shape of silver nanoparticles prepared by leaf extract. The image in plate I showed a clear and distinct spherical shapes of silver nanoparticles as observed by (Guzman *et al*., 2019), with particle size ranges from 5.3 to 29.33 nm, which is in close agreement with the ranges that was observed by (Moustafa, 2017).

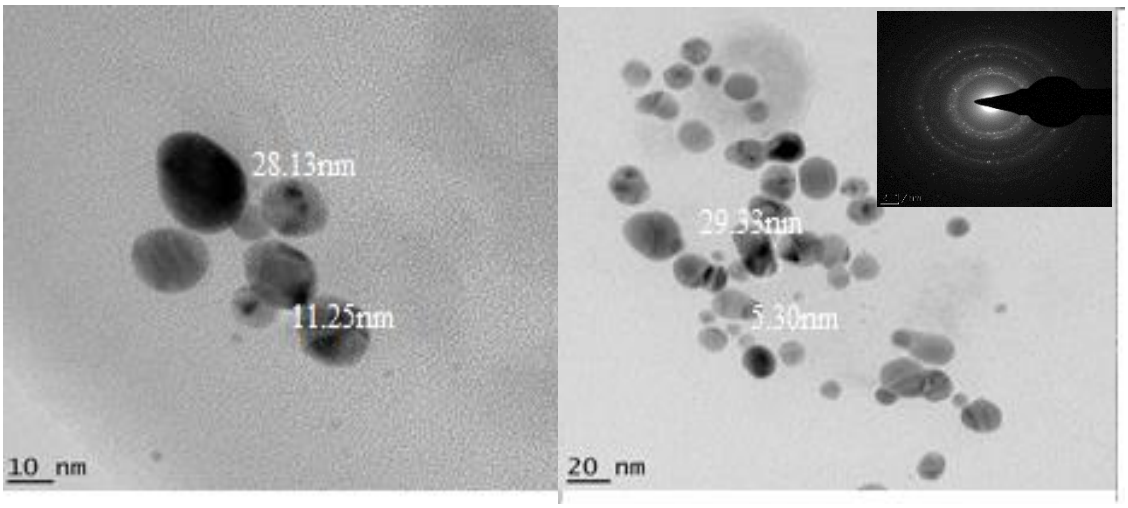

Plate I: TEM/SAED of synthesized AgNPS

The results of SAED pattern were in agreement with the XRD, as each of the diffraction rings was found to be consistent with the face centered cubic structure of Ag (111), (200), (220), (311) and (200) crystalline fringes.

4.1.4Energy dispersive x-ray spectroscopy (EDX) of silver nanoparticles

The EDX spectrum revealed the presence of elemental silver in the sample (Figure 4.3). The optical absorption of the silver metal peak in the EDX measurement was noticed in a range between ~3–4 Kev which is typically due to the absorbance of silver nano-crystals attributed to the surface Plasmon resonance.

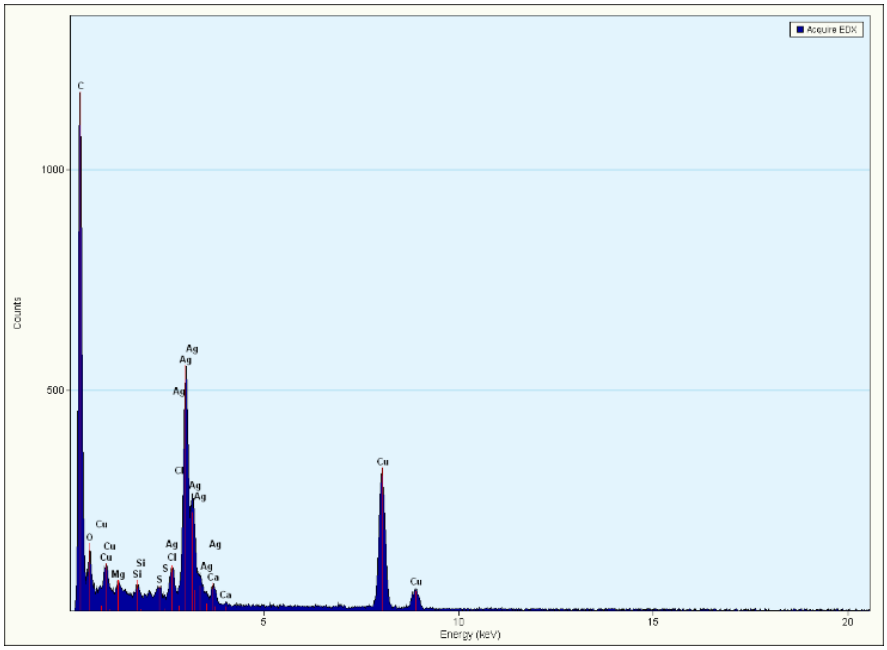

Figure 4.3: EDX of AgNPs

The carbon and oxygen peaks in the EDX spectra could be from the presence of surface hydroxyl group found in the *Carica papaya* leave extracts. The occurrence of other peaks (Ca and Si) was presumably related with the glass underneath, which held the sample. The peaks for Cu and C must have emanated as a result of grid used for the analysis.

4.1.5 X-Ray photoelectron spectroscopy (XPS) of silver nanoparticles

In this specimen there is a clear presence of Ag at binding energy of 368.4 eV (typical of Ag metal). The surface oxidation state of each element present in the prepared silver nanoparticles was determined using XPS and the results are shown in Figure 4.4,

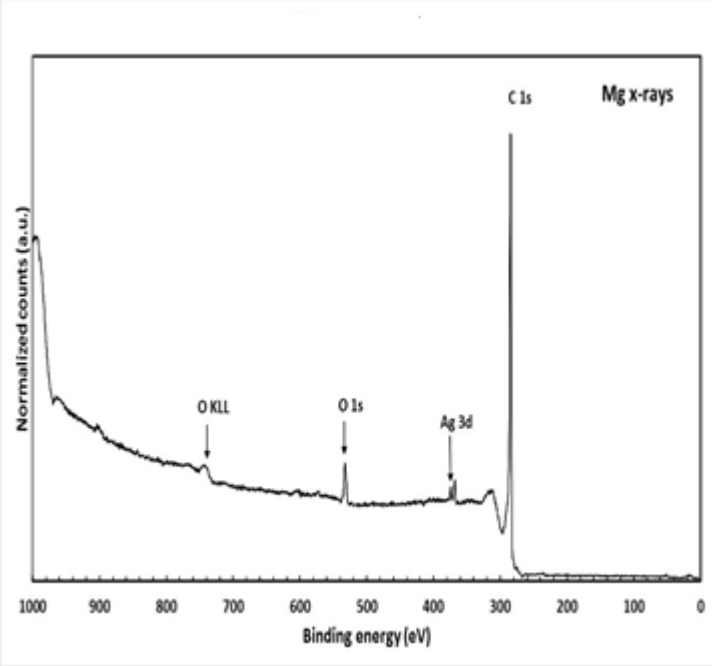

Figure 4.4: XPS of AgNPs

XPS measurements were performed on AgNPs the sputtered sample of AgNPs shows the presence of C, O and Ag. The carbon (C) was identified in the binding energy region of 280.5 eV, oxygen (O) at 535.5 eV while Ag was detected at 368 4 eV respectively. All this elements have multiple oxidation state since it is relatively easy to lose electrons, silver has +1, +2 and +3 silver is a normal transitional metals which have different electronic states, since their orbitals have large volume, the energy required to give away electrons is very less. It is easy to give 2 electrons from S orbital forming common oxidation state.

4.2 Characterization of Kaolin

Prior to the synthesis of bi-metallic catalyst for CNTs production, the support material (kaolin) was characterized to determine its suitability in CNTs production.

4.2.1 X-ray fluorescence analysis (XRF) of kaolin

The oxide compositional analysis of the kaolin sample was carried out using x-ray fluorescence (XRF) technique and the result was shown in Table 4.3. The chemical compositions of elements present in the kaolin sample and their corresponding percentage contributions were recorded and the results presented indicate the kaolin sample contains silica (54.21%), and alumina (28.43%) which were the major quantities, other oxides like iron oxide, potassium oxide, magnesium oxide, titanium oxide, calcium oxide and barium oxide are present in small quantities. the percentage loss on ignition (LOI) of the kaolin sample is 8.81 % which indicates the loss of volatile and organic content of the raw kaolin sample. Silica has been reported to constitute the highest percentage of kaolinite sample (Karim *et al.*, 2018). Also Aliyu *et al*. (2017) reported that alumina (Al_2O_3), titania (TiO_2) and silica (SiO_2) were the most widely used supports for catalyst synthesis because they have a high thermal stability, high surface area and porosity. More so, using kaolin as a catalyst support will complement the use of commercial support.

Table 4.2: Composition of the kaolin

Oxide	Kaolin (wt %)	Kaolin (wt %) (Mamudu *et al*.,2020)	Kaolin (wt %) (Salaudin *et al*.,2018)
SiO_3	54.21	58.50	52.04
Al_2O_3	28.43	16.62	27.81
Fe_2O_3	0.80	5.62	0.93
TiO_2	0.11	0.90	0.12
CaO	1.86	1.14	1.19
MgO	0.41	2.09	0.50
Na_2O	0.35	1.07	0.57
K_2O	3.90	1.50	1.89
MnO	0.03	0.01	-
BaO	0.73	-	--
SO_3	0.22	-	-
Cr_2O_3	0.04	-	-
V_2O_5	0.10	-	-
P_2O_5	-	0.10	-
CuO	-	0.02	0.02
LOI	8.81	12.35	14.70
Total	100.00	99.9	99.32

4.2.2 Thermal gravimetric analysis of kaolin

The effect of temperature on the thermal stability of the kaolin sample was investigated and the result is in Figure 4.5. The TGA plot of the kaolin sample with respect to weight loss against change in temperature as seen in Figure 4.5 show two well-defined weight loss regions due to the loss of hygroscopic water which occurred below 200^0C and at the temperature above 380^0C,dehydroxylation of coordinated and structural water bound.

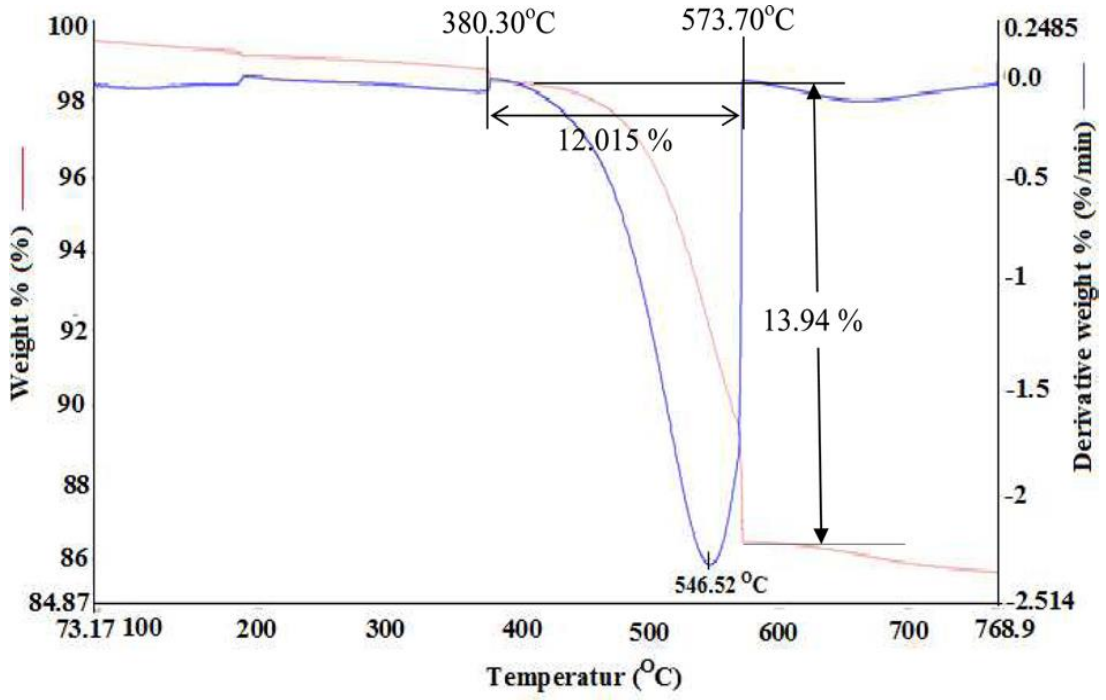

Figure 4.5: TGA and DTG Results for Kaolin

The TGA shows weight loss of 12.015 % which occurred between 380.30^{0}C and 573.70^{0}C and stabilized at 575^{0}C which corresponds to a phase change from the crystalline kaolin to amorphous metakaolin as shown in Equation 4.2, similar to the report of Edomwonyi-out *et al.* (2010).

$$2Al_2Si_2O_5(OH)_4 \rightarrow 2Al_2Si_2O_7 + 4H_2O \qquad 4.2$$
Kaolin Metakaolin

The DTG curve also in Figure 4.5 showed an endothermic peak at 546.52 ^{0}C with the corresponding weight loss of 13.94 % Thus, 85.80 % of the kaolin was left not decomposed. The endothermic peak at 546.52 ^{0}C is due to liberation of water caused by dehydroxylation of coordinated and structural water molecule (De Mejia *et al.*, 2008).Therefore, kaolin is thermally suitable as catalyst support for CNTs production.

4.2.3 Surface area, pore volume and pore sizes of kaolin

Determination of surface area, pore volume and pore size distribution of the kaolin is important to understand the extent and suitability of the kaolin as a support in the catalyst synthesis for the production of CNTs. Higher surface area of support results in higher dispersion of the active metal (Zhu *et al.,* 2016) hence supports with higher surface area are desirable. The BET surface area of the kaolin in this experiment was found to be 11.56m^2/g with corresponding pore volume and pore size of 0.00645 cm^3/g and 20.64Å respectively. These values are in good agreement with the work of Salaudeen. (2015), who reported the surface area of Kankara kaolin to be 12.95 m^2/g. Hence, the kaolin gives a promising surface area as catalyst support for bi-metallic catalyst synthesis in CNTs production using CCVD method.

Table 4.3: BET value of Kaolin

Sample catalyst	**SurfaceAream^2/g**	**Pore volume cm^3**	**Pore Size (Å)**
Kaolin	11.56	$6.45x10^{-3}$	20.64

4.2.4 Morphology of the kaolin

The micrograph depicts plate-like nature of kaolin with irregular particle shapes which contain of an aluminosilicate [$Al_2(Si_2O_7)(OH)_4$], constituent which is dominant in kaolin as shown in Plate II. The depicted structure might be related to the strong interaction bond which exists in aluminosilicate material.

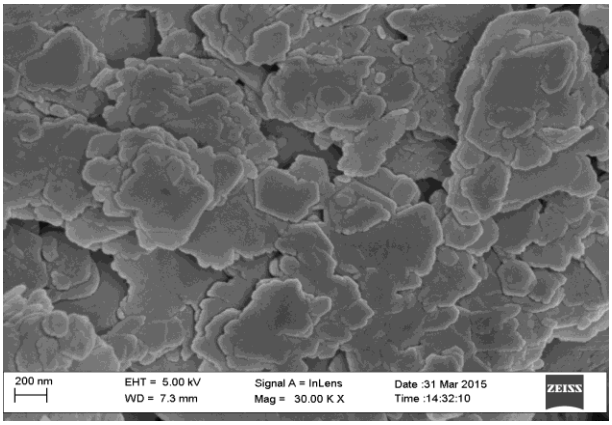

Plate II: HRSEM micrograph of kaolin sample

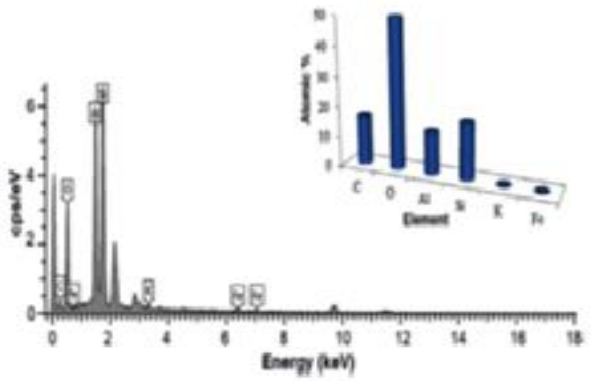

Figure 4.6: EDX micrograph of kaolin sample

The EDX revealed the presence of C, O, Al, Si, K and Fe with percentage weight of 16.35, 49.95, 14.25, 18.83, 0.32 and 0.3%, respectively. The higher percentage weight of oxygen presence might be due to the presence of oxides of the elements in the kaolin sample. While the carbon content is attributed to the presence of organic constituents due to the source of the kaolin and the carbon grid used during the scanning electron microscopy analysis. As shown from the EDX (Figure 4.6), the dominantly identified elements are aluminium and silicon which is similar to the work of Karim *et al.* (2018).

4.2.5 X-ray Diffraction analysis of kaolin

X-ray diffraction (XRD) was used to determine the crystal structure and phases present in the kaolin sample. In Figure 4.7 the XRD pattern of the kaolin used in this study is presented and observed from the XRD pattern that the kaolin was amorphous in nature.

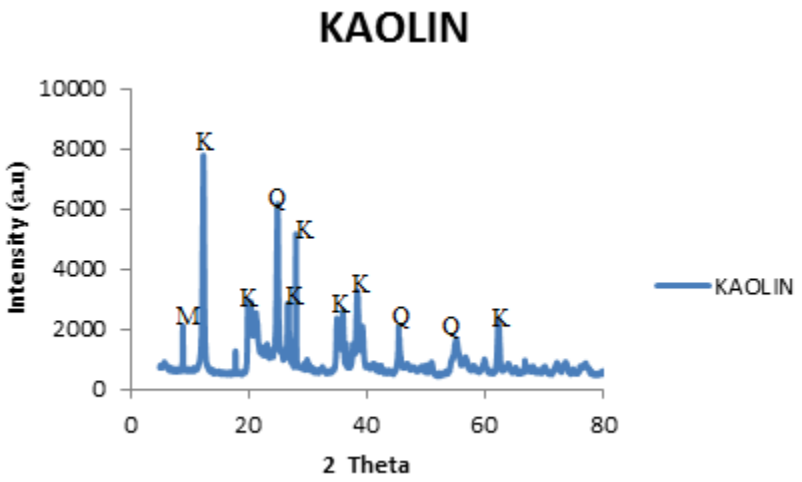

Figure 4.7: XRD Patterns of Kankara Kaolin

The results as presented in Figure 4.7 shows numerous peaks at varied diffraction angles and intensities. Each diffraction angle represents a pristine phase of compound. Hence, the phase identification of the component compound in the kaolin sample was done. The XRD shows the presence of kaolinite, mica, and quartz, the major peaks were identified at the diffraction angles (2Ɵ) of 8.75, 12.37, 19.9, 20.43, 24.88, 34.84, 35.95, 36.16, 38.37, 45.24, 54.88 and 62.23^0.This phase angles identification is in agreement with the report of Ishaq *et al*. (2018) with the combined effect of crystallinity it will have capacity since quartz (SiO_2) content was much higher in the XRF of kaoline in Table 4.2 to be used as a support in this research study for the synthesis of CNTs.

4.3. Characterization of Fe-Ni/kaolin Catalyst

4.3.1 Surface area, pore volume and pore sizes of Fe-N/kaolin catalyst

BET specific surface area, total pore volume and average pore size of the Fe-Ni/kaolin catalyst were determined. There was a significant increase in BET specific surface area and pore volume for the kaolin support after bi-metallic (Fe-Ni) impregnation. The specific surface area of kaolin was found to be 11.56 m^2/g while the pore volume was 0.00645cm^3/g with a pore size of 20.64 Å as seen in Table 4.3. However the surface area of Fe-Ni/kaolin catalyst was 21.68 m^2/g, pore volume and pore size of catalyst are 0.01479 cm^3/g and 25.986 Å respectively as presented in Table 4.4. BET specific surface area increase, and total pore volume, pore size after the impregnation of Fe-Ni on kaolin indicates that bi- metallic ions were successfully incorporated on the external surface of kaolin.

Table 4.4: ***BET value of Fe-Ni/ Kaolin catalyst***

Sample catalyst	**Surface Area m^2/g**	**Pore volume cm3/g**	**Pore Size(A)**
Fe-Ni/Kaolin catalyst	21.68	$1.48x10^{-2}$	25.99

4.3.2 Fourier transforms infrared spectroscopy (FTIR) of Fe-Ni/kaolin catalyst

The FTIR spectrum of Fe-Ni/kaolin catalyst is shown in Figure 4.8. The band at 591cm^{-1} corresponds to intrinsic stretching vibrations of the metal at the tetrahedral site (Fe-O), whereas the band at 437cm^{-1} was assigned to octahedral metal stretching (Ni-O). These two absorption bands are characteristics of inverse spinal ferrites and the positions of these infrared bands were in the ranges which correspond to spinal $NiFe_2O_4$as reported by

Gunjakar *et al*, (2008).

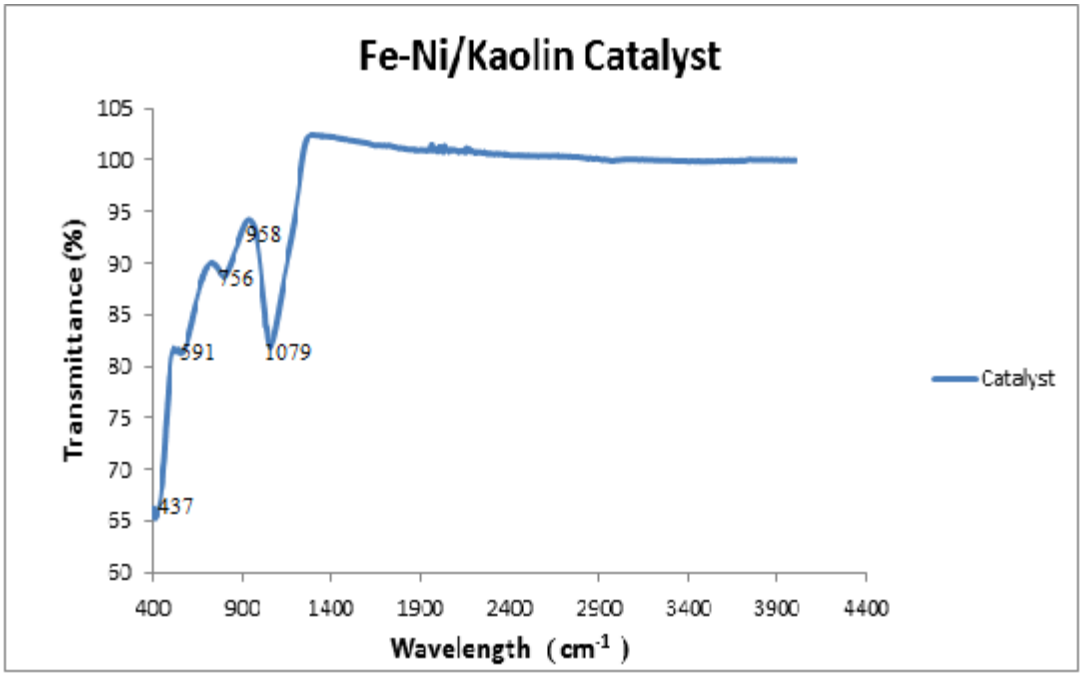

Figure 4.8: FTIR spectra of Fe-Ni/Kaolin catalyst by wet impregnation method

The Si-O-Si or Si-O-Al asymmetric stretching bands are observed at 1079cm^{-1} and 958 cm^{-1} respectively which confirms the adsorption of metals on the surface of the support material. The absorption band at 756 cm^{-1} corresponds to the O-Al-O symmetric bending vibration.

4.3.3Morphology of the catalyst

The microscopic structure of the developed bimetallic catalyst is shown in Plate III, and the detailed micrograph of the catalyst sample is revealed. The metal particles (Fe-Ni) are indicated by arrows which revealed the uniform deposition of Fe-Ni ($NiFe_2O_4$)compound obtained from the calcinations process of the catalyst material; the most participating component of the catalyst material during the CNTs nucleation process and randomly oriented nanoflakes texture (Karim *et al.*,2018).While Plate III revealed that the nanoflakes of metal catalysts were maximally distributed on the surface of the kaolin support material

with surface porous morphology, which is the key requirement for a catalyst to be used in CNTs synthesis Aliyu *et al.* (2017).

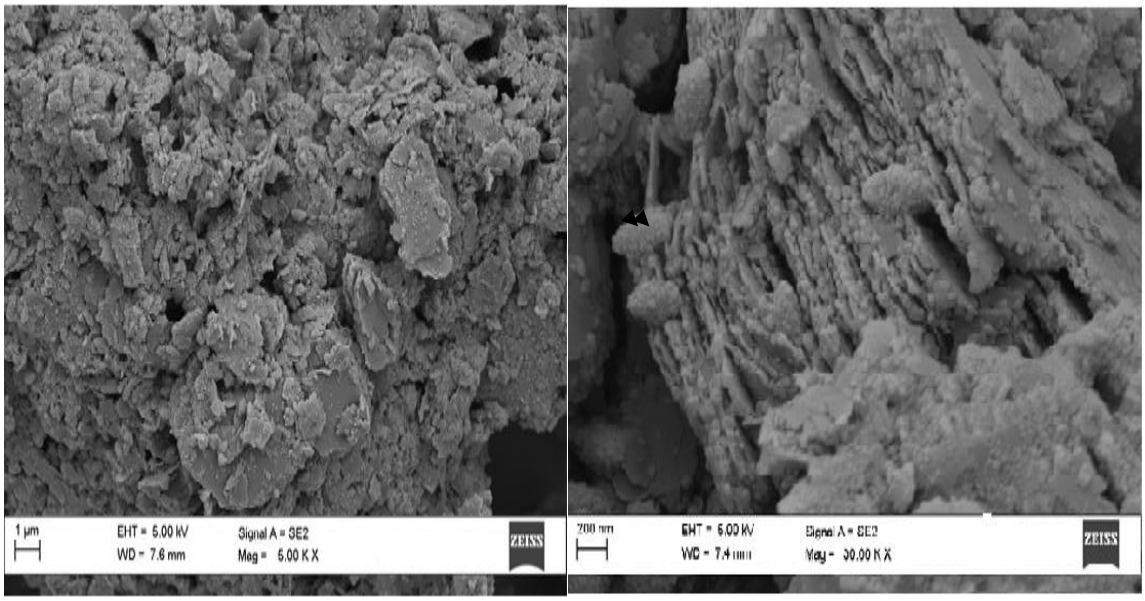

Plate III: The HRSEM image/micrograph of Fe-Ni/kaolin catalyst

In Figure 4.9 qualitative and quantitative elemental analysis of the prepared catalyst using energy dispersive X-ray spectroscopy (EDX) shows that all particles contained both Fe and Ni in a close to 1:1wt% ratio (50:50) which were in agreement with the expected chosen stoichiometry for the preparation of the catalyst,. The peaks attributed to carbon were derived from the carbon grid. As shown in Figure 4.9 the average atomic ratio of Ni to Fe were nearly1:1, indicating that pure $NiFe_2O_4$ was synthesized. The energy dispersive x-ray spectroscopy (EDX) indicates the presence of C, O, Mg, Ca, Fe, Ni observed at the lower energy levels. Meanwhile, the atomic percentage of C, O, Mg, Ca, Fe and Ni were determined to be 22.77, 61.38, 2.93, 7.38, 2.56 and 2.98 respectively. The presence of higher percentage weight of oxygen was due to the presence of oxides of the elements in the catalyst sample.

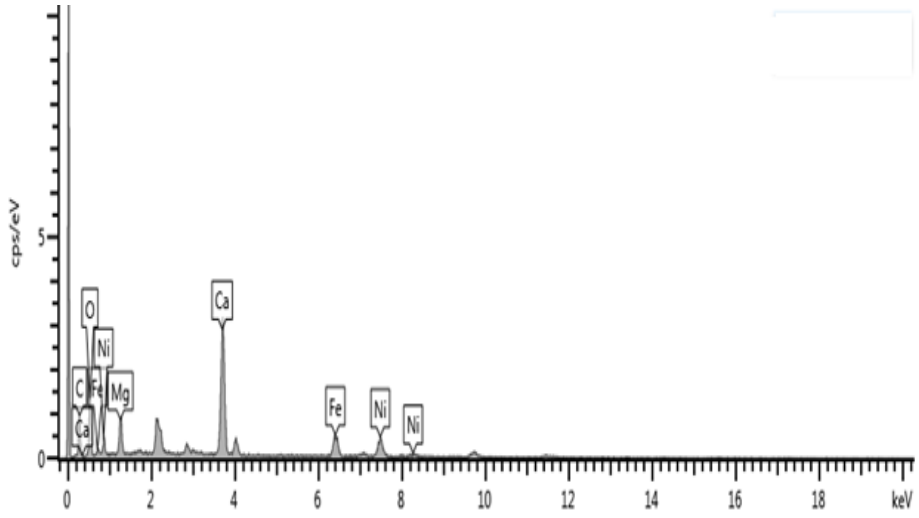

Figure 4.9: An EDX spectrum of the Fe-Ni/kaolin catalyst

Table 4.5: ***Elemental composition of prepared Fe-Ni/Kaolin catalyst***

Element	Atomic %
C	22.77
O	61.38
Mg	2.93
Ca	7.38
Fe	2.56
Ni	2.98
Total	100

4.3.4 High resolution transmission electron microscopic (HR-TEM) analysis of the catalyst

In From Plate III, it can be deduce from the results presented that the pores and pore walls can be distinguished due to different densities; dark region correspond to the pore wall, the bright one to the pore of the catalyst particles (Aliyu *et al.*, 2018) exhibited various sizes in the range of 29-33 nm. Also from the TEM images showed that some ($NiFe_2O_4$) particles had being effectively loaded on the kaolin.

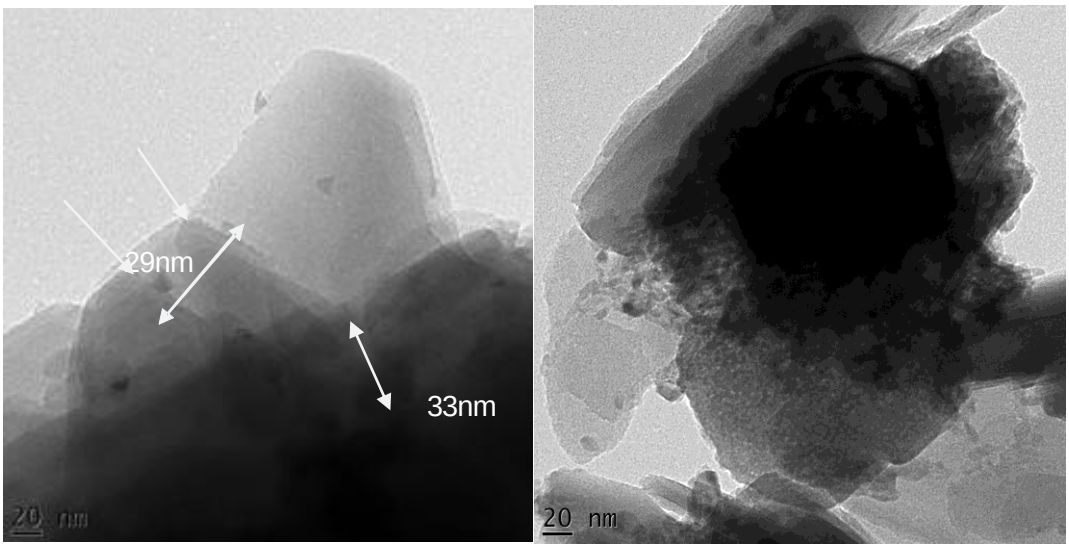

Plate IV: HRTEM of Fe-Ni/kaolin catalyst

4.3.5 Selected area electron diffraction (SAED) of Fe-Ni/kaolin

Selected area electron diffraction (SAED) pattern of the Fe-Ni/kaolin sample calcined at 500°C is shown in Plate V in SAED pattern, each spot of SAED becomes a disk, whose radii are approximately few hundred nanometers around the centre of the images. The SAED of Fe-Ni/kaolin catalyst exhibited a face centered cubic (FCC) pattern which implies successful loading of metal particles on the kaolin support. The lighter areas indicated heavy presence

of iron and nickel particles while darker areas revealed a breakdown of kaolin. A series of concentric rings resulting from many spots very close together at various rotations around the centre beam spot was noticed with each ring depicting reflection of the family of planes with different inter-planar spacing. From the diffraction rings, the type of crystal structure can be determined by measuring the ring radii (Cullity and Stock, 2001).The ring pattern observed in the SAED were indexed as (111) planes in the spinel structure (Fe-Ni) and (110), (210), (321) planes in the octahedral structure (kaolin).

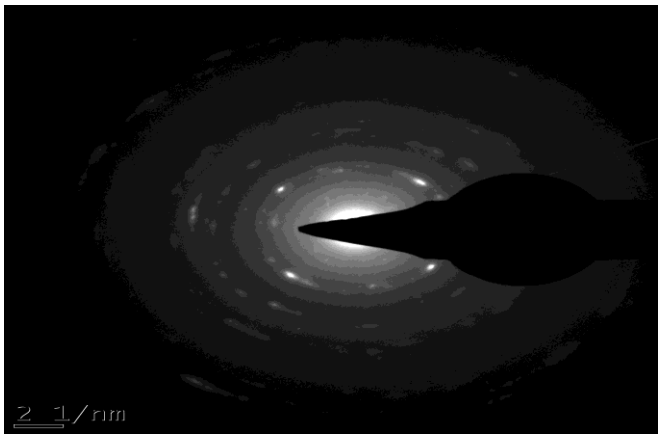

Plate V: SAED image of Fe-Ni/kaolin catalyst

4.4 Characterization of Synthesized Carbon Nanotubes (CNTs)

4.4.1Thermo gravimetric analysis of synthesized CNTs

Figure 4.10(a-c) summarized TGA curves of as-synthesized CNTs, purified CNTs and samples deposited with AgNPs examined under O_2 atmosphere.

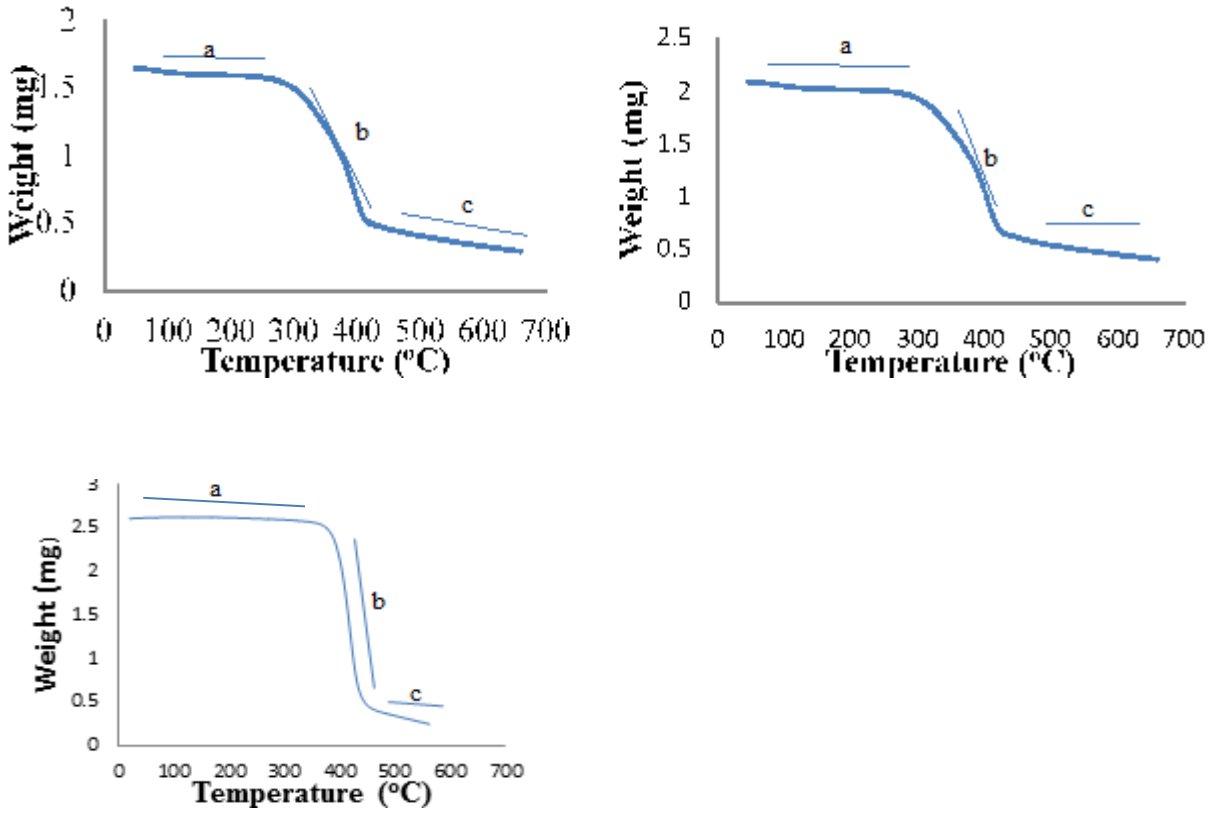

Figure 4.10: TGA Profile of (a) As-synthesized CNTs (b) Purified CNTs (c) Ag-CNTs

From Figure 4.10, the synthesized nanotubes consist of three different regions; (a, b and c) that is, initial, main and char decomposition region. The initial weight loss for both as-synthesized and purified CNTs around 0-300 °C can be attributed to the removal of water (ambient moisture). The changes of the thermal properties and weight loss of these samples at higher temperatures from around 300-420 °C are due to some physical damages occurring mostly to the amorphous carbon content. Herein, the main thermal stage (second region) occur in this region where the weight loss is significant. However, it is stated by Montazer *et al.* (2012) that the TGA of as-synthesized CNTs depends on various parameters such as irregular carbon cages, diameters of tubes and structural defects. In relation to the Ag doped CNTs nanocomposites, Figure 4.10 (c) showed decomposition at higher temperature

compared to both as-synthesized and purified carbon nanotubes. Although silver is an effective oxidative catalyst owing to their ability to split oxygen molecules into atoms, thus adsorbing those atoms lightly on the surface and providing sites for the oxidation of oncoming chemical compounds (Serve *et al.*,2019).The residual mass of silver doped CNTs examined was less than that of as-synthesized CNTs. The observed differences between as-synthesized and purified CNTs could be as a result of thermal oxidative destruction of the former which resulted from the defect site along the CNTs wall. Purification process introduces the defect sites and therefore provides the purified CNTs with enhanced air stability. Implying that the purity and crystalline carbon content of CNTs increases slightly from 63.83 % to 69.76 % after purification. This further suggest that the purified CNTs has a better thermal stability compared to as-synthesized CNTs. In summary, the results of this study indicated that the process produced highly thermal stabilized Ag-CNTs and the particles were neither damaged nor derivatized by the deposition process (Verma and Maheshwari 2019).

4.4.2 Surface area, pore volume and pore size of synthesized CNTs

The surface area, pore volume and pore size of the prepared materials (as-synthesized are presented in Table 4.6.

Table 4.6: BET Analysis

	As-synthesized CNTs	P- CNTs	Ag-CNTs
BETsurface area(m^2/g)	244.40	268.40	1068
Pore volume(cm^3/g)	0.086	0.105	0.381
Pore size (nm)	3.040	3.287	6.503

Therein, the N_2 adsorption-desorption isotherms of the as-synthesized CNTs, purified CNTs and Ag-CNTs at -196°C and relative pressure (P/Po = 5.84 x 10^{-2} to 0.307) are of a typical type IV hysteresis loop, which revealed the mesoporous properties of the adsorbent materials. The BET surface area of the as-synthesized CNTs was found to be 244.4 m^2/g. After purification processes, the BET surface area was recorded to be 268.40 m^2/g. The results indicate that the purification process led to an increase in the specific surface area of the nano-adsorbents (Burakova *et al.*, 2018). The increased specific surface area could be responsible for more active site on the adsorbent surfaces, which is of advantage to the occurrence of the redox reaction, and then improve the capacitance performance of the material (Cuong *et al.*, 2019). Further, the increase in the pore size of the purified CNTs facilitates the transport of particles during adsorption process, which enhances the performance efficiency of the adsorbent materials (Li *et al.*, 2016).BET surface area of Silver doped CNTs was found to be 1068 m^2/g which indicates a higher increase in the surface area. This increase in surfaces area could be attributed to the exterior space created by silver nanoparticles doped on the CNTs surface which have hollow structures with lower density as compare to synthesized nanoparticles (Mohammadreza *et al.*, 2020).Based on the International union of pure and applied chemistry (IUPAC) classification, pore size less than 2 nm are micro-porous in nature, material within 2-50 nm are mesoporous, while greater than 50 nm are said to be macroporous (Fletcher, 2008). Thus, the pore size of the prepared nano-adsorbent in this study revealed that they are mesoporous in nature (Table 4.6) In general, the obtained results thus confirmed the effectiveness of the purification process. Similar observations were reported by Aliyu *et al*. (2017) who reported increase in surface area of CNTs after purification.

4.4.3 HRSEM and EDX analysis of synthesized CNTs

The HRSEM images as presented in Plate VI (a) shows the possession of long-strands curly branched tube-like structure of agglomerated carbon nanotubes as indicated by arrows. An attempt was further made to investigate the effectiveness of the purification process using the HRSEM techniques (Plate VI b). The result showed that the P-CNTs are filaments with curve and interwoven web-like structures with shiny tips. The image (plate VII c) also indicates a typical structure with diameters size of from 16 to 38 nm (plate VII a), which is a characteristic properties of the MWCNTs produced by CVD techniques (Madian *et al.*, 2017).

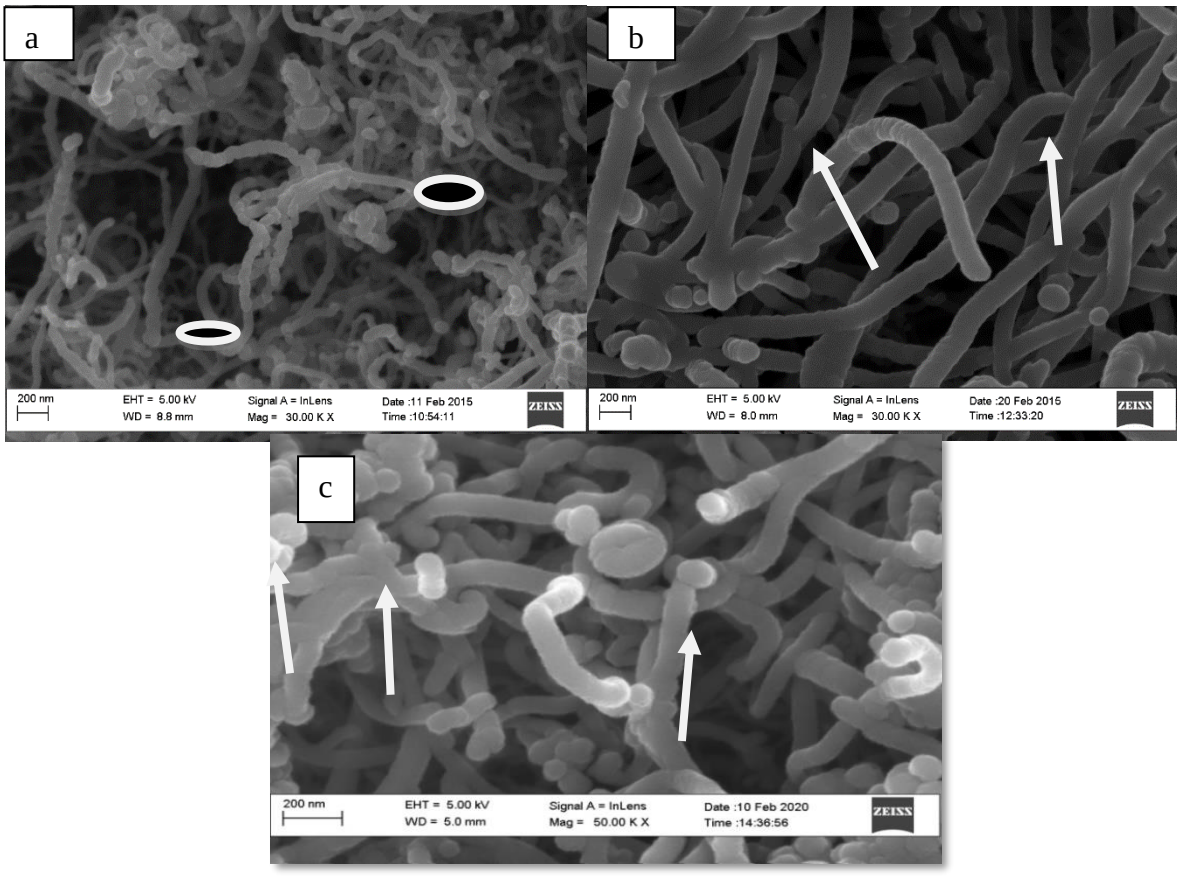

Plate VI: HRTEM micrograph (a) As-synthesized CNT (b) purified CNTs(c) Ag-CNTs

As depicted in plate VI (c), the HRSEM micrograph of Ag-CNTs were taken to verify the presence of synthesized nanoparticles on CNTs surfaces. The results affirm the deposition of silver on CNTs with indication of white crystals of Ag^0on the CNTs wall. Furthermore, the image demonstrates that upon incorporating silver nanoparticles, the carbon nanotubes (MWCNT) had shrunk in size when compared to that of purified CNTs, but equally kept its tube-like structure for a long time before its cleavage (Plate VI c).

Table 4.7 present the elemental composition of the synthesized CNTs. Higher content of metallic impurities were observed from the EDX results of as-synthesized carbon nanotubes. However, less content of metallic impurities were present in the purified CNTs samples. The presence of metallic impurities observed in these results could be attributed to the calcination process employed during the preparation of the samples.

Table 4.7: Energy dispersive x-ray (EDX) spectroscopy analysis of carbon nanotubes

Composite Samples	C	Ag	O	Al	Si	Ti	Fe	Ni	Cu
As-synthesized	91.59	-	3.02	1.41	1.35	0.05	1.62	0.86	0.10
P-CNTs	95.06	-	1.11	0.88	1.17	0.04	0.89	0.72	0.13
Ag-CNTs	85.82	5.65	5.86	0.9	0.87	0.08	0.45	0.26	0.11

According to EDX results shown in Table 4.7, the atomic weight (relative %) of metallic silver deposited on CNTs surface was 5.65 %. Other elemental compositions of silver doped CNTs reveal the presence of C, O, Fe, and Ni with other insignificant amount of metallic impurities.

4.4.4 High resolution transmission electron microscopy (HRTEM) of synthesized CNTs

The HRTEM micrograph of as-synthesized, purified CNTs and silver doped CNTs were obtained for more detailed morphology and diameter of the material. Plate VII (a) reveal a representative HRTEM image of carbon deposits grown on the surface of kaolin supported iron and nickel catalyst (as-synthesized CNTs). A high density of CNTs indicating a cluster of tube-like structures were observed, which cover thickly the catalyst particles. The as-synthesized CNTs contain some non-CNTs material such as the residual growth catalyst and the catalyst support. The HRTEM results as presented showed that the wall structure of CNTs vary, and their diameter distribution are not the same. Further, plate VII (b) reveal that the purified CNTs were predominantly consist of multiple layers. The image indeed demonstrates the well-graphitized wall structure without any indication of amorphous carbon coverage. The inner pore diameter of the P-CNTs is 6.9 nm, while the external diameter of the P-CNTs wall is 15.63 nm.

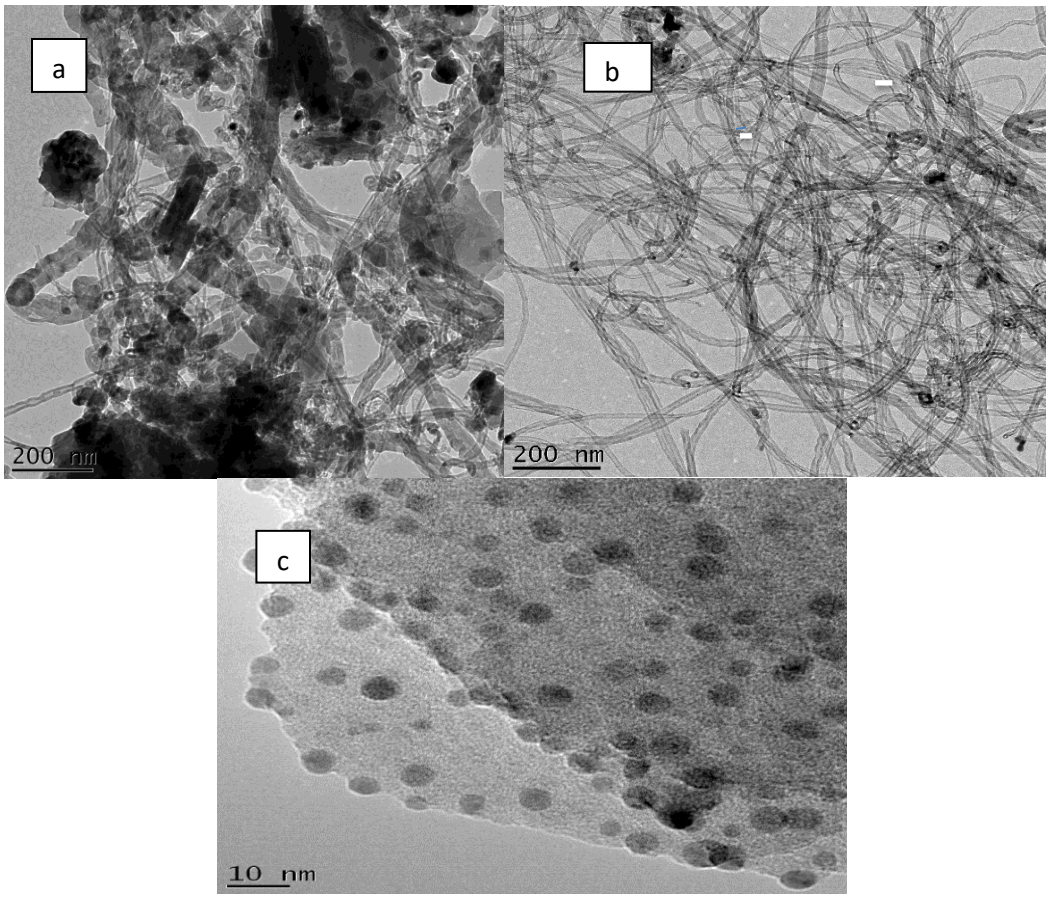

Plate VII: HRTEM micrographs of (a) unpurified CNT (b) purified CNT (c) Ag-CNTs Nano composites

Presented in plate VII (c) is the HRTEM result of Ag doped CNTs nano composites. It should be mentioned that it was AgNPs that were condensed within the lattice fringes of the CNT multi-layers, which was further confirmed by EDX result presented in Table 4.7.The distinct morphological features of these Ag nanoparticles are circular protrusions highly dispersed on the grafted CNT surface.

4.4.5 Selected area electron diffraction (SAED) of carbon nanotube

Plate VIII (a-c) presents the SAED pattern of As-synthesized CNTs, purified CNTs and Ag doped CNTs. The face centered cubic (FCC) patterns was found consistent with that of carbon nanotubes in both cases of purified and unpurified CNTs. There is presence of metallic impurities on the SAED pattern of as-synthesized CNTs as suggested by lighter areas as shown in Plate VIII (a) (Aliyu *et al.*, 2017).

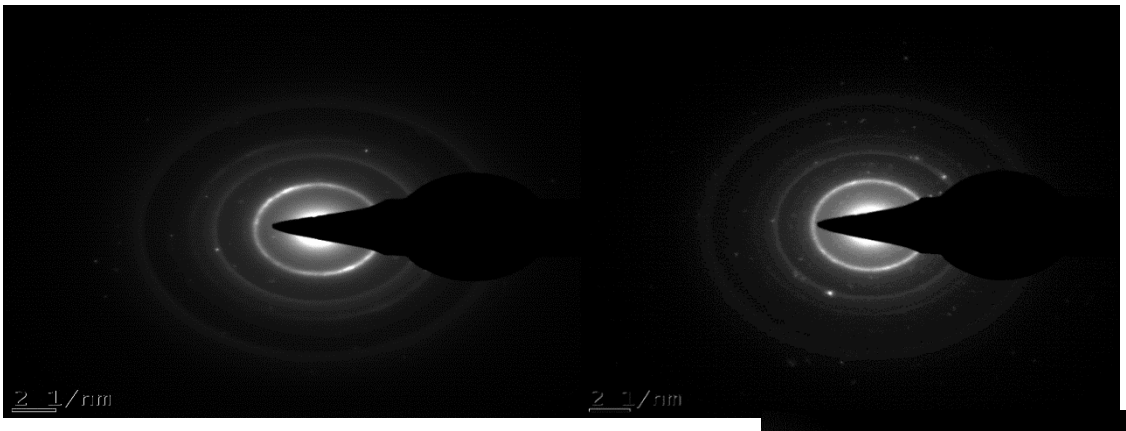

a

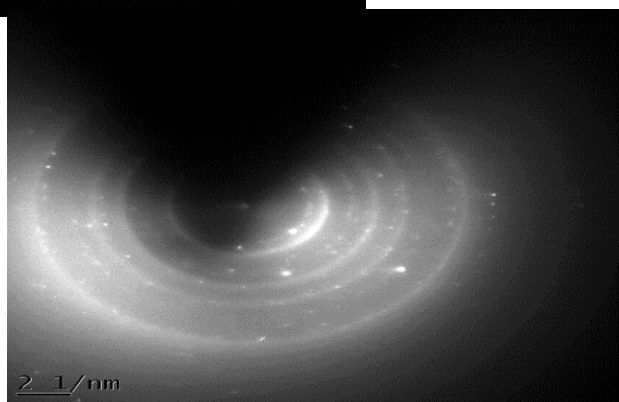

Plate VIII: SAED patterns of (a) As-synthesized CNTs (b) purified CNTs (c) Ag-CNTs

The obtained pattern were in line with was observed in HRTEM result of as-synthesized CNTs where the amorphous region and the entrapped impurities noticed on the micrograph may be ascribed to the period of time when the CNTs were removed from the electrical furnace. After purification process with the acids, the electron diffraction patterns revealed that the lighter areas in the FCC pattern becomes darker indicating that the catalyst residues were successfully removed. Thus implying that the surface area of the carbon nanotubes has increased (see Plate VIII b).

As shown in plate VIII (c), the multiple graphitic layer reveal an estimated values of 0.332 nm for the distance between two grapheme layers of Ag-CNTs nanocomposites. This obtained value is closely related to the figure reported by (Wu *et al.*, 2006) who employed CVD method for the synthesis of CNTs.

4.4.6 X-ray Diffraction (XRD) analysis of synthesized CNTs

As-synthesized CNTs along with purified and Ag doped CNTs were further characterized using powdered X-ray diffraction techniques to verify the mineralogical phase of the materials. As presented in figure 4.11, the XRD patterns of as-synthesized CNTs samples showed only two prominent diffraction angles. The patterns shows major peaks around 2Ɵ value of 26^0 and 44^0 with a corresponding plane of (002) and (100) which are usual characteristic planes for graphite-like carbon of the CNTs. The peaks were found at 30.49, 52.68, and $61.80^0$are indexed as the (110), (220) and (211) planes of kaolin. The peak around 34.88^0can be assigned to the (111) reflection of bi-metallic oxide ($NiFe_2O_4$)

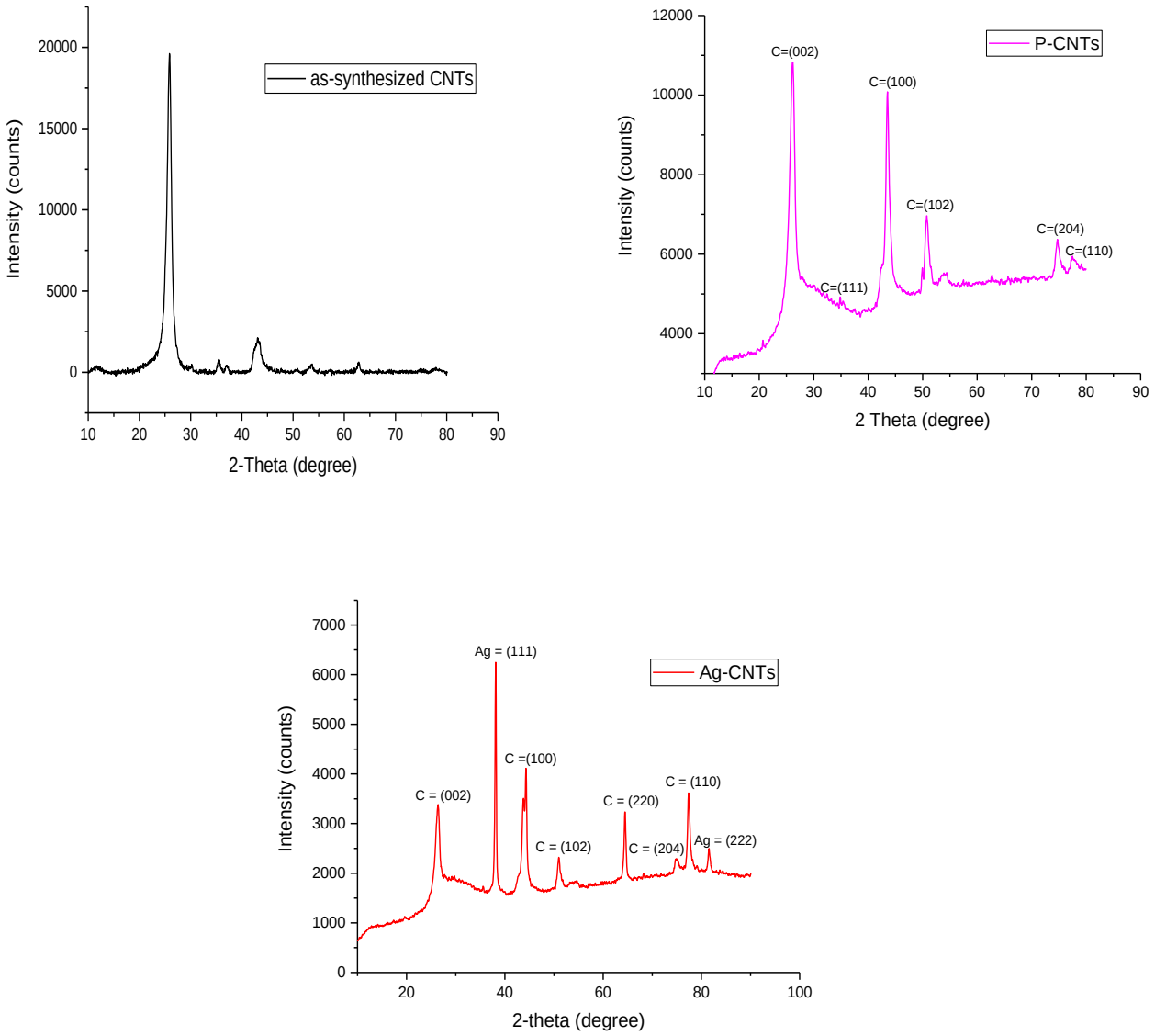

Figure 4.11: XRD Patterns of (a) as-synthesized CNTs (b) P-CNTs (c) Ag-CNTs

Also in Figure 4.11b for the purified CNTs the peaks appeared at 26.21^0, 43.47^0 and 74.72^0 are indexed as the (002), (100), and (204) planes of carbon, it was observed that more peaks of carbon came up which might be as the result of the removal of residue metal particles from the as-synthesized CNTs. Similar to the XRD results of the Ag-CNTs are shown in

Figure 4.11 (c). Only one characteristic peak was noticed at 2-theta value of 26.30°, which is attributed to the (002) plane of CNTs. The peaks at 38.13^0, 44.05^0, 64.45^0, 75.04^0, $77.42^0$and 81.56^o can be assigned to (111), (100), (220), (204), (110), (222) reflections of the face-centered lattice of Ag. No extra peaks were observed near the reflection angles of both AgNPs and CNTs, indicating a highly crystalline nature of the prepared adsorbent. This observed phenomenon in the XRD patterns of Ag-CNTs composite matches with the SAED pattern depicted in plate VIII (c).However, the crystallite sizes of the purified CNTs and silver doped CNTs were calculated from the XRD patterns based on the Debye Scherrer equation, and the results showed the average crystallite sizes to be 13 nm and 18 nm respectively.

4.3.7 Fourier transforms infrared spectroscopy (FTIR) of as-synthesized and purified carbon nanotubes (CNTs)

Figure 4.12 presence of C–C and C–O bending bond within the ranges of 800 cm^{-1}–1400 cm^{-1}, which is generally identified as the fingerprint region, was linked to the exposure of the MWCNTs to the surrounding environment after synthesis (Abdulkareem *et al.*, 2017). while the band wave number at 3759 cm^{-1} indicates the – OH vibrational bond that is out of the plane, which is a little higher than 3688 cm^{-1} which was similar to the report of Buang *et al.* (2012). The peaks at 1497 and 1902 cm^{-1} represents the possible presence of C=C double bond resulting from incomplete decomposition of acetylene during the catalytic cracking of the gaseous hydrocarbon material. The peaks at 1733 cm^{-1} presented the C=O group. The increase in the peak intensity of the C-H stretching mode at 2500 cm^{-1} and 2848 cm^{-1} suggests that oxidation of the CNTs successfully introduced the carboxylic group (-COOH) on the walls of carbon nanotubes.

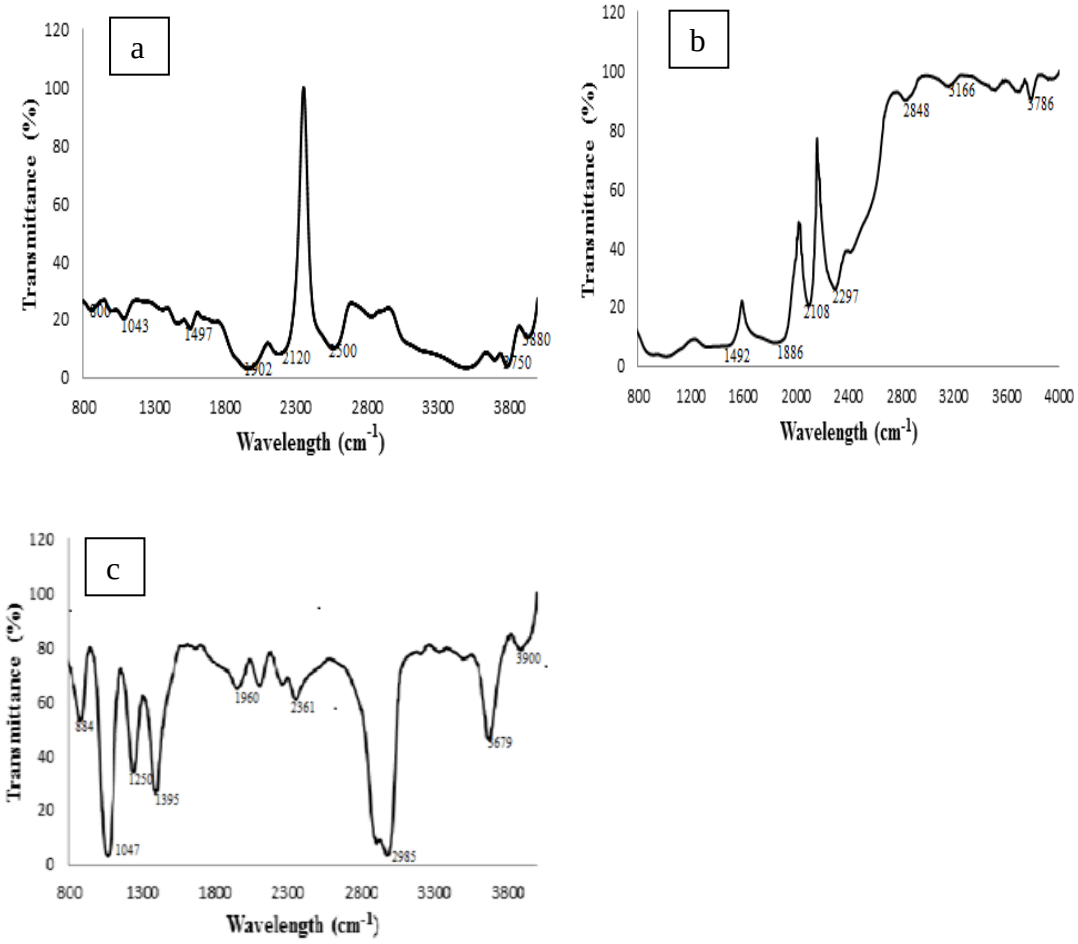

Figure 4.12: FTIR spectra of (a) as-synthesized CNT (b) purified CNT (c) Ag-CNT

The FTIR spectrum in Figure 4.12was employed for the surface functional group identification on chemical substances. The band wavenumber at 3894 cm^{-1} indicates the –OH vibrational bond that is out of the plane. The peak at 1926 cm^{-1} represents the possible presence of C=C double bond resulting from incomplete decomposition of acetylene during the catalytic cracking of the gaseous hydrocarbon material. Furthermore, the presence of C-C bending was observed at 864 and 1047 cm^{-1} (Ishaq *et al.*, 2018). The appearance of a peak approximately at 1378 cm^{-1} corresponds to the C— stretching, indicating the interaction and perturbation at the CNT surface due to adherence of metal particles .which is in agreement

with Hemant *et al.* (2015). The band at 1225 $cm^{-1}$was due to nitrogen-oxygen stretch bond. The functional groups obtained were in good agreement with the work of Anwar and Arthanareeswaran, (2019) who observed 1230 cm^{-1} of N-O bond. In addition, the 2951 cm^{-1} peak correspond to C-H stretching.

4.5. Physicochemical Parameters of Fish Pond Wastewater

4.5.1 Physicochemical parameters of fish pond wastewater before and after adsorptions

The wastewater samples were characterized for their physicochemical properties before and after adsorption process. The results are presented in Table 4.8. Along with the maximum required limit for drinking water WHO (2009); NESREA (2011).

The pH of fish pond wastewater sample was 7.88. While the pH value varied between 6.74 and 6.61 in the treated wastewater samples for P-CNTs and Ag-CNTs respectively. The results shows that the pH values reduced to the range of permissible limits set by NESREA standards (6.5-8.5) after treatment process, indicating that the treated wastewater sample is almost neutral. Up till now, pH measurements is a simple parameter which have direct influence on the solubility (amount that can be dissolved in the water) and biological availability (amount that can be utilized by aquatic life) of chemical constituents such as nutrients and heavy metals. The degree to which heavy metals are soluble determines their toxicity. Any substance or solution that is highly acidic or alkaline would affect the solubility, mobility and metal toxicity in the water and consequently kill marine lives living within the environment (Lokhande *et al.*, 2011). As such, the pH measurement possess some important properties in deciding the quality of wastewater. According to WHO classification, waters with pH value range of 6.5-9.0 are good for most aquatic creatures, while the range of pH values desirable for water prescribed as human tolerable levels by (WHO) and

(NESREA) standards is 6.5 to 8.5. (WHO, 2009; NESREA, 2011).Based on this fact, it can be concluded that the treated water can be reuse for a wide array of domestic purposes.

Table 4.8: Physicochemical parameters of fish pond wastewater before and after treatment with maximum permisible limit at different conditions of dosage (0.4 g/50 cm^3) Temperature at 60 ^{0}C, contact time of 100 min and stirring speed of (120 rpm)

Parameters	Raw water	Treatment using P-CNT	Treatment using Ag-CNT	WHO/NESREA
pH	7.88	6.74	6.61	6.5-8.5
Conductivity(µs/cm)	397	7.94	6.82	200
Nitrate (mg/l)	6.22	0.56	0.51	10
Phosphate(mg/l)	1.66	0.02	0.01	0.5
Chloride (mg/l)	252.57	8.31	9.70	250
DO (mg/l)	3.07	6.48	8.0	8-10
BOD (mg/l)	6.50	4.50	3.8	10/5-7
COD (mg/l)	42.64	39.25	35.75	40
TDS (mg/l)	240.10	3.00	2.83	500
Manganese (mg/l)	1.435	0.73	0.144	0.40
Zinc (mg/l)	3.75	2.56	1.22	3.00
Iron (mg/l)	4.43	0.64	0.108	0.3
Bacteria (cfu/ml)	7.2×10^2	65.0	0.00	-
TA (mg/l)	78	15.23	5.53	0-0.05
Ca (mg/l)	54.68	56.90	49.62	25-200
Na (mg/l)	16.59	13.96	13.72	200

K (mg/l)	3.80	3.24	3.19	12
Mg (mg/l)	10.41	10.36	8.48	50

The total dissolve solids are the inorganic matters and small organic matter which are present in water, the WHO and NESREA standard for the total dissolved solids (TDS) is 500 mg/l but for this sample, the TDS value for the raw wastewater sample was recorded to be 240 mg/L. After the wastewater sample undergoes treatment process with the nanoadsorbents, the TDS values obtained for P-CNTs and Ag-CNTs were 3.00 mg/l and 2.83 mg/l, respectively. Based on the obtained results, the TDS concentration values all lies below the permissible limit set by NESREA (500 mg/L).TDS gives information on the level of both organic and inorganic dissolved compound which may increase the turbidity of water (Khan *et al.*, 2013). Salt like chloride, sulphate, carbonate, bicarbonate, phosphate, and nitrate of sodium, magnesium, potassium, calcium, manganese and iron are found dissolved in water bodies. They are known to increase the density of water and affects the osmoregulation of freshwater in aquatic organisms, reduces the availability and utility of oxygen, water for drinking, irrigation and other industrial purposes. Conductivity is the ability of any medium, to carry an electric current, the presence of dissolved solids such as calcium, chloride, and magnesium in water samples carries the electric current through water. According to WHO and NESREA the maximum allowable level of conductivity is 200 μS/cm. The results obtained showed that the measured conductivity of the wastewater samples is 397 μS/cm while treated water samples are 7.94 μS/cm and 6.82 μS/cm for P-CNTs and Ag-CNTs respectively. Conductivity does not have direct impact on human health, but high conductivity may lead to lowering the aesthetic value of the water by giving mineral taste to

the water (Rahmanian *et al.*, 2015). The values of phosphate, nitrate, total ammonium. Dissolved oxygen, biological oxygen demand and chemical oxygen demand (PO_4,NO_4,TA,DO,BODand COD) measured in the aquaculture wastewater were significantly higher than the values observed in the treatment of wastewater. These differences could be explained by the ability of nanoadsorbents in removing nutrients and other related pollutants in aquaculture wastewater. Which is an indication that the pollutants in aquaculture wastewater are biodegradable. The DO value recorded in waste water is 3.07 mg/L this lower DO level in the wastewater may be as result of high aerobic microbial activities (BOD) and chemical oxidation demand which are indicators of pollution. Lower DO ranged of 3.00 mg/L to 3.20 mg/L was reported by (Omitoyin *et al.*, 2017) in wastewater drained from shrimp ponds. This is reflection of higher biodegradable organic substances from uneaten feed, fish fecal wastes and metabolites from microbial activities in the discharged wastewater. The low BOD value of wastewater was recorded as 6.50 mg/L which is higher than the value obtained from the treated wastewater 0.75 mg/L and 0.5 mg/L for P-CNTs and Ag-CNTs respectively (Ogwo and Ogu 2014) reported that high COD in aquaculture wastewater may be ascribed to the presence of high organic matter. Though the value of COD in wastewater (42.64 mg/L) was higher than WHO and NESREA value (40 mg/L)and values of treated wastewater which are 0.03 mg/L and 0.01 mg/L for P-CNTs and Ag-CNTs respectively.

Similarly, the parameters like phosphate, Nitrate and TA in the wastewater were higher than the values in treated wastewater, these maybe as a result of leached nutrients from fish feed which are proteinaceous feed components. The phosphate value in the wastewater is 1.66 mg/L which was higher than the phosphate values of treated wastewater is 0.02 mg/L and

0.01mg/L P-CNTs and Ag-CNTs respectively. It was reported that phosphate levels above 1.00 mg/L could prevent coagulation of wastewater in water treatment system (Omitoyin *et al.*, 2017). The nitrate value of 6.22 mg/L recorded in wastewater was higher than the nitrate values of treated wastewater is 0.56mg/L and 0.51 mg/L for P-CNTs and Ag-CNTs respectively. While TA of 78 mg/L for wastewater and the value for the treated water are 15.23mg/L and 5.53 mg/L for P-CNTs and Ag-CNTs respectively the WHO and NESREA limit of phosphate, Nitrate and TA are (0.5, 10, 0-0.05).The result of bacterial analysis showed that the bacterial count may be due to differences in management practices resulting in different level of organic loads in the pond system from the diet used in feeding the fish (Oni *et al.*, 2013).The source of microorganisms could be traced to sources of water fed into the pond. Bacterial counts of aquaculture wastewater was 7.2 $x10^2$ cfu/mL which is much higher than the values of treated wastewater which are 65.0 cfu/mL and 0.00 cfu/mL for P-CNTs and Ag-CNTs respectively. However in this study the chloride ion is 252.57 mg/Lin the wastewater which is slightly beyond acceptable limit of NESREA (2011) guideline value (250 mg/L)and the chloride value treated water are 8.31 mg/L and 9.70 mg/L for P-CNTs and Ag-CNTs respectively.

Table 4.8 shows the concentration of the selected heavy metal in aquaculture wastewater and revealed these metals in different proportions hence; the need to either completely remove or reduce the level of this contaminants in the wastewater before final discharge into the environment, in order to address this issue. Silver doped multi walled carbon nanotubes adsorbent synthesized was used for the adsorption of the selected heavy metals.

4.5.2 Adsorption parameters

In this study, influence of parameters such as contact time, adsorbent dosage and temperature on the removal efficiency of the selected heavy metals by nano-adsorbents were investigated.

4.5.2.1 *Effect of contact time*

The effect of contact time on nano-adsorbents are shown in Figure 4.13a and Figure 4.13b.It can be seen from Figure 4.13 (a) and (b) that the amount of the heavy metals removal increases slightly with increase in time irrespective of the nano-adsorbents and in both cases, a very fast adsorption rate was noticed and the optimum time for removal of Mn, Zn and Fe are 60 min,40 min and 60 min for P-CNTs while the optimum time for removal of Mn, Zn and Fe were60 min for Ag-CNTs.

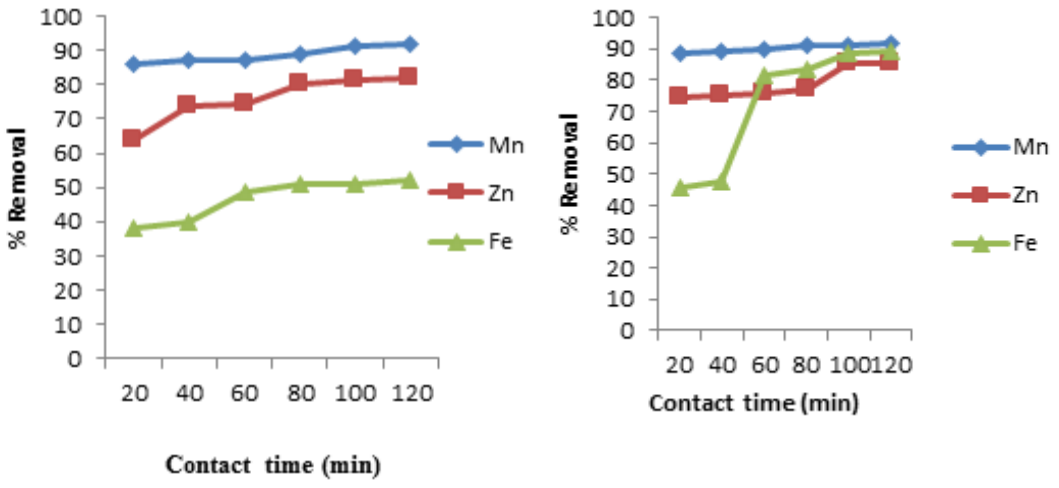

Figure 4.13: Effect of contact time on percentage removal of heavy metals on (a) P-CNT (b) Ag-CNT (adsorbent dosage (0.1 g), stirrer speed (120 rpm), and temperature (25 ^{0}C) volume of fish pond wastewater (50 mL), stirring time (90 min)

The equilibrium time occurred in the three metals (Mn, Zn and Fe**)** removal for the P-CNTs is at 100 minutes, at this time the amount of the heavy metals desorbing from the adsorbent

countered balanced the amount of the heavy metal being adsorbed onto the CNTs. The time required to attain this state of equilibrium is termed the equilibrium time and the amount of heavy metals adsorbed at the equilibrium time reflects the maximum adsorption capacity of adsorbent under those operating condition.

The efficiency of pollutants removal in relation to treatment time is shown in Figure 4.13 at the maximum percentage reduction achieved after a total treatment time of 120 min was Mn (91.85%), Zn (81.60%), and Fe (52.14%) respectively this higher value of Mn could be attributed the initial concentration of the heavy metals in the wastewater(Chaudhry *et al.*, 2016), (Mn is1.435 mg/g, Zn is 3.750 mg/g, Fe is 4.429 mg/g)which is fundamental to the mass transfer of molecules from the liquid to the solid surface during adsorption process and is also time dependent. This Equilibrium was achieved for Mn, Zn and Fe at 100min, the capacity for adsorption onto Nanoadsorbent is pore filling due to its porous nature in addition to other interfaces such as hydrogen bonding, cation exchange, electrostatic attraction, surface precipitation and so on, which rely on the characteristics of the porous nature of the adsorbent and the adsorbate characteristics. As the treatment time increased, the adsorbent sites had affinity towards saturation and equilibrium, which described the adsorbent-adsorbate affinity (Anijiofor *et al.*, 2018).

In other words, fast initial adsorption rate may be due to the higher driving force thus leading to the fast transfer mechanism between the adsorbed metals and the active site of the adsorbent. The percentage metal ions removed at equilibrium time of 60, 80 and 90 minutes for Mn (91.85 %), Zn (81.60%), and Fe (52.14%).

Figure 4.13b also shows that as the contact time increases, a corresponding increase in adsorption of the selected heavy metals was observed. It can also be observed at the initial stages, the slope was greater and later decreased with time suggesting that the rate of adsorption was rapid in initial stages and gradually decreases and subsequently become constant when equilibrium was attained 100 minutes amounting to Mn 91.92 %, Zn 88.53 % and Fe 89.23 % respectively. The maximum adsorption capacities of these metals are 0.116mg/g, 0.43 mg/g, and 0.477 mg/g. In similar manner, the optimum time for Mn, Zn and Fe are 60min while the three of them attained equilibrium at 100 min. Their percentage removal and adsorption capacities are Mn 88.64 % and 0.163 mg/g, Zn 74.40 % and 0.96 mg/g, Fe 45.69 % and 2.405 mg/g. the order of adsorption of heavy metals using Ag-CNTs in decreasing order are Mn> Fe>Zn. in decreasing trend order due to decreasing in ionic radius. It can be seen that equilibrium time is metal dependent adsorbent specific. Therefore, 100 minutes was considered to be sufficient for adsorption of heavy metals on Ag-CNTs. The Ag-CNTs successfully removed more of the metal ions than P-CNTs suggesting greater interaction between the adsorbent and the adsorbate in the former than the later. Alternatively, possible reason for high adsorption efficiency of Ag-CNTs may be due to its large surface area and pore sizes (BET in Table 4.6), crystallinity nature (TEM and XRD in Plate VII and Figure 4.11) and functional attachments(FTIR in Figure 4.12).

4.5.2.2 *Effect of Adsorbent Dosage*

The adsorbent dosage parameter has pronounced effect on the removal of adsorbate species from wastewater. In this study, the effects of different P-CNTs dosage (from 0.1 – 0.5g) on the selected heavy metals removal from fish pond wastewater were investigated. According to Figure 4.14a, it can be seen that the percentage removal increases with increasing amount

of adsorbent (up to 0.4 g/l for selected metals) except for Fe which was 0.2 g/l. From the three selected heavy metals, Mn was removed faster followed by zinc and iron, the removal efficiency increased for Mn increased from 40.00 to 48.92 % upon increasing the adsorbent from 0.1 to 0.5 g/l and Conversely, the percentage removal for Fe was low compared to the other selected heavy metals which however increased from 6.0 to 30.45 % with the maximum removal efficiency achieved under optimum dose of 0.5 g/l.

The effect of the Ag-CNTs dosage is shown in Figure 4.14b, the removal efficiency was found to increase proportionally with the amount of the Ag-CNTs until equilibrium was established and

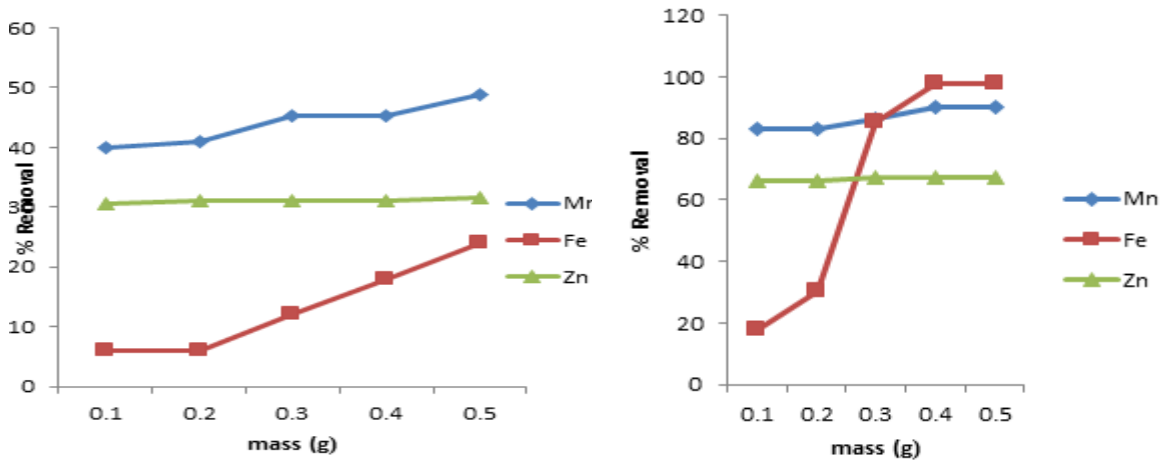

(a) **(b)**

Figure 4.14: Effect of dosage on percentage removal of heavy metals on (a) P-CNT (b) Ag-CNT (Experimental conditions: stirrer speed (120 rpm) and temperature (25 ^{0}C)volume of fish pond wastewater (50 mL), stirring time (90 min).

Afterwards, the removal efficiency remained constant despite the increment in the dosage of Ag-CNTs. Figure 4.14b shows the increasing of Ag-CNTs mass from 0.1 g to 0.3 g sharply enhances the percentage adsorption of Mn from 82.87 to 86.40 %, Zn from 66.45 to 67.09 % and Fe from 18 to 85.35 %. It was observed between 0.1 to 0.3 g for these three metals and

increasing Ag-CNTs mass above 0.3g had no effect on the increase in removal efficiency of the Mn and Zn but negligible effect on Fe in fish pond wastewater. In the same vein, increasing Ag-CNTs mass from 0.1 to 0.4 g increased the percentage adsorption of Mn from 82.87 to89.97 %, Zn from 66.45 to 67.30 %, Fe from 18 to 97.56 %. The observed increment in the removal efficiency may be ascribed to the availability of more adsorption sites for the metal ions adsorption Mohammad and Malack, (2016). The maintenance in adsorption uptake despite increase in adsorbent dosage is mainly due to saturation of adsorption sites through the adsorption reaction and subsequently resulted to desorption Nasir and Sohailer, (2010) comparatively, the results in Figure 4.14a and Fig 4.14b revealed that Ag-CNTs adsorbs heavy metal ions better than P-CNTs due to high surface area of the former than the latter.

4.5.2.3 *Effect of temperature*

The effect of temperature on removal efficiency of the selected heavy metal ion from fish pond wastewater was carried out and the result is shown in Figure 4.15a.

It was observed that increasing the temperature from 30^0 C to 70^0 C, gives a corresponding increase in the adsorption capacity and removal efficiency of heavy metal ions onto P-CNTs was observed. The removal efficiency increased from 36.93 % to 46.89 % for Mn, 81.17 % to 81.33 % for Zn and 72.16 % to 86.14 % for Fe as temperature increased from 30 to 60^0 C. This implies that the optimum temperature to achieved sufficient removal of Mn, Zn and Fe 60^0C. On the other hand, increasing the temperature beyond 60^0 C did not have a significant on the removal efficiency of the selected heavy metals in fish pond wastewater. Therefore, results showed that the removal of heavy metal ions using P-CNTs was potentially and comparatively favored at high temperature than lower temperature this is because of increase

in the mobility of metal as a result of temperature increment and sufficient interactions with the active sites. Moreover, an increasing temperature produced a swelling effect within the internal structure of adsorbent which invariably increase the rate of penetration of the active sites on the adsorbent by the metals (Nasir and Sohailer, 2010; Hongxia *et al.*, 2014).

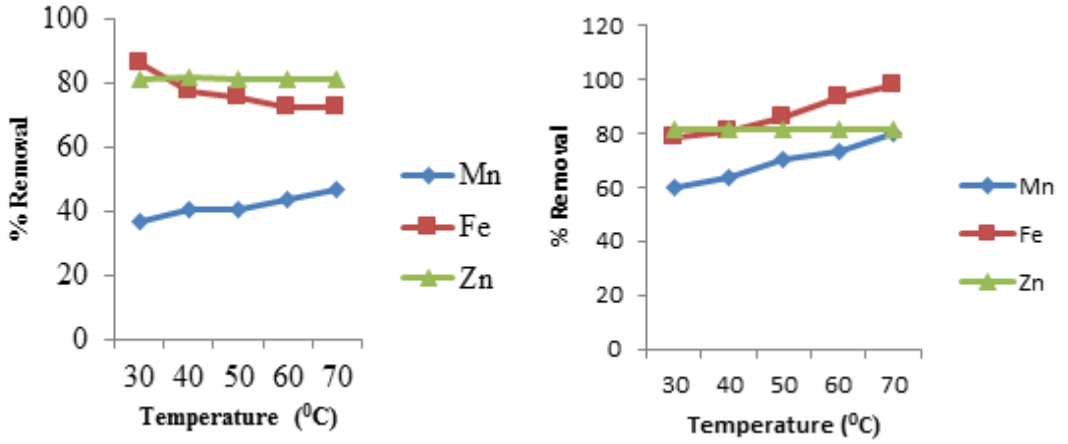

(a) **(b)**

Figure 4.15: Effect of temperature on percentage removal of heavy metals on (a)P-CNT, (b)Ag-CNT (Experimental conditions: stirrer speed(120 rpm),and dosage (0.4 g)volume of fish pond wastewater (50 mL), stirring time (90 min)

In Figure 4.15a shows a similar trend to Figure 4.15b, as the temperature increases from 30 to 70^{0}C was observed. The percentage removal and the adsorption capacity for all the selected metal increases for the chosen temperature range. The study undertaken here is governed by endothermic adsorption process. In the case of Mn, the removal efficiency was increased from 60.21% to 73.45% and Fe, from 73.59% to 93.65% and Zn from 81.89% to 81.52% as temperature increased from 30^{0}C to 60^{0}C .The temperature increases the rate of diffusion of the metal ions from the bulk of the solution to the bulk of the adsorbent. Secondly, the increase of temperature increases the adsorption active sites which increases their activity towards the adsorption from the solution (Badawi *et al.*,2017) by Zn from

81.89% to 81.52%, as temperature increased from 30^0C to 60^0C.This increase in temperature may cause decrease in binding forces between the adsorbent and adsorbate and perhaps responsible for the reduction in the adsorption capacity of the adsorbents at high temperature (Bankole *et al.*, 2017).Hence, from this research Ag-CNTs exhibited improved adsorption efficiency than P-CNTs due to high surface area, availability of more binding sites, nature of the adsorbent, electrostatic interaction between the adsorbent and adsorbate.

4.5.2.4 *Adsorption isotherm*

The Langmuir and Freundlich adsorption isotherm model were used to test the result of the adsorption process, to determine the model that best describe the adsorption mechanism. The value of regression correlation co-efficient (R^2) for the adsorption is used to determine which model indicates better applicability. The closer the value of R^2 to 1, the more fitting a model is for the adsorption process. (Sharma *et al.*, 2017).

Table 4.9: Isotherm parameters for the selected heavy metal removed from fish pond wastewater adsorption using purified CNTs and Ag-CNTs.

	P-CNTs			Ag-CNTs		
Isotherm parameter	Mn	Zn	Fe	Mn	Zn	Fe
Langmuir						
Kl (l/mg)	1.4478	0.3979	1.5390	8.1759	0.82473	10.1029
Q_0 (mg/g)	0.0137	0.0053	0.0397	0.06820	0.009871	0.12177
R^2	0.4952	0.1401	0.3424	0.8967	0.8697	0.6843
R_L	0.928	2.0320	0.1919	0.0931	0.4778	0.0228
Freundlich						
Kf	0.1753	6E+10	0.95120	0.1010	60.9223	0.6066
N	0.119	0.01618	0.51557	0.4329	0.0213	1.4073
R^2	0.5506	0.2821	0.8342	0.8499	0.7843	0.9274

The values of R^2 for Freundlich isotherm model is higher than that of Langmuir for the adsorption process of Mn on P-CNTs, a value of 0.4952 and 0.5506 were gotten for Langmuir and Freundlich isotherm respectively. Similarly, the uptake of Zn and Fe also follows the same trend with R^2 values of 0.1401 and 0.3424 for Langmuir, also 0.2821 and 0.8342 for Freundlich isotherm respectively. Another important parameter to consider before concluding if the Freundlich isotherm fits the adsorption mechanism better is the value of Freundlich correlation constant (*n)* adsorption is considered as satisfactory when the value of Freundlich constant *n* takes values between the ranges of 1 to 10. If *n* equals 1, this means that the adsorption process is linear; *n* greater than 1 indicates adsorption to be a chemical process and *n* less than 0 indicates that the adsorption process is a physical process. (Desta, 2013).Freundlich constant "*n*" values of 0.119, 0.01618 and 0.5156 are gotten for Mn, Zn and Fe respectively.

The values of *n* for Ag-CNTs is 0.4329, 0.0213 and 1.4073 with respect to Mn, Zn, and Fe which falls below zero. Likewise the R^2 values for Freundlich isotherm are 0.8499, 0.7843 and 0.9274 for Mn, Zn and Fe respectively, which is higher than 0.5506, 0.2821 and 0.8342 for Mn , Zn and Fe respectively which means that the isotherm follows Freundlich isotherm model. Qiang *et al*, (2017) reported that Freundlich model assumes that multilayer adsorption occurs. This suggests why the Freundlich isotherm fits the adsorption process on the multiwall CNTs walls which has multiple wall layers for adsorption.

4.5.2.5 *Adsorption kinetic studies*

The various adsorption isotherm parameters were calculated from the plots of the kinetic model equations and summarized with regression correlation coefficients *(R^2)* in Table 4.10. The relatively higher value is the more applicable model to the kinetics of heavy metals adsorption onto adsorbent. To investigate the adsorption kinetics, the pseudo first order and pseudo second order kinetic models were used.

Table 4.10: Kinetic parameters for the adsorption of selected heavy metals on P-CNTs and Ag-CNTs

	P-CNTs			Ag-CNTs		
Kinetic parameters	Mn	Zn	Fe	Mn	Zn	Fe
First order						
K(min)	0.0025	0.0228	0.0277	0.0022	0.012	0.0338
$q_e$exp(mg/g)	6.595	15.30	11.17	6.59	16.60	19.76
$q_e$cal(mg/g)	0.3575	3.6677	3.661	0.1347	4.2599	18.9714
R^2	0.0099	0.4265	0.3568	0.0078	0.6373	0.6924
Second order						
K (g/mg.min)	0.0490	0.0078	0.0073	0.0062	0.0062	0.0008
q_e(mg/g)	6.7024	16.3132	12.4378	6.6533	1.3310	27.5482
R^2	0.9992	0.9987	0.9927	0.9999	0.9869	0.9101
Elovich						
B	4.1305	0.5288	0.5421	7.6103	0.7224	0.1587
A	1E+09	57.6126	8.3197	5.74E18	1087.037	1.3550

R^2	0.8279	0.9523	0.8632	0.8952	0.6484	0.8582

As illustrated in Table 4.10, using the P-CNTs adsorbent, the first order model has R^2values of 0.0099, 0.4265 and 0.3568 for Mn, Zn and Fe respectively, which indicates that the first order model is not suitable for fitting the adsorption process, as the values of R^2 are not close to 1. On the other hand, using the Ag-CNTs adsorbent, the values of R^2 are 0.0078, 0.6373 and 0.6924 for Mn, Zn and Fe, this shows that the first order model does not fit the adsorption kinetic process for both the purified and Ag- CNTs adsorbents.

However, the second order parameters gotten shows higher value in correlation. 0.9999, 0.9869 and 0.9101 as the R^2 values for Mn, Zn and Fe respectively when the Ag- CNTs adsorbent was used. Likewise for the P- CNTs adsorbent, R^2values of 0.9992, 0.9987 and 0.9927 were gotten for Mn, Zn and Fe respectively. Which also shows best fit as the values are very close to 1.

Moreover the Elovich model has R^2valuesof 0.8279, 0.9523 and 0.8632 for Mn, Zn and Fe respectively for P-CNTs. While using the Ag-CNTs adsorbent, the values of R^2 are 0.8952, 0.6484 and 0.8582 for Mn, Zn and Fe respectively which indicates also that that the Elovich model is also suitable for fitting the adsorption process as the values of R^2 are also close to 1.

It can be observed that theR^2value of the pseudo-second-order kinetic model was higher than that of pseudo-first-order kinetic and the elovich model. The order of fitness of the kinetic model for the adsorption of Mn, Zn and Fe from the fish pond wastewater by Nanoadsorbents occurred in the following order; pseudo-second-order kinetic>elovich model>pseudo-first-order kinetic.

4.5.2.6 *Thermodynamic studies*

To study the adsorption thermodynamics, the fundamental parameter (Gibbs free energy (ΔG)) was determined in order to know the spontaneity of the adsorption process. Other thermodynamic parameters includes; Enthalpy (ΔH), and Entropy (ΔS) were also determined for both purified and functionalized CNTs as shown in Tables 4.11 and 4.12the ΔH value was calculated from the slope of the linear plot of lnKd versus 1/T. The standard entropy values (J/mol K), (ΔS), were calculated by using Gibbs–Helmholtz equation.

Table 4.11: Thermodynamic parameters of the selected heavy metals adsorption using P-CNTs

Adsorbate	Temp(^{0}K)	ΔH	ΔS kjmol^{-l}k^{-1}	ΔG (kjmol^{-l})
Mn	303	-13643.27	54.67453	-30209.66
	313			-30756.4
	323			-31303.15
	333			-31849.89
	343			-32396.64
Zn	303	104.5652	-13.6375	4236.714
	313			4373.088
	323			4509.463
	333			4645.837
	343			4782.212
Fe	303	-3475.418	6.294529	-5382.661
	313			-5445.606
	323			-5508.551
	333			-5571.497
	343			-5634.44

Table 4.12: Thermodynamic parameters of the selected heavy metals adsorption using Ag-CNTs.

Adsorbate	Temp(^{0}k)	ΔH	ΔS kjmol^{-1}k^{-1}	ΔG(kjmol^{-1})
Mn	303	-14773.98	35.7352	-25601.75
	313			-25959.11
	323			-26316.46
	333			-26673.81
	343			-27031.16
Zn	303	-336.717	15.1506	-4927349
	313			-5078.855
	323			-5230.362
	333			-5381.868
	343			-5533.743
Fe	303	-50910.78	138.2701	-92806.63
	313			-94189.33
	323			-95572.03
	333			-96954.73
	343			-98337.43

The values ΔG in Tables 4.11 and 4.12, the adsorption process was carried out over the temperature range of 303 to 343K.The negative values of ΔG show that the adsorption of Mn and Fe on purified CNTs is spontaneous, while that of Zn is not spontaneous, this implies that the process will proceed at this temperature range. It could be observed that the negative values of ΔG obtained increases with increase in temperature, this shows that increase in

temperature favors the spontaneity of the adsorption process. The negative values ΔH for Mn and Fe while Zn has positive values of ΔH for the adsorption on purified CNTs and the negative values of ΔH for the adsorption of Mn, Zn and Fe respectively on Ag-CNTs. The negative values of enthalpy (ΔH°) indicate that the nature of the adsorption is exothermic and its magnitude gives information on the type of adsorption, which can be either physical or chemical adsorption. Furthermore, the positive values of entropy (ΔS°) shows increase in the randomness at sorbate-solution interface during the adsorption process. A negative ΔG° value means the reaction is favorable. Increase in the value of ΔG° with rise in temperature show that the adsorption is more favorable at lower temperature (Jodeh *et al.,* 2015). Furthermore, the positive value of ΔS° signified a better adsorption of Ag-CNTs for the selected heavy metals and increase in randomness at the solid/liquid interface during the adsorption process (Chungsying, 2016).

CHAPTER FIVE

5.0 CONCLUSION AND RECOMMENDATIONS

5.1 Conclusion

This study involves the synthesis of silver doped multi walled carbon nanotubes for the treatment of fishpond wastewater.

1. Bimetallic catalyst on kaolin support Fe–Ni/kaolin was prepared via a wet impregnation method; at the experimental conditions of 8 g mass of support, oven drying temperature of 140 °C, oven drying time of 8 hr, and a stirring speed of 2400 rpm, and calcination temperature of 500 ^{0}C for 16 hrs and the catalyst prepared is suitable for the CNTs production. The prepared catalyst was used for the production of CNTs via the CCVD method, under the following experimental conditions 750 ^{0}C reaction temperature, 60 min reaction time, 230 ml/min argon flow rate and 200 ml/min C_2H_2.The as-synthesized CNTs was then purified by 30 % (v/v) HNO_3/H_2S0_4, the as-synthesized CNTs and purified CNTs were characterized using standard analytical techniques.
2. The silver nanoparticles was successfully synthesized using *Carica Papaya* leaf extract via green synthesis method. The result of AgNPs prepared, characterized shown that this plant can be used as a reducing and stabilizing agent. The UV-visible spectroscopy, HRTEM and XRD analysis confirms the existence of elemental silver, and the Surface Plasmon Resonance (SPR) peak, corresponds to the silver nanoparticles 419.50 nm and the particle size of as-synthesized AgNPs was calculated to be 17.32 nm.

3. Silver nanoparticles was doped on the surface of purified carbon nanotubes by wet impregnation method. Purified carbon nanotubes were synthesized, the active sites provided by purification process permitted ready formation of Ag nanoparticles on the CNT surfaces. TEM revealed that the well-dispersed, spherical nanoparticles were being anchored on the external walls of the MWNTs, The surface chemistry investigated using FTIR spectroscopy analyses confirmed the formation of Ag-CNTs and the size range of Ag-CNT was about 18 nm.
4. The adsorption efficiency of P-CNTs and Ag-CNTs for the removal of Fe, Mn and Zn metals from fish pond wastewater was studied and was found to depend on contact time, adsorbent dosage and temperature. The removal efficiency of selected heavy metal was in order of Ag-CNTs>P-CNTs, the performance of the adsorbent is dependent on the individual water holding capacity of each material.

5. The adsorption isotherm and kinetic model was best fitted to Freundlich isotherm and pseudo-second-order model, which shows that it is a multilayer phenomenon. The adsorption process of the selected heavy metal ions from fish pond wastewater was feasible and spontaneous, random and exothermic in nature. This study showed that Ag-CNTs is a better promising nano-adsorbent compare to its counterpart for the adsorption of heavy metals from fish pond wastewater.

5.2 Recommendations

From the research performed and study, the following recommendations are been made;

1. Further research should look into methods of desorption of adsorbent so as to optimize the use of CNTs adsorbent.
2. Regeneration of Ag-CNTs absorbent should be studied to limit the cost of water treatment using CNTs.
3. The effect of other doping methods should be employed in order to know the most effective and economical route.
4. Other ponds from different states should be studied in other to test the effectiveness of the as-synthesised nano adsorbent.

5.3 Contribution to knowledge

1. In this research work, carbon nanaotubes were produced using Fe-Ni/ kaolin catalyst and silver nanaoparticles were successfully synthesized via green method.
2. The doping of silver nanaoparticles on the matrix of carbon nanotubes were achieved.
3. The synthesized nanoadsorbent (Ag-CNT) was use to remove organic pollutants and heavy metals present in FAIB construction international fishpond wastewater Minna and the water is safe for reuse in irrigation farming.

REFERENCES

Abdel-Tawwab, M., M. N. Monier, A. M. Abdelrhman and M. A. Dawood (2020). "Effect of dietary multi-stimulants blend supplementation on performance, digestive enzymes, and antioxidants biomarkers of common carp, Cyprinus carpio L. and its resistance to ammonia toxicity." Aquaculture, **528**, 735529.

Ahmad, A., S. R. S. Abdullah, H. A. Hasan, A. R. Othman and N. I. Ismail (2021). "Aquaculture industry: Supply and demand, best practices, effluent and its current issues and treatment technology." *Journal of Environmental Managemen*t, **287**, 112271.

Ajitha, B., Y. A. K. Reddy and P. S. Reddy (2015). "Green synthesis and characterization of silver nanoparticles using Lantana camara leaf extract." *Materials science and engineering*, **49**, 373-381.

Al Moustafa, A.-E., E. Mfoumou, D. E. Roman, V. Nerguizian, A. Alazzam, I. Stiharu and A. Yasmeen (2016). "Impact of single-walled carbon nanotubes on the embryo: a brief review." *International journal of Nanomedicine,* **11**, 349.

Alfarisa, S., R. Safitri and W. Dwandaru (2016). "Effect of catalyst concentrations on the growth of carbon nanotubes from waste engine oil." EDUCATUM *Journal of Science, Mathematics and Technology,* **3**(1), 6-12.

Alguacil, F. J., F. López, O. Rodriguez, S. Martinez-Ramirez and I. Garcia-Diaz (2016). "Sorption of indium (III) onto carbon nanotubes." *Ecotoxicology and environmental safety,* **130**, 81-86.

Alisawi, H. A. O. (2020). "Performance of wastewater treatment during variable temperature." Applied Water Science, **10**(4), 1-6.

Aliyu, A., A. Abdulkareem, A. Kovo, O. Abubakre, J. Tijani and I. Kariim (2017). "Synthesize multi-walled carbon nanotubes via catalytic chemical vapour deposition method on Fe-Ni bimetallic catalyst supported on kaolin." Carbon letters, **21**, 33-50.

Aliyu, A., I. Kariim and S. A. Abdulkareem (2017). "Effects of aspect ratio of multi-walled carbon nanotubes on coal washery waste water treatment." *Journal of environmental management, **202**, 84-93.*

Aliyu, U. S., H. M. Kamari, A. M. Hamza and A. A. Awshah (2018). "The structural, physical and optical properties of borotellurite glasses incorporated with silica from rice husk." *Journal of Science and Mathematics* Letters, **6**, 32-46.

Almahdi, A. M. A. (2017). A Development of a Water Quality Monitoring System Using Wireless Sensors Network 20, University of Gezira.

Amendola, V., R. Pilot, M. Frasconi, O. M. Maragò and M. A. Iatì (2017). "Surface plasmon resonance in gold nanoparticles: a review." *Journal of Physics: Condensed Matter,* **29**(20), 203002.

Ang, M. B. M. Y., C. A. Trilles, M. R. De Guzman, J. M. Pereira, R. R. Aquino, S.-H. Huang, C.-C. Hu, K.-R. Lee and J.-Y. Lai (2019). "Improved performance of thin-film nanocomposite nanofiltration membranes as induced by embedded polydopamine-coated silica nanoparticles." *Separation and Purification Technology,* **224**, 113-120.

Anijiofor, S. C., N. N. N. Daud, S. Idrus and H. C. Man (2018). "Recycling of fishpond wastewater by adsorption of pollutants using aged refuse as an alternative low-cost adsorbent." *Sustainable Environment Research,* **28**(6), 315-321.

Annu, A., B. Bhattacharya, P. K. Singh, P. Shukla and H.-W. Rhee (2017). "Carbon nanotube using spray pyrolysis: recent scenario." *Journal of Alloys and Compounds,* **691**, 970-982.

Anwar, F. and G. Arthanareeswaran (2019). "Silver nano-particle coated hydroxyapatite nano-composite membrane for the treatment of palm oil mill effluent." *Journal of Water Process Engineering* **31**, 100844.

Arezoo, E., E. Mohammadreza, M. Maryam and M. N. Abdorreza (2020). "The synergistic effects of cinnamon essential oil and nano TiO2 on antimicrobial and functional properties of sago starch films." *International journal of biological macromolecules*,**157**, 743-751.

Arnold, W. R. and A. J. Rainbow (1996). "Host cell reactivation of irradiated adenovirus in UV-sensitive Chinese hamster ovary cell mutants." Mutagenesis, **11**(1), 89-94.

Aroca, R. (2006). Surface-enhanced vibrational spectroscopy, John Wiley & Sons.

Ayangbenro, A. S. and O. O. Babalola (2017). "A new strategy for heavy metal polluted environments: a review of microbial biosorbents." International journal of environmental research and public health, **14**(1), 94.

Ayawei, N., A. N. Ebelegi and D. Wankasi (2017). "Modelling and interpretation of adsorption isotherms." *Journal of chemistry, **2017***.

Ayawei, N., A. Ekubo, D. Wankasi and E. Dikio (2015). "Synthesis and Application of Layered Double Hydroxide for the removal of Copper in Wastewater." *International Journal of Chemistry,* **7**(1), 122-132.

Ayawei, N., A. T. Ekubo, D. Wankasi and E. D. Dikio (2015). "Adsorption of congo red by Ni/Al-CO3: equilibrium, thermodynamic and kinetic studies." *Oriental Journal of Chemistry,* **31**(3), 1307.

Bagherzade, G., M. M. Tavakoli and M. H. Namaei (2017). "Green synthesis of silver nanoparticles using aqueous extract of saffron (Crocus sativus L.) wastages and its antibacterial activity against six bacteria." *Asian Pacific Journal of Tropical Biomedicine,* **7**(3), 227-233.

Bajpai, M., S. S. Katoch and N. K. Chaturvedi (2019). "Comparative study on decentralized treatment technologies for sewage and graywater reuse–a review." *Water Science and Technology,* ***80***(11), 2091-2106.

Baker, C., A. Pradhan, L. Pakstis, D. J. Pochan and S. I. Shah (2005). "Synthesis and antibacterial properties of silver nanoparticles." *Journal of nanoscience and nanotechnology,****5***(2), 244-249.

Baker, R., M. Barber, P. Harris, F. Feates and R. Waite (1972). "Nucleation and growth of carbon deposits from the nickel catalyzed decomposition of acetylene." *Journal of catalysis,* **26**(1), 51-62.

Baker, R., P. Harris, J. Henderson and R. Thomas (1975). "Formation of carbonaceous deposits from the reaction of methane over nickel." Carbon, **13**(1), 17-22.

Bang, Y.-J., S. Shankar and J.-W. Rhim (2019). "In situ synthesis of multi-functional gelatin/resorcinol/silver nanoparticles composite films." Food Packaging and Shelf Life, **22**, 100399.

Bankole, M., A. Abdulkareem, J. Tijani, S. Ochigbo, A. Afolabi and W. Roos (2017). "Chemical oxygen demand removal from electroplating wastewater by purified and polymer functionalized carbon nanotubes adsorbents." Water Resources and Industry, **18**, 33-50.

Barua, S., H. S. Dutta, S. Gogoi, R. Devi and R. Khan (2017). "Nanostructured MoS2-based advanced biosen,sors: a review." ACS Applied Nano Materials, **1**(1), 2-25.

Bousskri, A., A. Anejjar, M. Messali, R. Salghi, O. Benali, Y. Karzazi, S. Jodeh, M. Zougagh, E. E. Ebenso and B. Hammouti (2015). "Corrosion inhibition of carbon steel in aggressive acidic media with 1-(2-(4-chlorophenyl)-2-oxoethyl) pyridazinium bromide." *Journal of Molecular Liquids,* **211**, 1000-1008.

Boyd, C. and A. McNevin (2015). Aquaculture, resource use, and the environment, John Wiley & Sons.

Burakov, A. E., E. V. Galunin, I. V. Burakova, A. E. Kucherova, S. Agarwal, A. G. Tkachev and V. K. Gupta (2018). "Adsorption of heavy metals on conventional and nanostructured materials for wastewater treatment purposes: A review." *Ecotoxicology and environmental safety,* ***148***, 702-712.

Burakova, E. A., T. P. Dyachkova, A. V. Rukhov, E. N. Tugolukov, E. V. Galunin, A. G. Tkachev and I. Ali (2018). "Novel and economic method of carbon nanotubes synthesis on a nickel magnesium oxide catalyst using microwave radiation." *Journal of Molecular Liquids*, ***253***, 340-346.

Cao, C.-F., P.-H. Wang, J.-W. Zhang, K.-Y. Guo, Y. Li, Q.-Q. Xia, G.-D. Zhang, L. Zhao, H. Chen and L. Wang (2020). "One-step and green synthesis of lightweight, mechanically flexible and flame-retardant polydimethylsiloxane foam nanocomposites via surface-assembling ultralow content of graphene derivative." *Chemical Engineering Journal*, **393**, 124724.

Cao, S., G. Chen, X. Hu and P. L. Yue (2003). "Catalytic wet air oxidation of wastewater containing ammonia and phenol over activated carbon supported Pt catalysts." *Catalysis Today*, **88**(1-2), 37-47.

Chandhru, M., R. Logesh, S. K. Rani, N. Ahmed and N. Vasimalai (2019). "One-pot green route synthesis of silver nanoparticles from jack fruit seeds and their antibacterial activities with escherichia coli and salmonella bacteria." *Biocatalysis and Agricultural Biotechnology*, ***20***, *101241*.

Chandhru, M., S. K. Rani and N. Vasimalai (2020). "Reductive degradation of toxic six dyes in industrial wastewater using diaminobenzoic acid capped silver nanoparticles." *Journal of Environmental Chemical Engineering*, **8**(5), 104225.

Chen, B., M. Han, K. Peng, S. Zhou, L. Shao, X. Wu, W. Wei, S. Liu, Z. Li and J. Li (2018). "Global land-water nexus: Agricultural land and freshwater use embodied in worldwide supply chains." *Science of the Total Environment*, **613**, 931-943.

Cheo, A. (2016). "Understanding seasonal trend of rainfall for the better planning of water harvesting facilities in the Far-North region, Cameroon." Water Util.**13**, 3-11.

Chernousova, S. and M. Epple (2013). "Silver as antibacterial agent: ion, nanoparticle, and metal." *Angewandte Chemie International Edition*, **52**(6), 1636-1653.

Chinnappan, A., C. Baskar, H. Kim and S. Ramakrishna (2016). "Carbon nanotube hybrid nanostructures: future generation conducting materials." *Journal of Materials Chemistry*, A**4**(24), 9347-9361.

Cobos, M., I. De-La-Pinta, G. Quindós, M. J. Fernández and M. D. Fernández (2020). "Graphene oxide–silver nanoparticle nanohybrids: Synthesis, characterization, and antimicrobial properties." Nanomaterials, **10**(2), 376.

Craig,S., Helfrich,L.A.,Kuhn, D., & Schwarz, M. H. (2017). "Understading fish nutrition,feeds and feeding.

Cullity, B. and S. Stock (2001). "Elements of x-ray diffraction, Prentice Hall." Upper Saddle River, NJ, 388.

Cuong, D. V., P.-C. Wu, N.-L. Liu and C.-H. Hou (2020). "Hierarchical porous carbon derived from activated biochar as an eco-friendly electrode for the electrosorption of inorganic ions." Separation and Purification Technology, **242**, 116813.

Daniels, B. and N. Mesner (2010). "Drinking Water Treatment Systems."

Dauda, A. B., A. Ajadi, A. S. Tola-Fabunmi and A. O. Akinwole (2019). "Waste production in aquaculture: sources, components and managements in different culture systems." *Aquaculture and Fisheries*, **4**(3), 81-88.

Dauda, A. B., N. Romano, W. W. Chen, I. Natrah and M. S. Kamarudin (2018). "Differences in feeding habits influence the growth performance and feeding efficiencies of African catfish (Clarias gariepinus) and lemon fin barb hybrid (Hypsibarbus wetmorei♂× Barboides gonionotus♀) in a glycerol-based biofloc technology system versus a recirculating system." *Aquacultural Engineering*, ***82***, 31-37.

Dauda, M., C. Basheer, M. H. Al-Malack and M. N. Siddiqui (2021). "Efficient Co-MoS2 electrocatalyst for cathodic degradation of halogenated disinfection by-products in water sample." *Separation and Purification Technology*, ***259***, 118085.

Dawadi, S., S. Katuwal, A. Gupta, U. Lamichhane, R. Thapa, S. Jaisi, G. Lamichhane, D. P. Bhattarai and N.Parajuli (2021). "Current Research on Silver Nanoparticles: Synthesis, Characterization, and Applications." *Journal of Nanomaterials*, **2021**.

Demeke, A. and A. Tassew (2016). "A review on water quality and its impact on fish health." *International journal of fauna and biological studies*, **3**(1), 21-31.

Desta, M. B. (2013). "Batch sorption experiments: Langmuir and Freundlich isotherm studies for the adsorption of textile metal ions onto teff straw (Eragrostis tef) agricultural waste." *Journal of thermodynamics*, **2013**.

Di Fraia, S., N. Massarotti and L. Vanoli (2018). "A novel energy assessment of urban wastewater treatment plants." *Energy Conversion and Managemen*t, **163**, 304-313.

Dixit, S. and A. Tripathi (2019). "A review on biosynthesis, characterization and Antimicrobial effect of silver nanoparticles of Moringa olifera (MO-AgNPs)." *Journal of Pharmaceutical Sciences and Research*, **11**(5), 1937-1943.

Doraiswamy, N. and L. Marks (1996). "Electron beam induced small particle transformations: temperature." Surface Science, **348**(1-2), L67-L69.

Dresselhaus, G., M. S. Dresselhaus and R. Saito (1998). Physical properties of carbon nanotubes, World scientific.

Dresselhaus, M., G. Dresselhaus and R. Saito (1995). "Physics of carbon nanotubes." Carbon, **33**(7), 883-891.

Eatemadi, A., H. Daraee, H. Karimkhanloo, M. Kouhi, N. Zarghami, A. Akbarzadeh, M. Abasi, Y. Hanifehpour and S. W. Joo (2014). "Carbon nanotubes: properties, synthesis, purification, and medical applications." *Nanoscale research letters,* **9**(1), 1-13.

El-Sayed, M. A. (2001). "Some interesting properties of metals confined in time and nanometer space of different shapes." *Accounts of chemical research,* **34**(4), 257-264.

Elmorsi, T. M. (2011). "Equilibrium isotherms and kinetic studies of removal of methylene blue dye by adsorption onto miswak leaves as a natural adsorbent." *Journal of Environmental Protection,* **2**(06), 817.

Elsayed, A., D. Osman, S. Attia, H. Ahmed, E. Shoukry, G. A. Mahmoud, Y. Moustafa and A. Taman (2020). "Synthesis of super magnetite (Fe3O4)/bentonite nanocomposite for efficient remediation for industrial wastewater effluents." *Egyptian Journal of Chemistry,* **63**(12), 5-5.

Fang, H.-T., C.-G. Liu, C. Liu, F. Li, M. Liu and H.-M. Cheng (2004). "Purification of single-wall carbon nanotubes by electrochemical oxidation." *Chemistry of Materials,* **16**(26), 5744-5750.

Farid, M., S. Ali, M. Zubair, R. Saeed, M. Rizwan, R. Sallah-Ud-Din, A. Azam, R. Ashraf and W. Ashraf (2018). "Glutamic acid assisted phyto-management of silver-contaminated soils through sunflower; physiological and biochemical response." *Environmental Science and Pollution Research,* **25**(25), 25390-25400.

Feng, Y., Q. Yang, X. Wang and B. E. Logan (2010). "Treatment of carbon fiber brush anodes for improving power generation in air–cathode microbial fuel cells." *Journal of Power Sources,* **195**(7), 1841-1844.

Ferreira, N., C. Bonetti and W. Seiffert (2011). "Hydrological and water quality indices as management tools in marine shrimp culture." *Aquaculture,* **318**(3-4), 425-433.

Ferroudj, N., J. Nzimoto, A. Davidson, D. Talbot, E. Briot, V. Dupuis, A. Bée, M. S. Medjram and S. Abramson (2013). "Maghemite nanoparticles and maghemite/silica nanocomposite microspheres as magnetic Fenton catalysts for the removal of water pollutants." *Applied Catalysis B: Environmental,* **136**, 9-18.

Fetouh, H., A. Hefnawy, A. Attia and E. Ali (2020). "Facile and low-cost green synthesis of eco-friendly chitosan-silver nanocomposite as novel and promising corrosion inhibitor for mild steel in chilled water circuits." *Journal of Molecular Liquids,* **319**, 114355.

Galasso, H. L., M. D. Callier, D. Bastianelli, J.-P. Blancheton and C. Aliaume (2017). "The potential of near infrared spectroscopy (NIRS) to measure the chemical composition of aquaculture solid waste." *Aquaculture,* **476**, 134-140.

Gao, J., K. Powers, Y. Wang, H. Zhou, S. M. Roberts, B. M. Moudgil, B. Koopman and D. S. Barber (2012). "Influence of Suwannee River humic acid on particle properties and toxicity of silver nanoparticles." Chemosphere, **89**(1), 96-101.

Geurts, K., S. P. Fletcher, A. W. van Zijl, A. J. Minnaard and B. L. Feringa (2008). "Copper-catalyzed asymmetric allylic substitution reactions with organozinc and Grignard reagents." *Pure and Applied Chemistry,* **80**(5), 1025-1037.

Gleick, P. H. (2019). "Water as a weapon and casualty of armed conflict: A review of recent water-related violence in Iraq, Syria, and Yemen." Wiley Interdisciplinary Reviews: Water, **6**(4), e1351.

Gogoi, A., P. Mazumder, V. K. Tyagi, G. T. Chaminda, A. K. An and M. Kumar (2018). "Occurrence and fate of emerging contaminants in water environment: a review." *Groundwater for Sustainable Development*, **6**, 169-180.

Gottschalk, F. and B. Nowack (2011). "The release of engineered nanomaterials to the environment." *Journal of Environmental Monitoring*, **13**(5), 1145-1155.

Gribble, G. W. (2003). "Natural production of organohalogen compounds."

Gunjakar, J., A. More, K. Gurav and C. Lokhande (2008). "Chemical synthesis of spinel nickel ferrite (NiFe2O4) nano-sheets." *Applied Surface Science*, ***254***(18), 5844-5848.

Gurunathan, S., J. W. Han, J. H. Park, E. Kim, Y.-J. Choi, D.-N. Kwon and J.-H. Kim (2015). "Reduced graphene oxide–silver nanoparticle nanocomposite: a potential anticancer nanotherapy." *International journal of nanomedicine*, **10**: 6257.

Hamzat, W. A., A. S. Abdulkareem, M. T. Bankole, J. O. Tijani, A. S. Kovo and O. K. Abubakre (2019). "Adsorption studies on the treatment of battery wastewater by purified carbon nanotubes (P-CNTs) and polyethylene glycol carbon nanotubes (PEG-CNTs)." *Journal of Environmental Science and Health*, Part A, **54**(9), 827-839.

Hemant, P. and V. Sharma (2015). "Thermal conductivity of carbon nanotube–silver composite." *Transactions of Nonferrous Metals Society of China,* **25**(1), 154-161.

Hirlekar, R., M. Yamagar, H. Garse, M. Vij and V. Kadam (2009). "Carbon nanotubes and its applications: a review." *Asian journal of pharmaceutical and clinical research,* **2**(4), 17-27.

Huang, X., J. Tu, B. Zhang, C. Zhang, Y. Li, Y. Yuan and H. Wu (2006). "Electrochemical properties of NiO–Ni nanocomposite as anode material for lithium ion batteries." *Journal of power sources,* **161**(1), 541-544.

Iravani, S., H. Korbekandi, S. V. Mirmohammadi and B. Zolfaghari (2014). "Synthesis of silver nanoparticles: chemical, physical and biological methods." *Research in pharmaceutical sciences*, **9**(6), 385.

Ishaq, K., A. A. Saka, A. O. Kamardeen, A. Abdulrahman, I. K. Adekunle and A. S. Afolabi (2018). "Application of γ-alumina as catalyst support for the synthesis of CNTs in a CVD reactor." *Advances in Natural Sciences: Nanoscience and Nanotechnology,* **9**(3), 035012.

Jamshaid, A., A. Hamid, N. Muhammad, A. Naseer, M. Ghauri, J. Iqbal, S. Rafiq and N. S. Shah (2017). "Cellulose-based Materials for the Removal of Heavy Metals from Wastewater–An Overview." *ChemBioEng Reviews,* **4**(4), 240-256.

Jethave, G., U. Fegade, S. Attarde and S. Ingle (2017). "Facile synthesis of lead doped zinc-aluminum oxide nanoparticles (LD-ZAO-NPs) for efficient adsorption of anionic dye: kinetic, isotherm and thermodynamic behaviors." *Journal of industrial and engineering chemistry,* **53**, 294-306.

Junyu, Z., D. Jianjun, W. Haipeng, S. Hongxia, Z. Dongmei and L. Lin (2014). "Meta analysis." *Chinese medical journa*l, **127**(15), 2837-2843.

Kalantari, K., A. B. M. Afifi, S. Bayat, K. Shameli, S. Yousefi, N. Mokhtar and A. Kalantari (2019). "Heterogeneous catalysis in 4-nitrophenol degradation and antioxidant activities of silver nanoparticles embedded in Tapioca starch." *Arabian Journal of Chemistry,* **12**(8), 5246-5252.

Kar, S., M. Salam and K. Rana (2017). "Artificial feed development through fishmeal replacement with non-conventional feed stuff for mud crab (Scylla serrata) fattening." *Indian Journal of Applied Research,* **3**(6), 237-242.

Karim, M. N., S. R. Anderson, S. Singh, R. Ramanathan and V. Bansal (2018). "Nanostructured silver fabric as a free-standing NanoZyme for colorimetric detection of glucose in urine." *Biosensors and Bioelectronics,* **110**, 8-15.

Kean, T. and M. Thanou (2010). "Biodegradation, biodistribution and toxicity of chitosan." *Advanced drug delivery reviews,* **62**(1), 3-11.

Kemigabo, C., J. Kang'ombe, C. Masembe, L. Jere and D. Sikawa (2017). "Effects of protease enzyme supplementation on protein digestibility of legume and/or fish meal-based fish feeds." *International Journal of Fisheries and Aquaculture,* **9**(7), 73-80.

Khan, M. Y. A., K. M. Gani and G. J. Chakrapani (2016). "Assessment of surface water quality and its spatial variation. A case study of Ramganga River, Ganga Basin, India." Arabian *Journal of Geosciences, **9***(1), 28.

Khan, N., S. T. Hussain, A. Saboor, N. Jamila and K. S. Kim (2013). "Physicochemical investigation of the drinking water sources from Mardan, Khyber Pakhtunkhwa, Pakistan." *International journal of physical sciences,* **8**(33), 1661-1671.

Kharlamova, M. V. and D. Eder (2020). "Carbon Nanotubes: Synthesis, Properties, and New Developments in Research." *Synthesis and Applications of Nanocarbons*, 107-147.

Khiriya, P. K. and J. Chauhan "Theoretical Studies of Single Wall Carbon Nanotubes for Synthesis and Growth Mechanism."

Khodashenas, B. and H. R. Ghorbani (2019). "Synthesis of silver nanoparticles with different shapes." *Arabian Journal of Chemistry,* **12**(8), 1823-1838.

Kim, J. H., S. Lee, M. Wajahat, H. Jeong, W. S. Chang, H. J. Jeong, J.-R. Yang, J. T. Kim and S. K. Seol (2016). "Three-dimensional printing of highly conductive carbon nanotube microarchitectures with fluid ink." ACS nano, **10**(9), 8879-8887.

Kohnen, W., S. Teske-Keiser, H.-G. Meyer, A. H. Loos, M. Pietsch and B. Jansen (2005). "Microbiological quality of carbonated drinking water produced with in-home carbonation systems." *International journal of hygiene and environmental health* **208**(5), 415-423.

Konnola, R. and K. Joseph (2016). "Effect of side-wall functionalisation of multi-walled carbon nanotubes on the thermo-mechanical properties of epoxy composites." RSC advances, **6**(28), 23887-23899.

Kotakadi, V. S., S. A. Gaddam, Y. S. Rao, T. Prasad, A. V. Reddy and D. S. Gopal (2014). "Biofabrication of silver nanoparticles using Andrographis paniculata." European *Journal of Medicinal Chemistry, **73***, 135-140.

Krenkel, P. (2012). Water quality management, *Elsevier*.

Kumar, A., J. Kumar and T. Bhaskar (2020). "Utilization of lignin: A sustainable and eco-friendly approach." *Journal of the Energy Institute,* **93**(1), 235-271.

Kumar, M. and Y. Ando (2010). "Chemical vapor deposition of carbon nanotubes: a review on growth mechanism and mass production." *Journal of nanoscience and nanotechnology*, **10**(6), 3739-3758.

Kyzas, G. Z. and K. A. Matis (2015). "Nanoadsorbents for pollutants removal: a review." *Journal of Molecular Liquids*, **203**, 159-168.

Li, L., Y. Hu and L. Ling (2016). "Wave propagation in viscoelastic single-walled carbon nanotubes with surface effect under magnetic field based on nonlocal strain gradient theory." Physica E: Low-dimensional Systems and Nanostructures,**75**, 118-124.

Liu, H., B. Xu, M. Jia, M. Zhang, B. Cao, X. Zhao and Y. Wang (2015). "Polyaniline nanofiber/large mesoporous carbon composites as electrode materials for supercapacitors." *Applied Surface Science*, **332**, 40-46.

Liu, L., F. Liu and J. Zhao (2014). "Curved carbon nanotubes: From unique geometries to novel properties and peculiar applications." Nano Research, **7**(5), 626-657.

Lokhande, R. S., P. U. Singare and D. S. Pimple (2011). "Toxicity study of heavy metals pollutants in waste water effluent samples collected from Taloja industrial estate of Mumbai, India." *Resources and Environment*, **1**(1), 13-19.

Lounsbury, A. W., J. S. Yamani, C. P. Johnston, P. Larese-Casanova and J. B. Zimmerman (2016). "The role of counter ions in nano-hematite synthesis: implications for surface area and selenium adsorption capacity." *Journal of hazardous materials*, **310**, 117-124.

Lu, L., R. Sun, R. Chen, C.-K. Hui, C.-M. Ho, J. M. Luk, G. Lau and C.-M. Che (2008). "Silver nanoparticles inhibit hepatitis B virus replication." Antiviral therapy, **13**(2), 253.

Luo, J., J.-H. Im, M. T. Mayer, M. Schreier, M. K. Nazeeruddin, N.-G. Park, S. D. Tilley, H. J. Fan and M. Grätzel (2014). "Water photolysis at 12.3% efficiency via perovskite photovoltaics and Earth-abundant catalysts." Science, **345**(6204), 1593-1596.

Ma, X., R. Jian, P. R. Chang and J. Yu (2008). "Fabrication and characterization of citric acid-modified starch nanoparticles/plasticized-starch composites." *Biomacromolecules*, **9**(11), 3314-3320.

Mabena, L. F., S. S. Ray, S. D. Mhlanga and N. J. Coville (2011). "Nitrogen-doped carbon nanotubes as a metal catalyst support." *Applied Nanoscience*, **1**(2), 67-77.

Mader, M., C. Schmidt, R. van Geldern and J. A. Barth (2017). "Dissolved oxygen in water and its stable isotope effects: a review." *Chemical Geology*, **473**, 10-21.

Mahmoodian, H., O. Moradi, B. Shariatzadeha, T. A. Salehf, I. Tyagi, A. Maity, M. Asif and V. K. Gupta (2015). "Enhanced removal of methyl orange from aqueous solutions by poly HEMA–chitosan-MWCNT nano-composite." *Journal of Molecular Liquids*, ***202***, 189-198.

Mahmoud, M. E., M. F. Amira, S. M. Seleim and A. K. Mohamed (2020). "Amino-decorated magnetic metal-organic framework as a potential novel platform for selective removal of chromium (Vl), cadmium (II) and lead (II)." *Journal of hazardous materials*, **381**, 120979.

Makarov, V., A. Love, O. Sinitsyna, S. Makarova, I. Yaminsky, M. Taliansky and N. Kalinina (2014). ""“Green” nanotechnologies: synthesis of metal nanoparticles using plants." Acta Naturae, **6**(1 (20)).

Mohanta, Y. K., S. K. Panda, R. Jayabalan, N. Sharma, A. K. Bastia and T. K. Mohanta (2017). "Antimicrobial, antioxidant and cytotoxic activity of silver nanoparticles synthesized by leaf extract of Erythrina suberosa (Roxb.)." *Frontiers in molecular biosciences*, **4**, 14.

Montazer, M., F. Alimohammadi, A. Shamei and M. K. Rahimi (2012). "In situ synthesis of nano silver on cotton using Tollens’ reagent." *Carbohydrate Polymers*, **87**(2), 1706-1712.

Montoneri, E. (2017). Municipal waste treatment, technological scale up and commercial exploitation: The case of bio-waste lignin to soluble lignin-like polymers. *Food Waste Reduction and Valorisation, Springer***,** 79-120.

Moustafa, M. T. (2017). "Removal of pathogenic bacteria from wastewater using silver nanoparticles synthesized by two fungal species." *Water Science*, ***31***(2), 164-176.

Nassehiniaa, H., H. Rahmanib, K. Rahmanic and A. Rahmania (2020). "Solar photocatalytic degradation of Reactive Black 5: by-products, bio-toxicity, and kinetic study." *Desalination and Water Treatment, **206***, 385-395.

Niu, W.-J., Y.-P. Wang, J.-Z. He, W.-W. Liu, M.-C. Liu, D. Shan, L. Lee and Y.-L. Chueh (2019). "Highly stable nitrogen-doped carbon nanotubes derived from carbon dots and metal-organic frameworks toward excellent efficient electrocatalyst for oxygen reduction reaction." Nano Energy, **63**, 103788.

Novak, I., C. Morgan, L. Adde, J. Blackman, R. N. Boyd, J. Brunstrom-Hernandez, G. Cioni, D. Damiano, J. Darrah and A.-C. Eliasson (2017). "Early, accurate diagnosis and early intervention in cerebral palsy: advances in diagnosis and treatment." JAMA pediatrics, **171**(9), 897-907.

Obaid, A. Y., S. A. Al-Thabaiti, E. El-Mossalamy, L. M. Al-Harbi and Z. Khan (2017). "Extracellular bio-synthesis of silver nanoparticles." *Arabian Journal of Chemistry,* **10**(2), 226-231.

Obasogie, O. E., A. S. Abdulkareem, I. h. A. Mohammed, M. T. Bankole, J. O. Tijani and O. K. Abubakre (2018). "Empirical relationship between band gap and synthesis parameters of chemical vapor deposition-synthesized multiwalled carbon nanotubes." *Carbon letters,* **28**, 72-80.

Ogwo, P. and O. Ogu (2014). "Impact of Industrial Effluents Discharge on the Quality of Nwiyi River Enugu South Eastern Nigeria." IOSR *Journal of Environmental Science, Toxicology and Food Technology* (IOSRJESTFT), 2319-2402.

Olsson, C., R. Zangana and J. Swenson (2020). "Stabilization of proteins embedded in sugars and water as studied by dielectric spectroscopy." *Physical Chemistry Chemical Physics,* **22**(37), 21197-21207.

Omitoyin, B., E. Ajani, O. Okeleye, B. Akpoilih and A. Ogunjobi (2017). "Biological treatments of fish farm effluent and its reuse in the culture of Nile Tilapia (Oreochromis niloticus)." *Journal of Aquaculture Research & Development,* **8**(2).

Oni, S. K., M. N. Futter, K. Bishop, S. Köhler, M. Ottosson-Löfvenius and H. Laudon (2013). "Long-term patterns in dissolved organic carbon, major elements and trace metals in boreal headwater catchments: trends, mechanisms and heterogeneity." Biogeosciences, **10**(4), 2315-2330.

Oprica, L., M. Andries, L. Sacarescu, L. Popescu, D. Pricop, D. Creanga and M. Balasoiu (2020). "Citrate-silver nanoparticles and their impact on some environmental beneficial fungi." *Saudi Journal of Biological Sciences,* **27**(12), 3365-3375.

Otunola, B. O. and O. O. Ololade (2020). "A review on the application of clay minerals as heavy metal adsorbents for remediation purposes." *Environmental Technology & Innovation, **18**, 100692.*

Papagiannis, F., P. Gazzola, O. Burak and I. Pokutsa (2018). "Overhauls in water supply systems in Ukraine: A hydro-economic model of socially responsible planning and cost management." *Journal of cleaner production*, ***183***, 358-369.

Perala, S. R. K. and S. Kumar (2013). "On the mechanism of metal nanoparticle synthesis in the Brust–Schiffrin method." Langmuir, **29**(31), 9863-9873.

Polte, J. (2015). "Fundamental growth principles of colloidal metal nanoparticles–a new perspective." CrystEngComm, **17**(36), 6809-6830.

Pomerantz, N., Y. Ladizhansky, E. Korin, M. Waisman, N. Daltrophe and J. Gilron (2006). "Prevention of scaling of reverse osmosis membranes by "zeroing" the elapsed nucleation time. Part I. Calcium sulfate." Industrial & engineering chemistry research, **45**(6), 2008-2016.

Poulsen, S. S., A. T. Saber, A. Williams, O. Andersen, C. Købler, R. Atluri, M. E. Pozzebon, S. P. Mucelli, M. Simion and D. Rickerby (2015). "MWCNTs of different physicochemical properties cause similar inflammatory responses, but differences in transcriptional and histological markers of fibrosis in mouse lungs." Toxicology and applied pharmacology, **284**(1), 16-32.

Prazeres, A. R., F. Fernandes, L. Madeira, S. Luz, A. Albuquerque, R. Simões, F. Beltran, E. Jerónimo and J. Rivas (2019). "Treatment of slaughterhouse wastewater by acid precipitation (H2SO4, HCl and HNO3) and oxidation (Ca (ClO) $_2$, H2O2 and CaO_2)." *Journal of environmental management*, **250**, 109558.

Rahman, G., Z. Najaf, A. Mehmood, S. Bilal, S. A. Mian and G. Ali (2019). "An overview of the recent progress in the synthesis and applications of carbon nanotubes." C—*Journal of Carbon Research*, **5**(1), 3.

Rahmania, N. A., B. S. Rahardja and D. K. Meles "Addition of Gryllus bimaculatus flour in commercial feeds to retention of protein and energy of Oreochromis Sp."

Rahmanian, N., S. H. B. Ali, M. Homayoonfard, N. Ali, M. Rehan, Y. Sadef and A. Nizami (2015). "Analysis of physiochemical parameters to evaluate the drinking water quality in the state of Perak, Malaysia." *Journal of Chemistry*, ***2015***.

Rajkumar, P., A. Prakasam, S. Rajeshkumar, M. Gomathi, P. Anbarasan and R. Chandrasekaran (2020). "Green synthesis of silver nanoparticles using Gymnema sylvestre leaf extract and evaluation of its antibacterial activity." *South African Journal of Chemical Engineering*, **32**(1), 1-4.

Rakotondrabe, F., J. R. N. Ngoupayou, Z. Mfonka, E. H. Rasolomanana, A. J. N. Abolo and A. A. Ako (2018). "Water quality assessment in the Bétaré-Oya gold mining area (East-Cameroon): multivariate statistical analysis approach." Science of the total environment, **610**, 831-844.

Ramoraswi, N. O. (2014). Physical and chemical properties of carbon nanotubes and silica nano-composites on the photo-catalytic activity of titania nanoparticles for selected organic pollutants.

Rananga, L. E. (2013). Synthesis, characters and application of silver-doped cabon Nanotubes and nanoporous polymers for purification of water samples, University of Limpopo (Turfloop Campus).

Rasheed, T., M. Bilal, C. Li, F. Nabeel, M. Khalid and H. M. Iqbal (2018). "Catalytic potential of bio-synthesized silver nanoparticles using Convolvulus arvensis extract for the degradation of environmental pollutants." *Journal of Photochemistry and Photobiology* B: Biology, **181**, 44-52.

Ronga, D., E. Francia, F. Rizza, F.-W. Badeck, F. Caradonia, G. Montevecchi and N. Pecchioni (2019). "Changes in yield components, morphological, physiological and fruit quality traits in processing tomato cultivated in Italy since the 1930's." *Scientia Horticulturae*, **257**, 108726.

Roul, M. K., B. Obasogie, G. Kogo, J. Skuza, R. Mundle and A. Pradhan (2017). "Transparent and flexible heaters based on Al: ZnO degenerate semiconductor." *Journal of Applied Physics*, **122**(13), 135110.

Rycenga, M., C. M. Cobley, J. Zeng, W. Li, C. H. Moran, Q. Zhang, D. Qin and Y. Xia (2011). "Controlling the synthesis and assembly of silver nanostructures for plasmonic applications." *Chemical reviews*, **111**(6), 3669-3712.

Sagadevan, S., S. Vennila, A. R. Marlinda, Y. Al-Douri, M. R. Johan and J. A. Lett (2019). "Synthesis and evaluation of the structural, optical, and antibacterial properties of copper oxide nanoparticles." *Applied Physics* A, **125**(8), 1-9.

Saifuddin, N., A. Raziah and A. Junizah (2013). "Carbon nanotubes: a review on structure and their interaction with proteins." *Journal of Chemistry*, **2013**.

Salaudeen, I., M. Olajuwon, A. Ajala, T. Abdulkareem, S. Adeniyi, S. Jisu, M. Omisore, M. Abdulahi, J. Abdulazeez and J. Igbalaye (2021). "Green Synthesis, Characterization and In-vitro Antioxidant Property of Silver Nanoparticles Using the Aqueous Leaf Extract of Justicia carnea." *Asian Journal of Biochemistry, Genetics and Molecular Biology*, 20-30.

Savary, S. (2020). Looking back on 2019: a selection of Food Security articles, Springer.

Sawyer, C. N., P. L. McCarty and G. F. Parkin (2003). Chemistry for environmental engineering and science, McGraw-Hill New York.

Schmid, G. and L. F. Chi (1998). "Metal clusters and colloids." Advanced Materials, **10**(7), 515-526.

Selvaraj, V., S. Sagadevan, L. Muthukrishnan, M. R. Johan and J. Podder (2019). "Eco-friendly approach in synthesis of silver nanoparticles and evaluation of optical, surface morphological and antimicrobial properties." *Journal of Nanostructure in Chemistry,* ***9***(2), 153-162.

Semwal, V. and B. D. Gupta (2017). "LSPR-and SPR-based fiber-optic cholesterol sensor using immobilization of cholesterol oxidase over silver nanoparticles coated graphene oxide nanosheets." *IEEE Sensors Journal,* **18**(3), 1039-1046.

Shankar, S. S., A. Ahmad and M. Sastry (2003). "Geranium leaf assisted biosynthesis of silver nanoparticles." *Biotechnology progress,* **19**(6), 1627-1631.

Shao, W., X. Liu, H. Min, G. Dong, Q. Feng and S. Zuo (2015). "Preparation, characterization, and antibacterial activity of silver nanoparticle-decorated graphene oxide nanocomposite." *ACS applied materials & interfaces,* ***7***(12), 6966-6973.

Sharma, J., B. S. Kaith, A. K. Sharma and A. Goel (2018). "Gum xanthan-psyllium-cl-poly (acrylic acid-co-itaconic acid) based adsorbent for effective removal of cationic and anionic dyes: adsorption isotherms, kinetics and thermodynamic studies." *Ecotoxicology and environmental safety*, **149**, 150-158.

Sharma, V. K., R. A. Yngard and Y. Lin (2009). "Silver nanoparticles: green synthesis and their antimicrobial activities." Advances in colloid and interface science, **145**(1-2), 83-96.

Shiosaki, A., M. Goto and T. Hirose (1994). "Frontal analysis of protein adsorption on a membrane adsorber." *Journal of Chromatography* A, **679**(1), 1-9.

Shirke, S., S. M. Pinto, V. K. Kushwaha, T. Mardikar and R. Vijay (2016). "Object-based image analysis for the impact of sewage pollution in Malad Creek, Mumbai, India." Environmental monitoring and assessment, **188**(2), 95.

Shirley, A. D., A. Dayanand, B. Sreedhar and S. Dastager (2010). "Antimicrobial activity of silver nanoparticles synthesized from novel Streptomyces species." *Digest Journal of Nanomaterials and Biostructures,* **5**(2), 447-451.

Shrivastava, S., T. Bera, A. Roy, G. Singh, P. Ramachandrarao and D. Dash (2007). "Characterization of enhanced antibacterial effects of novel silver nanoparticles." Nanotechnology, **18**(22), 225103.

Siddiqui, E. and J. Pandey (2019). "Assessment of heavy metal pollution in water and surface sediment and evaluation of ecological risks associated with sediment contamination in the Ganga River: a basin-scale study." *Environmental Science and Pollution Research,* **26**(11), 10926-10940.

Sinnott, S., R. Andrews, D. Qian, A. M. Rao, Z. Mao, E. Dickey and F. Derbyshire (1999). "Model of carbon nanotube growth through chemical vapor deposition." Chemical Physics Letters, **315**(1-2), 25-30.

Smith, K. L., S. Moriarty, K. Kenney and G. Barbatsis (2004). Handbook of visual communication: Theory, methods, and media, Routledge.

Solgi, E., E. Mirzaei-Rajeouni and A. Zamani (2020). "Feathers of Three Waterfowl Bird Species from Northern Iran for Heavy Metals Biomonitoring." Bulletin of environmental contamination and toxicology, **104**(6), 727-732.

Soni, M., P. Mehta, A. Soni and G. K. Goswami (2018). "Green nanoparticles: Synthesis and applications." IOSR J. Biotechnol. Biochem, **4**, 78-83.

Suzuki, Y., T. Maruyama, H. Numata, H. Sato and M. Asakawa (2003). "Performance of a closed recirculating system with foam separation, nitrification and denitrification units for intensive culture of eel: towards zero emission." *Aquacultural Engineering,* **29**(3-4), 165-182.

Talavera-Prieto, N. M., A. G. Ferreira, A. n. T. Portugal and A. P. Egas (2019). "Viscosity of cottonseed oil and biodiesel." *Journal of Chemical & Engineering* Data, **64**(3), 1166-1176.

Tang, Z., L. Zhang, N. Wang, X. Zhang, G. Wen, G. Li, J. Wang, C. T. Chan and P. Sheng (2001). "Superconductivity in 4 angstrom single-walled carbon nanotubes." Science, **292**(5526), 2462-2465.

Teh, C. Y., P. M. Budiman, K. P. Y. Shak and T. Y. Wu (2016). "Recent advancement of coagulation–flocculation and its application in wastewater treatment." *Industrial & Engineering Chemistry Research, **55***(16), 4363-4389.

Thostenson, E. T., Z. Ren and T.-W. Chou (2001). "Advances in the science and technology of carbon nanotubes and their composites: a review." Composites science and technology, **61**(13), 1899-1912.

Tilley, E. (2014). Compendium of sanitation systems and technologies, Eawag.

Tiwari, D. K., J. Behari and P. Sen (2008). "Application of nanoparticles in waste water treatment 1."

Uchymiak, M., A. R. Bartman, N. Daltrophe, M. Weissman, J. Gilron, P. D. Christofides, W. J. Kaiser and Y. Cohen (2009). "Brackish water reverse osmosis (BWRO) operation in feed flow reversal mode using an ex situ scale observation detector (EXSOD)." Journal of Membrane Science, **341**(1-2), 60-66.

Van Tung, T., Q. B. Tran, N. T. P. Thao, T. T. Hieu, S. Le, N. Q. Tuan, C. Sonne, S. S. Lam and Q. Van Le (2021). "Recycling of aquaculture wastewater and sediment for sustainable corn and water spinach production." Chemosphere, **268**, 129329.

van Vliet, M. T., E. R. Jones, M. Flörke, W. H. Franssen, N. Hanasaki, Y. Wada and J. R. Yearsley (2021). "Global water scarcity including surface water quality and expansions of clean water technologies." Environmental Research Letters, **16**(2), 024020.

Vardevanyan, P. O., A. P. Antonyan, M. A. Parsadanyan, M. A. Torosyan and A. T. Karapetian (2016). "Joint interaction of ethidium bromide and methylene blue with DNA. The effect of ionic strength on binding thermodynamic parameters." Journal of Biomolecular Structure and Dynamics, **34**(7), 1377-1382.

Varshney, K. (2014). "Carbon nanotubes: a review on synthesis, properties and applications." *International journal of engineering research and general science*, **2**(4), 660-677.

Verma, P. and S. K. Maheshwari (2019). "Applications of Silver nanoparticles in diverse sectors." *International Journal of Nano Dimension*, **10**(1), 18-36.

Vijay, R., T. Mardikar and R. Kumar (2016). "Impact of sewage discharges on coastal water quality of Mumbai, India: present and future scenarios." Environmental monitoring and assessment, **188**(7), 1-13.

Vlaanderen, J., A. Pronk, N. Rothman, A. Hildesheim, D. Silverman, H. D. Hosgood, S. Spaan, E. Kuijpers, L. Godderis and P. Hoet (2017). "A cross-sectional study of changes in markers of immunological effects and lung health due to exposure to multi-walled carbon nanotubes." Nanotoxicology, **11**(3), 395-404.

Wang, L., Z. Qiang, Y. Li and W. Ben (2017). "An insight into the removal of fluoroquinolones in activated sludge process: Sorption and biodegradation characteristics." *Journal of Environmental Sciences*, **56**, 263-271.

Wang, S., M. Shen, Y. Ma, G. Chen, Y. You and W. Liu (2019). "Application of Remote Sensing to Identify and Monitor Seasonal and Interannual Changes of Water Turbidity in Yellow River Estuary, China." *Journal of Geophysical Research*: Oceans, **124**(7), 4904-4917.

Wei, L., J. Lu, H. Xu, A. Patel, Z.-S. Chen and G. Chen (2015). "Silver nanoparticles: synthesis, properties, and therapeutic applications." Drug discovery today, **20**(5), 595-601.

Westall, F. and A. Brack (2018). "The importance of water for life." Space Science Reviews, **214**(2), 1-23.

Westerhoff, P., H. Moon, D. Minakata and J. Crittenden (2009). "Oxidation of organics in retentates from reverse osmosis wastewater reuse facilities." Water research, **43**(16), 3992-3998.

Willmon, E. (2018). "Microbial Quality of Aquaculture Water Used for Produce Irrigation."

Xu, J., Z. Cao, Y. Zhang, Z. Yuan, Z. Lou, X. Xu and X. Wang (2018). "A review of functionalized carbon nanotubes and graphene for heavy metal adsorption from water: Preparation, application, and mechanism." Chemosphere, **195**, 351-364.

Yadav, J. P., S. C. Das, P. Dhaka, D. Vijay, M. Kumar, P. Chauhan, R. Singh, K. Dhama, S. Malik and A. Kumar (2016). "Isolation, genotyping and antibiogram profile of

Clostridium perfringens isolates recovered from freshwater fish and fish products from Kolkata region." *Journal of Pure and Applied Microbiology,* **10**(4), 2807-2814.

Yasunori, T., M. Katsunori, Y. Masatoshi, M. Masatomo, H. Katsutoshi and U. Hajime (2002). "Fate of coliphage in a wastewater treatment process." *Journal of bioscience and bioengineering,* ***94***(2), 172-174.

Younas, M., M. Sohail, L. Leong, M. J. Bashir and S. Sumathi (2016). "Feasibility of CO 2 adsorption by solid adsorbents: a review on low-temperature systems." *International journal of environmental science and technology,* ***13***(7), 1839-1860.

Yu, J., N. Grossiord, C. E. Koning and J. Loos (2007). "Controlling the dispersion of multi-wall carbon nanotubes in aqueous surfactant solution." Carbon, **45**(3), 618-623.

Zambrano, M., E. Tondi, I. Korneva, E. Panza, F. Agosta, J. M. Janiseck and M. Giorgioni (2016). "Fracture properties analysis and discrete fracture network modelling of faulted tight limestones, Murge Plateau, Italy." *Italian Journal of Geosciences,* **135**(1), 55-67.

Zamora-Ledezma, C., D. Negrete-Bolagay, F. Figueroa, E. Zamora-Ledezma, M. Ni, F. Alexis and V. H. Guerrero (2021). "Heavy metal water pollution: A fresh look about hazards, novel and conventional remediation methods." *Environmental Technology & Innovation*: 101504.

Zargar, M., K. Shameli, G. R. Najafi and F. Farahani (2014). "Plant mediated green biosynthesis of silver nanoparticles using Vitex negundo L. extract." *Journal of Industrial and Engineering Chemistry,* **20**(6), 4169-4175.

Zawani, Z. (2009). "Equilibrium, kinetics and thermodynamic studies: adsorption of Remazol Black 5 on the palm kernel shell activated carbon." Eng. J. Sci. Res, **37**(1), 67-76.

Zhang, D., W. Luo, Y. Li, G. Wang and G. Li (2018). "Performance of co-composting sewage sludge and organic fraction of municipal solid waste at different proportions." Bioresource technology, **250**, 853-859.

Zhang, X.-F., Z.-G. Liu, W. Shen and S. Gurunathan (2016). "Silver nanoparticles: synthesis, characterization, properties, applications, and therapeutic approaches." *International journal of molecular sciences,* **17**(9), 1534.

Zhang, X., M. Feng, R. Qu, H. Liu, L. Wang and Z. Wang (2016). "Catalytic degradation of diethyl phthalate in aqueous solution by persulfate activated with nano-scaled magnetic CuFe2O4/MWCNTs." *Chemical engineering journal,* **301**, 1-11.

Zhang, Y., D. Petibone, Y. Xu, M. Mahmood, A. Karmakar, D. Casciano, S. Ali and A. S. Biris (2014). "Toxicity and efficacy of carbon nanotubes and graphene: the utility of carbon-based nanoparticles in nanomedicine." Drug metabolism reviews, **46**(2), 232-246.

Zhang, Y., Y. Zhang, K. Sun, Z. Meng and L. Chen (2019). "The SLC transporter in nutrient and metabolic sensing, regulation, and drug development." *Journal of molecular cell biology* ***11***(1), 1-13.

Zhu, B., Y. Li, Z. Lin, M. Zhao, T. Xu, C. Wang and N. Deng (2016). "Silver nanoparticles induce HePG-2 cells apoptosis through ROS-mediated signaling pathways." Nanoscale research letters, **11**(1), 1-8.